

# **THESIS**

## **DEVELOPMENT AND VALIDATION OF A PHYSICAL MODEL FOR A MODERN TWIN TUBE DAMPER**

Submitted by

Christopher Ryan Meissen

Mechanical Engineering

In partial fulfillment of the requirements

For the Degree of Master of Science

Colorado State University

Fort Collins, Colorado

Summer 2009

COLORADO STATE UNIVERSITY

April 16, 2009

WE HEREBY RECOMMEND THAT THE THESIS PREPARED UNDER OUR  
SUPERVISION BY CHRISTOPHER RYAN MEISSEN ENTITLED DEVELOPMENT  
AND VALIDATION OF A PHYSICAL MODEL FOR A MODERN TWIN TUBE  
DAMPER BE ACCEPTED AS FULFILLING IN PART REQUIREMENTS FOR THE  
DEGREE OF MASTER OF SCIENCE.

Committee on Graduate Work

---

Dr. Suren Chen

---

**Advisor** Dr. Patrick Fitzhorn

---

**Department Head and Committee Member** Dr. Allan Kirkpatrick

# **ABSTRACT OF THESIS**

## **DEVELOPMENT AND VALIDATION OF A PHYSICAL MODEL FOR A MODERN TWIN TUBE DAMPER**

Dampers, commonly referred to as shock absorbers, are very important to racecar development and performance. Combined with springs, they control the body motions of the vehicle. A spring mass damper model was developed to examine the effect of the damper characteristics on the response of a simple vehicle suspension.

A mathematical model of a modern twin tube damper was developed to accurately predict the force output as a function of velocity. The flow restrictions in the damper are determined from the physical properties of the damper and its fluid. Then the pressure differential across the damper piston and the consequent force outputted by the damper was calculated. The accuracy of the model was validated with experimental testing of a Cane Creek Double Barrel damper.

The fluid inertia and viscous effects in the twin tube damper were studied using the model. The effects of the fluid inertia were found to be negligible. The viscous effects were found to contribute significantly to the damper force. The model was also used to compare other differences between a monotube and modern twin tube damper. It was found that the gas pressure in a twin tube damper could be set significantly lower than in a comparable monotube damper without the risk of fluid cavitation. Parameter studies were performed to evaluate the effect of different adjustments and properties of the valves and orifices on the performance of the damper.

Christopher Ryan Meissen  
Mechanical Engineering Department  
Colorado State University  
Fort Collins, CO 80523  
Summer 2009

## **ACKNOWLEDGMENTS**

I would especially like to thank Dr. Patrick Fitzhorn for this research opportunity. I have greatly appreciated the support and guidance you have provided to me. Thank you to my other committee members, Dr. Allan Kirkpatrick and Dr. Suren Chen for your participation in my thesis.

I would like to thank Josh Coaplen and Malcolm Smith of Cane Creek for their assistance and interest in this project. I appreciate them for helping me to better understand the intricacies of the damper being modeled and their willingness to share specific properties of the damper internals with me.

Thank you to Eric Neeley of PUSH Industries for allowing me to use one of their dampers for measurements to ensure the accuracy of this work.

I greatly appreciate the 2009 Colorado State University Formula SAE team for allowing me to perform testing on their dampers to complete this research.

The support and love that my parents and sister have provided over the past two years have kept me positive and driven me to succeed. I want to thank my parents for the opportunities they have given me and everything else they have done for me. Especially the sacrifices they made to be with me throughout my treatment.

Thanks to Randy Leech for helping me during my second semester by keeping me updated on my classes and providing me with notes. Thanks again to Eric Neeley for understanding and taking some of the pressure off of me while we were graduate teaching assistants.

## TABLE OF CONTENTS

	Page
ABSTRACT.....	iii
ACKNOWLEDGMENTS .....	iv
TABLE OF CONTENTS.....	v
LIST OF FIGURES .....	vii
LIST OF SYMBOLS .....	xi
1. INTRODUCTION .....	1
2. FUNDAMENTALS OF DAMPING .....	4
2.1 Spring Mass Damper Model .....	5
2.2 Monotube Dampers.....	17
2.3 Twin Tube Dampers .....	22
2.4 Damper Characterization .....	26
3. LITERATURE REVIEW .....	34
4. MODEL DEVELOPMENT.....	41
4.1 Static Damper Properties .....	41
4.2 Monotube Damper Model.....	43
4.2.1 Total Flow Rate.....	46
4.2.2 Constant Area Orifice Flow .....	47
4.2.3 Bleed Orifice Flow.....	49
4.2.4 Piston Orifice Flow .....	50
4.2.5 Piston Valve Flow.....	51
4.2.6 Leakage around Piston.....	54
4.2.7 Gas Chamber Model .....	55
4.3 Twin Tube Damper Model.....	57
4.4 Fluid Inertia and Viscous Effects.....	61
4.5 Model Execution.....	65

4.6 Solution Method.....	67
<b>5. EXPERIMENTAL PROCEDURE .....</b>	<b>70</b>
5.1 Experimental Apparatus.....	70
5.2 Damper Parameters .....	73
5.3 Validation Procedure .....	76
<b>6. RESULTS .....</b>	<b>80</b>
6.1 Validation Results.....	80
6.1.1 Static and Friction Force.....	81
6.1.2 Bleed Orifice Correlation.....	82
6.1.3 Knee Location Correlation.....	90
6.1.4 Valve Correlation.....	92
6.2 Fluid Inertia and Viscous Effects .....	98
6.3 Twin Tube and Monotube Damper Comparison .....	104
6.4 Parameter Studies .....	111
6.4.1 Bleed Orifice Area .....	111
6.4.2 Valve Orifice Area .....	113
6.4.3 Valve Spring Stiffness .....	115
6.4.4 Piston Leakage Gap .....	117
6.4.5 Fluid Passage Width .....	120
6.5 Spring Mass Damper Model .....	122
<b>7. CONCLUSIONS AND RECOMMENDATIONS .....</b>	<b>128</b>
<b>REFERENCES .....</b>	<b>131</b>

## LIST OF FIGURES

FIGURE	Page
2.1 Spring Mass Damper System.....	6
2.2 Simulink Model .....	8
2.3 Effect of Damping Ratio on a Second Order System .....	10
2.4 Sprung Mass Displacement .....	11
2.5 Sprung Mass Acceleration .....	12
2.6 Damper Force .....	12
2.7 Tire Load Variation .....	13
2.8 Segments of the Characteristic Diagram .....	16
2.9 Monotube Damper Components [2] .....	17
2.10 Flow through Piston during Compression [10].....	19
2.11 Flow through Piston during Extension [10].....	20
2.12 Monotube Damper Varieties [11] .....	21
2.13 Twin Tube and Monotube Dampers [9].....	22
2.14 Modern Twin Tube Damper [12].....	24
2.15 Modern Twin Tube Damper in Low Speed Compression [12] .....	25
2.16 Roehrig Engineering 5VS Damper Dynamometer [14].....	27
2.17 Damper Test Motion Profile .....	28
2.18 Continuous Velocity Characteristic Diagram .....	30
2.19 Peak Velocity Characteristic Diagram.....	31
2.20 Work Diagram .....	32

4.1	Damper at Static State.....	42
4.2	Damper with Gas Chamber at Static State.....	42
4.3	Damper during Compression [1] .....	44
4.4	Piston and Rod Free Body Diagram .....	45
4.5	Compression Flow Diagram .....	46
4.6	Piston Orifice and Valve.....	50
4.7	Valve Free Body Diagram .....	52
4.8	Piston Leakage [1] .....	55
4.9	Gas Piston Free Body Diagram.....	56
4.10	Modern Twin Tube Damper Compression Flow Diagram .....	59
4.11	Modern Twin Tube Damper Rebound Flow Diagram .....	60
4.12	Fluid Inertia .....	62
4.13	Newton's Method .....	67
5.1	Instron 8501 Damper Dynamometer .....	71
5.2	Damper Displacement .....	72
5.3	Damper Velocity.....	73
5.4	Cane Creek Double Barrel Damper .....	74
5.5	Cane Creek Double Barrel Adjusters.....	75
5.6	Cane Creek Double Barrel Internal Valve .....	76
6.1	Damper Friction.....	82
6.2	Bleed Correlation at Soft Low Speed Adjustment and .8 Hz .....	83
6.3	Bleed Correlation at Soft Low Speed Adjustment and 1.6 Hz .....	84
6.4	Variance at Soft Low Speed Adjustment and .8 Hz .....	85

6.5	Bleed Correlation at Medium Low Speed Adjustment and .8 Hz .....	87
6.6	Bleed Correlation at Medium Low Speed Adjustment and 1.6 Hz .....	87
6.7	Variance at Medium Low Speed Adjustment and .8 Hz .....	88
6.8	Model Sensitivity to the Discharge Coefficient .....	89
6.9	Knee Correlation at Soft High Speed Adjustment.....	90
6.10	Knee Correlation at Medium High Speed Adjustment.....	91
6.11	Knee Correlation at Stiff High Speed Adjustment .....	91
6.12	Valve Correlation at Soft High Speed Adjustment .....	93
6.13	Variance at Soft High Speed Adjustment and 3.2 Hz .....	94
6.14	Valve Correlation at Medium High Speed Adjustment .....	95
6.15	Variance at Medium High Speed Adjustment and 3.2 Hz .....	96
6.16	Valve Correlation at Stiff High Speed Adjustment .....	97
6.17	Variance at Stiff High Speed Adjustment and 3.2 Hz .....	97
6.18	Characteristic Diagram with Combined Inertia and Viscous Effects .....	99
6.19	Damper Pressure with Combined Inertia and Viscous Effects .....	100
6.20	Characteristic Diagram with Viscous Effects .....	101
6.21	Damper Pressure with Viscous Effects .....	102
6.22	Characteristic Diagram with Fluid Inertia Effects .....	103
6.23	Damper Pressure with Fluid Inertia Effects .....	103
6.24	Characteristic Diagram of Twin Tube and Monotube Damper .....	105
6.25	Twin Tube Damper Chamber Pressures at 5 bar .....	107
6.26	Monotube Damper Chamber Pressures at 5 bar .....	108
6.27	Monotube Damper Chamber Pressures at 10 bar .....	109

6.28 Characteristic Diagram of Twin Tube and Monotube Damper with Different Initial Gas Pressures .....	110
6.29 Characteristic Diagram of Bleed Orifice Area Parameter Study .....	112
6.30 Pressure from Bleed Orifice Area Parameter Study .....	112
6.31 Characteristic Diagram of Valve Orifice Area Parameter Study .....	114
6.32 Valve Deflection from Valve Orifice Area Parameter Study .....	115
6.33 Characteristic Diagram of Valve Stiffness Parameter Study .....	116
6.34 Valve Deflection from Valve Stiffness Parameter Study .....	117
6.35 Plot of Piston Leakage Gap Parameter Study .....	118
6.36 Flow Rate of Piston Leakage Gap .....	119
6.37 Characteristic Diagram of Fluid Passage Width Parameter Study .....	120
6.38 Pressure Differential over Fluid Passage .....	121
6.39 Characteristic Diagram for the Spring Mass Damper Model .....	123
6.40 Sprung Mass Displacement with Damper Model Input .....	124
6.41 Sprung Mass Acceleration with Damper Model Input .....	125
6.42 Damper Force from Damper Model Input .....	126
6.43 Tire Load Variation from Damper Model Input .....	126

## LIST OF SYMBOLS

Symbol	Definition, Units
$A$	Area, m <sup>2</sup>
$A_b$	Bleed Orifice Area, m <sup>2</sup>
$A_c$	Piston Area on Compression Chamber Side, m <sup>2</sup>
$A_{gp}$	Gas Piston Area, m <sup>2</sup>
$A_o$	Piston Orifice Area, m <sup>2</sup>
$A_r$	Piston Area on Rebound Chamber Side, m <sup>2</sup>
$A_{rod}$	Area of Rod, m <sup>2</sup>
$A_v$	Area of Pressure Acting on Valve, m <sup>2</sup>
$A_{vf}$	Flow Area from Valve Deflection, m <sup>2</sup>
$Amp$	Amplitude, m
$b$	Piston/Cylinder Clearance, m
$b_t$	Twin Tube Passage Width, m
$c$	Damping Coefficient, N/(m/s)
$c_{crit}$	Critical Damping Coefficient, N/(m/s)
$C_d$	Steady State Discharge Coefficient
$C_D$	Dynamic Discharge Coefficient
$C_{Db}$	Bleed Orifice Dynamic Discharge Coefficient
$C_{Do}$	Piston Orifice Dynamic Discharge Coefficient
$C_{Dv}$	Valve Dynamic Discharge Coefficient
$C_f$	Momentum Force Coefficient
$C_s$	Suspension Damping Coefficient, N/(m/s)

Symbol	Definition, Units
$C_t$	Tire Damping Coefficient, N/(m/s)
$C_w$	Wetted Circumference, m
$D_H$	Hydraulic Diameter, m
$Di$	Inner Passage Diameter, m
$D_o$	Outer Passage Diameter, m
$D_p$	Piston Diameter, m
$D_v$	Valve Diameter, m
$f$	Frequency, Hz
$F$	Damper Force, N
$F_c$	Compression Chamber Force, N
$F_{exp}$	Experimental Force, N
$F_f$	Piston Friction Force, N
$F_m$	Fluid Momentum Force, N
$F_{model}$	Force from Model, N
$F_p$	Valve Preload Force, N
$F_r$	Rebound Chamber Force, N
$F_s$	Damper Static Force, N
$F_{sc}$	Damper Static Force in Compression, N
$F_{sr}$	Damper Static Force in Rebound, N
$k$	Valve Spring Stiffness, N/m
$K$	Spring Stiffness, N/m
$K_s$	Suspension Spring Stiffness, N/m

Symbol	Definition, Units
$K_t$	Tire Spring Stiffness, N/m
$l$	Piston Length, m
$L$	Length, m
$L_c$	Leakage Circumference, m
$L_g$	Length of Gas Chamber, m
$m$	Mass, kg
$m_{gp}$	Mass of Gas Piston, kg
$m_{rp}$	Mass of Rod/Piston Assembly Piston, kg
$P$	Pressure, Pa
$\Delta P$	Pressure Differential, Pa
$P_c$	Compression Chamber Pressure, Pa
$P_g$	Gas Chamber Pressure, Pa
$P_{gi}$	Initial Gas Chamber Pressure, Pa
$P_r$	Rebound Chamber Pressure, Pa
$P_t$	Pressure after the Valve, Pa
$P_v$	Pressure in the Valve, Pa
$P_i$	Initial Pressure, Pa
$P_2$	Final Pressure, Pa
$Q$	Flow Rate, $\text{m}^3/\text{s}$
$Q_b$	Flow Rate through Bleed Orifice, $\text{m}^3/\text{s}$
$Q_f$	Flow Rate across Boundary, $\text{m}^3/\text{s}$
$Q_{lp}$	Flow Rate through Piston Leakage, $\text{m}^3/\text{s}$

Symbol	Definition, Units
$Q_p$	Total Flow Rate, m <sup>3</sup> /s
$Q_r$	Flow Rate through External Valve, m <sup>3</sup> /s
$Q_v$	Flow Rate through Valve, m <sup>3</sup> /s
$\dot{Q}$	Volumetric Flow Acceleration, m <sup>3</sup> /s <sup>2</sup>
$SSW$	Sum of Squares within Samples
$s_w^2$	Mean Square within Samples
$v_T$	Theoretical Fluid Velocity, m/s
$v_{x,in}$	Fluid Entrance Velocity, m/s
$v_{x,out}$	Fluid Exit Velocity, m/s
$v_I$	Initial Fluid Velocity, m/s
$v_2$	Final Fluid Velocity, m/s
$\Delta V$	Change in Volume, m <sup>3</sup>
$V_I$	Initial Volume, m <sup>3</sup>
$V_2$	Final Volume, m <sup>3</sup>
$x$	Piston Displacement, m
$\dot{x}$	Piston Velocity, m/s
$\dot{x}_{max}$	Maximum Piston Velocity, m/s
$\ddot{x}$	Piston Acceleration, m/s <sup>2</sup>
$y$	Valve Deflection, m
$z$	Gas Piston Displacement, m
$\ddot{z}$	Gas Piston Acceleration, m/s <sup>2</sup>
$z_{road}$	Road Input Displacement, m

Symbol	Definition, Units
$\dot{z}_{road}$	Road Input Velocity, m/s
$z_s$	Sprung Mass Displacement, m
$\dot{z}_s$	Sprung Mass Velocity, m/s
$\ddot{z}_s$	Sprung Mass Acceleration, m/s <sup>2</sup>
$z_{us}$	Unsprung Mass Displacement, m
$\dot{z}_{us}$	Unsprung Mass Velocity, m/s
$\ddot{z}_{us}$	Unsprung Mass Acceleration, m/s <sup>2</sup>
$\alpha$	Area Flow Correction Factor
$\zeta$	Damping Ratio
$\mu$	Fluid Viscosity, Pa-s
$\pi$	pi
$n_T$	Number of samples collected
$\rho$	Fluid Density, kg/m <sup>3</sup>
$\omega_d$	Damped Natural Frequency, radians/s
$\omega_n$	Undamped Natural Frequency, radians/s
$\zeta$	Damping Ratio



## **1. INTRODUCTION**

Dampers, commonly referred to as shock absorbers, are very important to racecar development and performance. Combined with springs, they control the body motions of the vehicle. This is very important because most modern racecars are very dependent on aerodynamics. Being able to precisely control the ride height, pitch, and roll of the vehicle is crucial to maximizing the aerodynamic performance. Dampers also affect the vertical load on the tire during transient conditions. Minimizing the variation of the tire vertical load is very important because it allows the tires to produce maximum lateral and longitudinal force [1]. A spring mass damper model will be used to examine the effect of the damper characteristics on the response of a simple vehicle suspension.

Dampers are generally characterized through experimental testing that generates a characteristic diagram, expressing the damping force as a function of the damper velocity. While these tests allow the effect of the damper on the vehicle response to be determined, they give little insight to how and where the actual forces in the damper are generated. Also many dampers are externally adjustable and revalvable to give a wide range of characteristics. This allows the damper to be made suitable for different cars, tracks, and ambient conditions. Therefore to fully characterize a damper with multiple adjustments extensive experimental testing is performed. If the damper is rebuilt or revalved this testing must be repeated to see the effects.

A damper model could be used to limit the need for extensive testing to determine the range and resolution of the damper adjustment. It could also be used to predict what valving is needed to produce a desired characteristic diagram, without actually revalving and testing the damper. This could significantly reduce the testing and revalving time required for the damper.

This research focuses on developing and experimentally validating a parametric model of a modern twin tube damper. There has been no other research published on the modeling of a modern twin tube damper. The model developed will generate characteristic diagrams from the physical parameters of a damper. These parameters include the dimensions of the damper internals, the inertia of the damper, properties of the damper oil, and the initial gas pressure in the damper. The model will also calculate the internal pressures in the damper and flow rates through the different flow paths in the damper. This will give insight to how and why the physical parameters of the damper affect the force outputted by the damper.

A model of a monotube damper will first be developed. This has been done before and has been experimentally validated by both Talbot and Starkey [1] and Rhoades [2]. This model will be developed because many aspects of a monotube damper model can be applied to the twin tube damper model. Also with both models the difference in the operation and performance characteristics of these types of dampers will be compared.

One of the significant differences in the operation of the twin tube and monotube dampers is the movement and subsequent acceleration of the damper fluid through an external circumferential passage. Twin tube dampers move a significantly greater volume

of fluid. Therefore the effect of the inertial and viscous attributes of this fluid movement on the damper performance will be examined.

## **2. FUNDAMENTALS OF DAMPING**

Despite being commonly referred to as shock absorbers, dampers do not absorb shocks. The shocks are actually absorbed by the deflection of the tire and suspension springs. Basic vibration theory explains that a spring-mass system once excited will oscillate continuously at a specific amplitude and frequency. This is commonly referred to as harmonic motion. This is achieved by the system exchanging potential and kinetic energy without any net energy loss. Therefore to control this movement energy must be dissipated from the system. The damper dissipates this energy in a controlled manner by converting the kinetic energy of the mass into thermal energy.

Dampers are commonly treated as being solely velocity dependent. However, this is not true. Most dampers are also position and acceleration dependent to some extent. Coulumb friction is also present in dampers, mainly due to the seals around the rod and piston that prevent leakage and contamination entering the damper. These forces are normally treated as constant and do not depend on the position, velocity, or acceleration of the damper. Reducing the friction and position and acceleration dependencies is one of the main goals of damper design.

Before the development of the damper model is described the effect of the damper force on a vehicle suspension will be examined. A spring mass damper model of a vehicle suspension will be used for this. Then a brief description and explanation of the

operation and characteristics of both a monotube and modern twin tube damper will follow. Also the typical testing procedure of the damper is explained, as well as the generation of characteristic and work diagrams.

## 2.1 Spring Mass Damper Model

In racecar suspensions the damper operates at a minimum in parallel with the suspension springs and in series with the tire. The tire is both displacement and velocity sensitive therefore it acts as another spring and damper acting in parallel. However the damping component of the tire is generally small and is often neglected [3]. Racecar suspensions often include other sources of restoring, damping, and friction force but those are beyond the scope of this research.

The effects of different damper and spring rates can be determined by writing the equations of motion for a typical vehicle suspension system. Figure 2.1, on the next page, shows the physical representation of the system that will be described. It represents one corner of a vehicle with a simple suspension. More complex suspension systems or a more complete, two or four wheel, vehicle suspension systems can be modeled in a similar manner.

In the figure  $m_s$  is the sprung mass of the vehicle that acts on this corner of the suspension. For a vehicle that is laterally and longitudinally symmetric it would be one quarter of the total sprung mass. The unsprung mass is represented by  $m_{us}$ . This includes any mass that moves with the wheel and tire. For an independent suspension a portion of the suspension links and half shafts should be included. This can be measured or determined analytically but assuming half of the weight of the links is unsprung mass is

generally accurate enough [3].  $K_s$  and  $C_s$  are the spring rate and damper coefficient of the suspension, and  $K_t$  and  $C_t$  are of the tire. The displacement of the sprung and unsprung masses and the road are  $z_s$ ,  $z_{us}$ , and  $z_{road}$ , respectively.

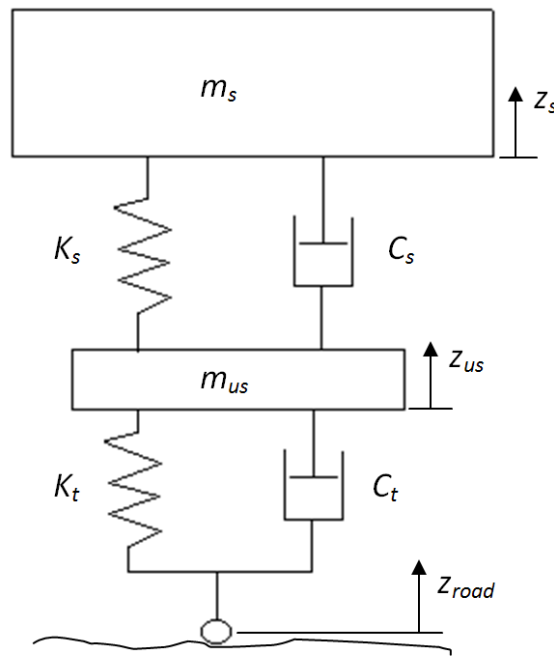


Figure 2.1: Spring Mass Damper System

The equations of motion for the sprung and unsprung masses can be determined by summation of the spring, damper, and inertial forces. Equation (2.1) is the equation of motion of the sprung mass, and Equation (2.2) is for the unsprung mass.

$$m_s \ddot{z}_s + C_s(\dot{z}_s - \dot{z}_{us}) + K_s(z_s - z_{us}) = 0 \quad (2.1)$$

$$m_{us} \ddot{z}_{us} + C_t(\dot{z}_{us} - \dot{z}_{road}) + K_t(z_{us} - z_{road}) - C_s(\dot{z}_s - \dot{z}_{us}) - K_s(z_s - z_{us}) = 0 \quad (2.2)$$

It is not necessary to include the effect of gravity in these equations because the static equilibrium of the system is taken as the initial positions. The static equilibrium accounts for the deflection of the spring and tire due to gravity [4].

This system was modeled in Matlab Simulink. Simulink was used because it allows many types of disturbances to be introduced into the system including displacements from the road surface and forces from load transfer or aerodynamic effects. The primary outputs monitored were the sprung mass displacement and acceleration, the damper force, and the tire load variation. These outputs can be plotted by Simulink, but for more detailed analysis they are automatically outputted to the Matlab workspace. From there the data can be analyzed and plotted in Matlab or easily outputted to Excel. The flexibility of Simulink allows virtually any parameter of the system to be plotted or outputted for further analysis.

The Simulink model is displayed in Figure 2.2. The blocks on the left are the inputs for the masses, spring rates, tire damping coefficient, and road disturbances. Additional blocks allow force to be applied separately to the sprung and unsprung masses. This is important because load transfer from lateral and longitudinal acceleration is proportioned into geometric and elastic components depending on the height of the center of gravity and the roll or pitch center. Geometric load transfer is transferred through the suspension links to the unsprung mass, while the elastic load transfer is transferred through the sprung mass and the springs and dampers. The two large circles sum the forces on the sprung and unsprung masses. The force is then divided by the mass to determine its acceleration. These accelerations are then integrated to determine the velocities and displacements of the masses. The block to the far right outputs the data to

the Matlab workspace. Multiple scopes can be seen in the model. These allow the user to look at different aspects of the system and evaluate the effect of the changes made to the inputs.

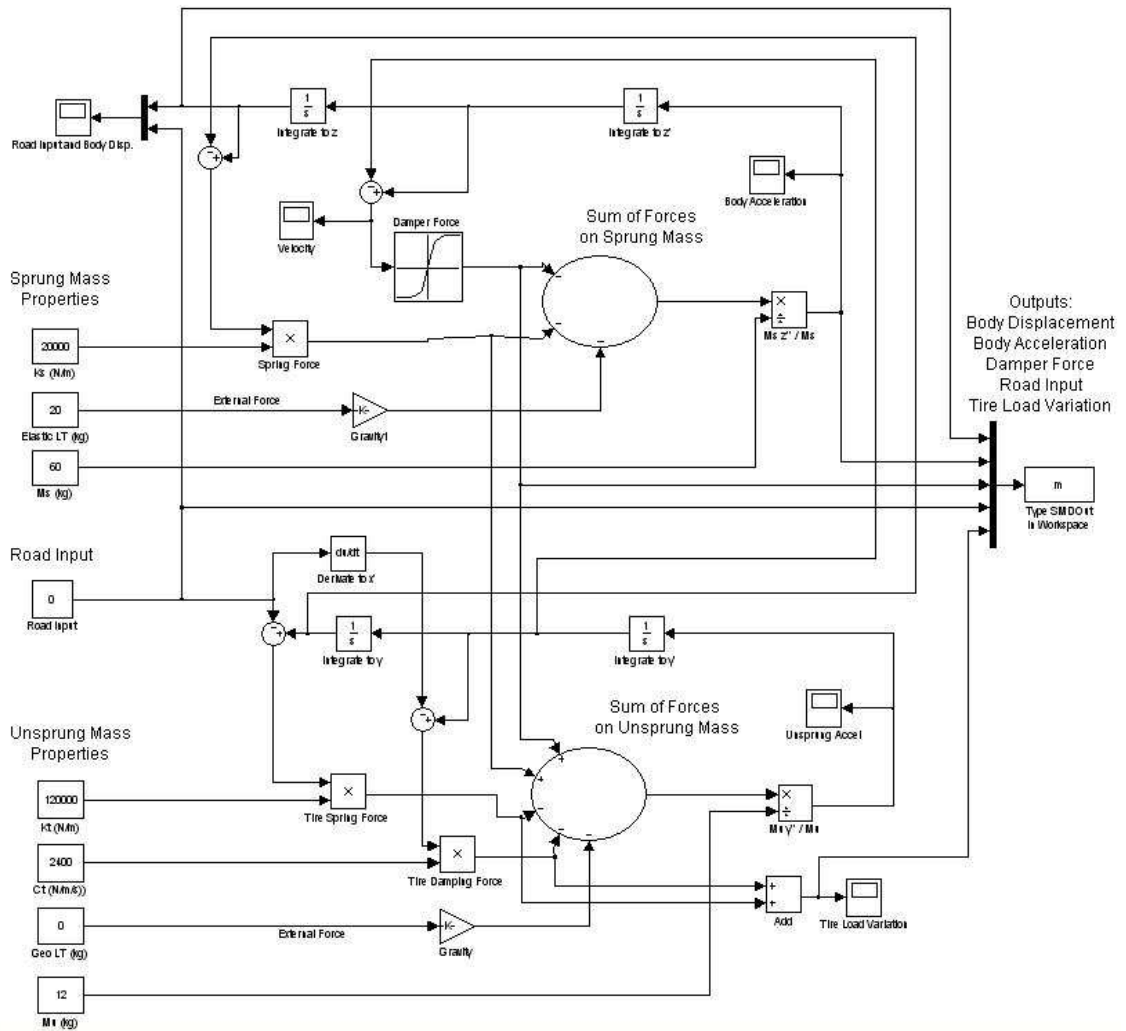


Figure 2.2: Simulink Model

A look up table was used to import data from the damper model into the spring mass damper model. The velocity of the damper is the input for the look up table. The

data from the damper model is interpolated and the damper force is outputted. This model neglects the effect of the hysteresis in the characteristic diagram of the damper. Thus the damper force is assumed to be the same regardless of the direction of the acceleration of the damper.

In order to better evaluate the outputs given by this model the characteristics of typical second order system shall be reviewed. The damping of a second order system is usually defined by the damping ratio. It is the damping coefficient of the system divided by the critical damping coefficient.

$$\zeta = \frac{c}{c_{crit}} \quad (2.3)$$

The critical damping coefficient is a function of the mass and the spring rate as shown in equation (2.4).  $\omega_n$  is the undamped natural frequency of the system. If the system had no damping and was disturbed it would oscillate at that frequency. Physically the critical damping is the damping required so that the system responds as quickly as possible without any oscillation or overshoot of the steady state value.

$$\omega_n = \sqrt{\frac{K}{m}} \quad (2.4)$$

$$c_{crit} = 2 \sqrt{\frac{K^2}{\omega_n^2}} = 2\sqrt{K m} \quad (2.5)$$

The damped natural frequency is the frequency the system will actually oscillate at. It is a function of the undamped natural frequency and the damping ratio. As can be seen from equation (2.6) as the damping ratio increases the damped natural frequency of the system decreases. If the damping ratio is one or greater the system will not oscillate and therefore will not have a damped natural frequency.

$$\omega_d = \omega_n \sqrt{1 - \zeta^2} \quad (2.6)$$

The effect of the damping ratio on the response of a second order system to a unit step is shown below in Figure 2.3. As can be seen if the damping ratio is less than one the system is under damped and will overshoot and oscillate about the steady state value before reaching it. If the value is greater than one the system is over damped and the response will not overshoot the steady state value but will have a larger settling time. The settling time is the time for the response to reach and stay within a percentage of the final value. This value is difficult to determine analytically but can easily be determined from the plotted response [5]. As can be seen from the figure below the 5% settling time for the .7 damping ratio is approximately .4 seconds versus approximately 1 second for the damping ratio of 1.5.

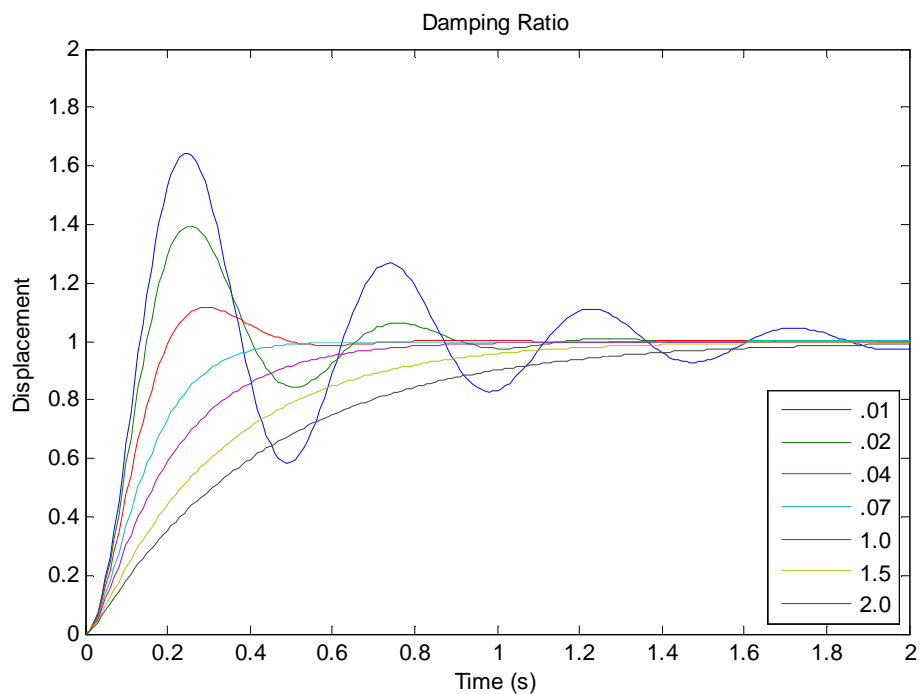


Figure 2.3: Effect of the Damping Ratio on a Second Order System

The data in the figures below was outputted from the Simulink model. The figures show the response of the system to an applied force of 200 N to the sprung mass. This is representative of elastic load transfer to the outer wheel during lateral acceleration. The model uses a tire stiffness of 120,000 N/m, a spring stiffness of 20,000 N/m, and sprung and unsprung masses of 60 and 12 kg, respectively. Linear damping coefficients of 660, 1530, and 2630 N/(m/s) were used. These values correlate to damping ratios of the sprung mass of .3, .7, and 1.2, respectively. Figure 2.4 is the sprung mass displacement, 2.5 is the sprung mass acceleration, 2.6 is the damper force, and 2.7 is the tire load variation.

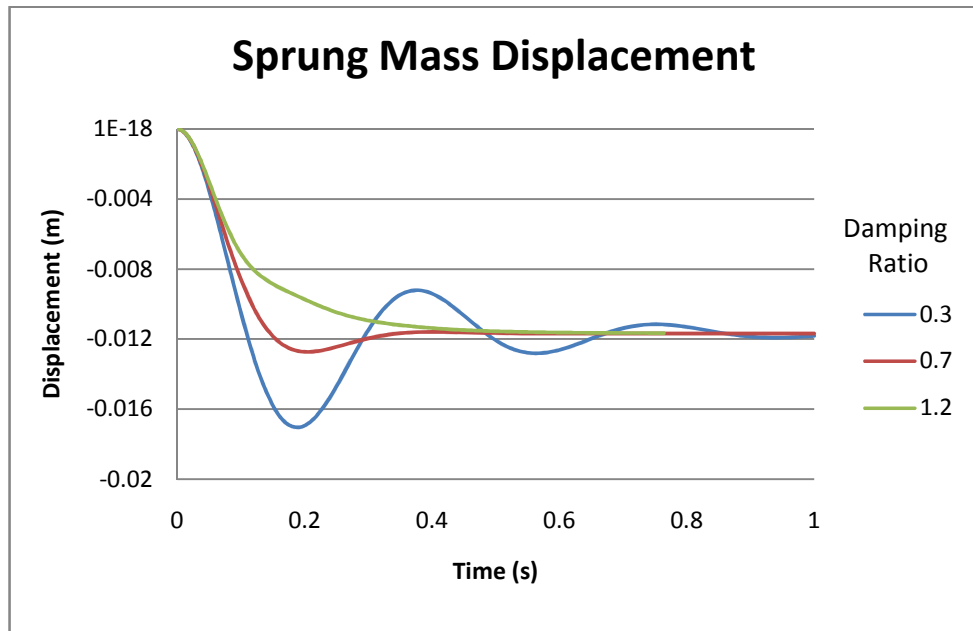


Figure 2.4: Sprung Mass Displacement

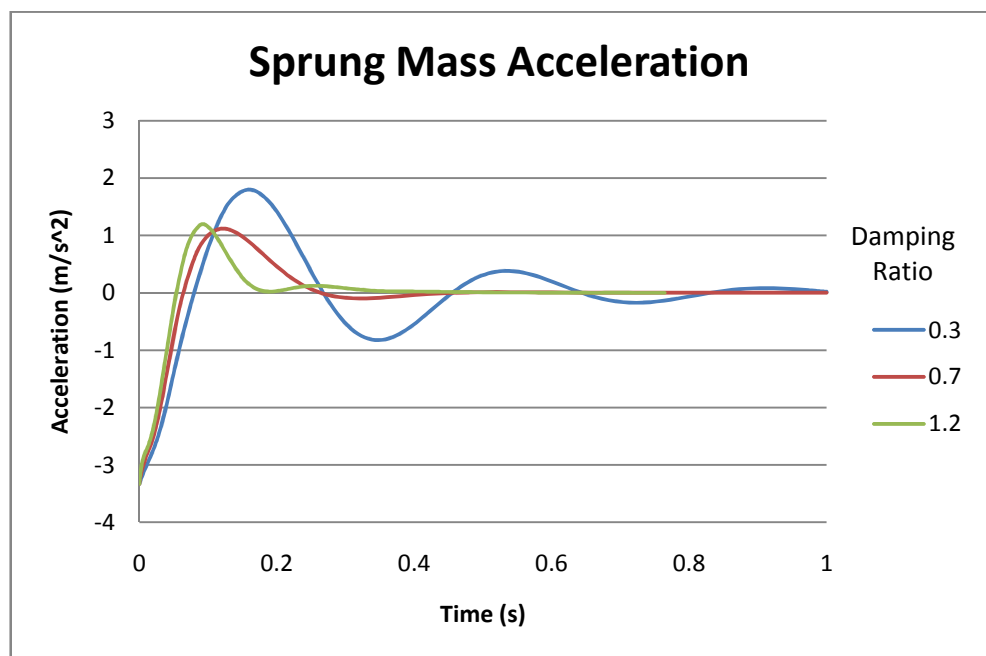


Figure 2.5: Sprung Mass Acceleration

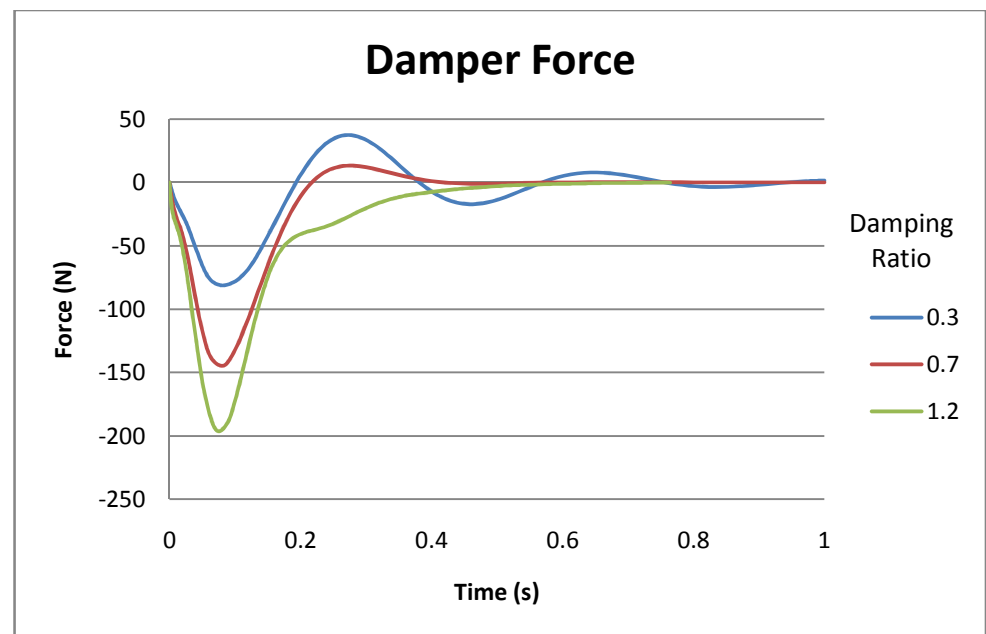


Figure 2.6: Damper Force

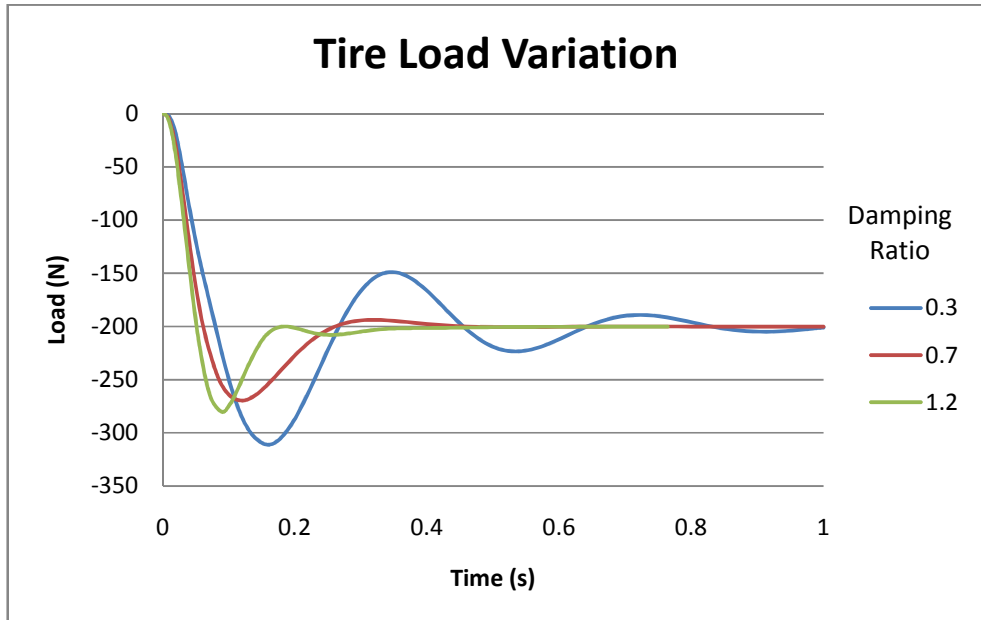


Figure 2.7: Tire Load Variation

It can be seen in all four figures that the steady state values do not depend on the damping ratio. Thus the dampers have no effect on the system once it reaches steady state. They affect the transient state before the system settle. The damping ratios can extend or shorten this transient period because they affect the time delay of the system until it reaches steady state.

The damping ratios of .3, .7, and 1.2 were chosen for specific reasons. A damping ratio of between .2 and .4 is often used on modern passenger cars because it provides good ride comfort [6]. However, a damping ratio between .65 and .7 is a typical baseline used for optimum handling [7]. For race cars that are very dependent on aerodynamic downforce for maximum performance damping ratios of 1.0 and much greater are often used [8]. However, these damping ratios are only for heave of the vehicle. The damping ratios for the roll and pitch of the vehicle will be different and must

be calculated separately because they depend on the moments of inertia of the sprung mass not the mass itself.

The displacement of the sprung mass can be seen in Figure 2.4. It varies significantly depending on the damping ratio. Excessive displacement can be very detrimental to the performance of a race car. It makes the car very slow to respond and requires large ground clearance raising the center of gravity. If the car relies heavily on aerodynamics it will be very unpredictable and difficult to drive because the front and rear ride heights and subsequently the pitch of the body will vary significantly with the body displacement. This will cause large changes in the downforce, pitching moment, center of gravity height of the vehicle affecting the maximum lateral acceleration and the handling balance. A damping ratio greater than 1 will make these changes happen slower giving the driver more time to account for them.

Figure 2.5 shows the acceleration of the sprung mass. Minimizing this is one of the main criteria for developing suspension systems for good ride properties [1]. However in the figure it can be seen that the system with a damping ratio of .3 has the highest accelerations. This is primarily a result of the large force from spring deflections caused by the large displacement of the body not the force of the damper. With inputs of higher velocity and smaller displacement, like typical road roughness a damping ratio of around .3 would minimize the acceleration of the sprung mass.

The damper force is shown in Figure 2.6. For the damping ratios of .7 and 1.2 the damper force quickly peaks and then returns to steady state. This is because the large damping force quickly dissipates the kinetic energy and causes the vehicle to return to steady state. This damping force is directly proportional to the difference in velocity of

the sprung and unsprung masses. The system with a damping ratio of .3 has much lower damping force and takes much longer to return to steady state. With small, high velocity road inputs this lower damper force combined with small spring displacements would limit the transferred to the sprung mass and reduce the sprung mass acceleration.

The tire load variation shown in Figure 2.7 is very important for race cars, especially those not extremely dependant on aerodynamics. Reducing the load variation of the tires will increase the maximum grip that they can provide. It can be seen that a damping ratio of .7 gives a good compromise between the magnitude and rate of change of the load variation. A higher damping ratio may have less overall variation because it reaches steady state quicker but the rate of change of the load can be quite significant. Tire load variation is not a significant factor when optimizing the ride properties of a vehicle.

Many modern dampers try to compromise between high damping ratios at low damper speeds and lower damping ratios at high speeds. Typically low damper speeds are considered between approximately 0 and .05 m/s [7]. This corresponds to the movements of the sprung mass from lateral and longitudinal acceleration. High damper speeds above approximately .05m/s correspond to the response of the vehicle due to road inputs. A compromise between these speeds can be achieved in the damper by preloading the valve springs. The dampers will be very stiff, having a high damping ratio at low velocities. Once the damper velocity required to overcome the preload on the valve is reached the dampers will become much softer, having a lower damping ratio. The characteristic diagram of a damper like this is shown below in Figure 2.8.

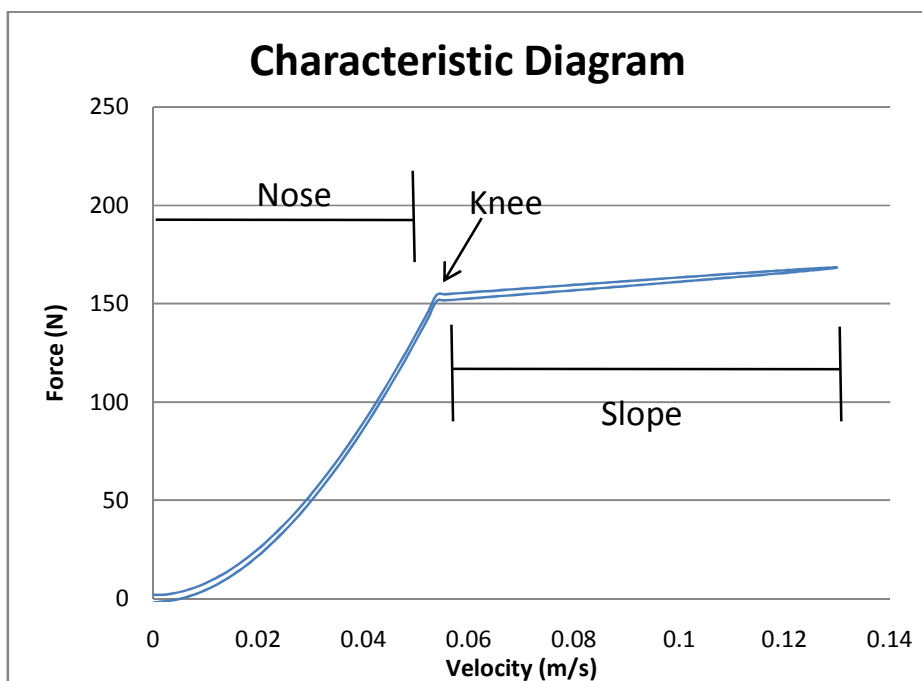


Figure 2.8: Segments of the Characteristic Diagram

In the characteristic diagram above the slope of the curve is the damping coefficient. It can be seen at lower velocities that the damping coefficient and subsequently the damping ratio is much greater from approximately 0 to .05 m/s. Above .05 m/s the coefficient is significantly less. The section of the curve at approximately .05 m/s where an inflection in the slope occurs is commonly referred to as the knee. The knee is not necessarily an abrupt change of slope like shown in this figure. Often it is much more gradual and in that case the knee would be defined over a range of velocities. The section of the curve between zero velocity and the knee is referred to as the nose and the section at higher velocity than the knee is referred to as the slope.

## 2.2 Monotube Damper

Monotube dampers are very common in motorsports. Figure 2.9 below shows the major components of a monotube damper. The damper is attached to the sprung and unsprung mass of the vehicle by the spherical bearings at each end. Generally the body of the damper is connected to the chassis of the vehicle. The rod side of the damper is connected to the suspension members to minimize the unsprung mass of the vehicle. The compression and rebound chambers are filled with mineral or synthetic oil. Extension or compression of the damper causes fluid to flow through valves and orifices in the piston. The gas chamber is separated from the oil by a floating piston and is pressurized with nitrogen.

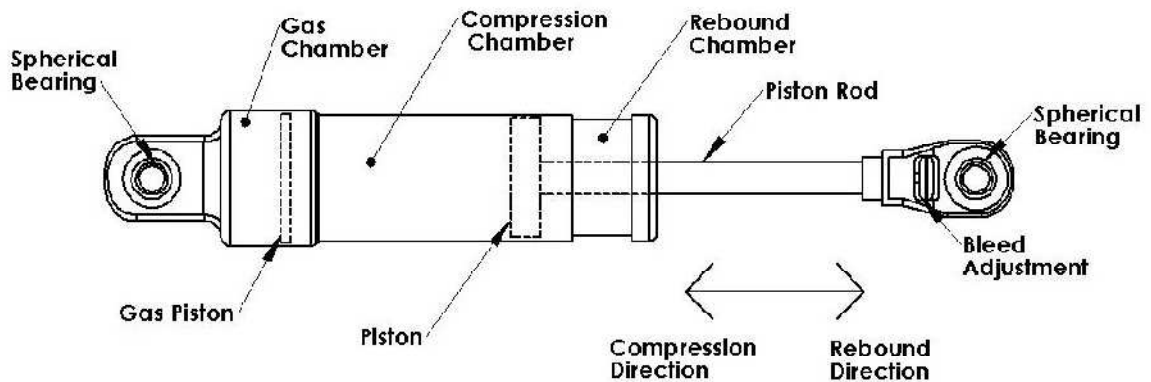


Figure 2.9: Monotube Damper Components [2]

The compressibility of the gas allows for changes in volume, caused primarily by the insertion of the rod, but also by expansion or contraction of the damper and fluid under different temperatures and pressures. The gas chamber is pressurized to prevent

cavitation of the oil. Cavitation is vaporization of the damper fluid, caused by the pressure of the fluid dropping below its vapor pressure [9]. The gas chamber also creates a gas spring effect because the areas on each side of the piston are not equal. That is why a damper will rebound without any force.

The gas chamber in a monotube damper is always acting on the compression chamber. Therefore, the pressure has to be nearly equivalent in these two chambers. In order to generate a damping force a pressure differential across the piston must be created. In compression the pressure in the rebound chamber will have to be lower than that in the compression chamber. Therefore, a high gas pressure is necessary to keep the rebound chamber pressure above the vapor pressure of the fluid.

Compression of the damper causes fluid to flow through the piston from the compression chamber to the rebound chamber. The flow through the piston is restricted by valves and orifices. This is the primary mechanism of generating damping force. These flow restrictions create a pressure differential across the piston. Energy is dissipated through the hydraulic shearing of the fluid. The energy is dissipated thermally increasing the temperature of the fluid and damper [1].

Figure 2.10, on the next page, shows a cutaway of a damper body and piston. The damper is undergoing compression. The figure shows a very common valve and orifice configuration. It combines a small bleed orifice in the rod and larger orifices covered by shims in the piston. The shims act as a spring and can be preloaded to prevent flow at low velocities. Since fluid is flowing from the compression to the rebound chamber, the pressure in the compression chamber must be greater than the pressure in the rebound chamber. This pressure differential acting on the piston generates damping force.

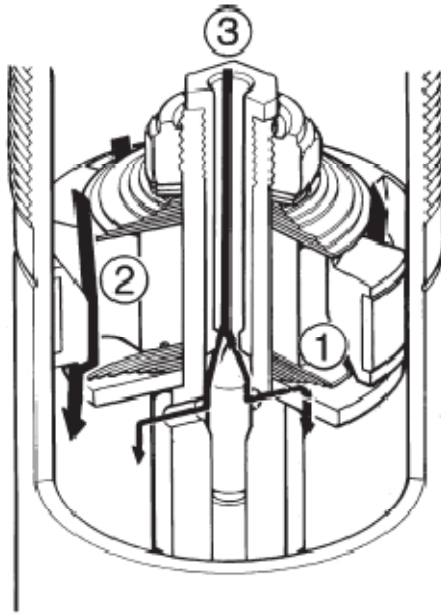


Figure 2.10: Flow through Piston during Compression [10]

Only a small amount of fluid is allowed to flow through the bleed orifice, path 3.

The flow through the piston orifices is restricted by the shim stack in path 2. As the velocity of the damper increases the shim stacks deflect more allowing more flow through path 2. No fluid flows through path 1 during compression. The shim stack on the rebound side of the piston acts as a check valve to prevent this flow. A very small amount of fluid will also leak around the piston through the piston seal from the compression to the rebound chamber. Since the rod is being inserted into the damper, the gas chamber will be compressed and the pressure of both the gas and damper fluid will increase.

Figure 2.11, on the next page, shows the same valve and orifice configuration except that the damper is extending. The flow through the bleed orifice, path 3, has reversed. The flow through the piston orifices is now path 1. Similarly to path 1 in

compression no fluid flows through path 2 during rebound. The shim stack on the compression chamber side of the piston acts as a check valve to prevent this flow. Leakage around the piston will act in the opposite direction. The gas chamber will expand and the pressure will decrease.

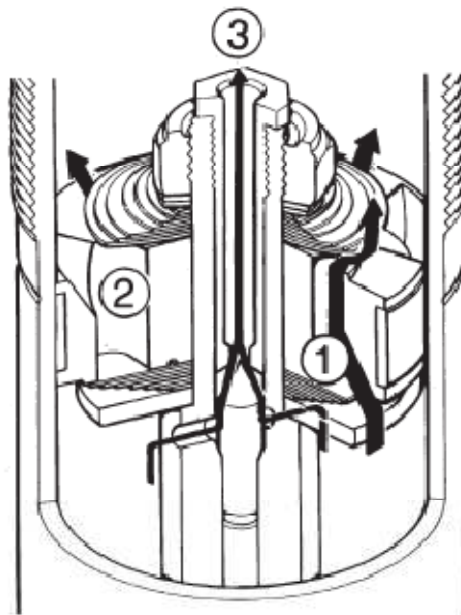


Figure 2.11: Flow through Piston during Extension [10]

The multiple flow paths in the dampers are used to give different characteristics depending on the velocity and direction of the damper. The bleed orifices primarily control the damping at low velocities, while the piston orifices and shim stack control the damping at high velocities. The damper is also able to give different characteristics for rebound or compression.

External adjustment of these characteristics is available in many dampers designed for motorsports applications. Because of the different flow paths the

adjustments can independently control certain characteristics of the damper. For example a 4-way adjustable damper will have separate low and high speed compression and rebound adjusters. Normally low speed adjustments will change the size of the bleed orifice. This is often achieved by a cone shaped needle in the orifice that can be adjusted in and out. High speed adjustment will normally change the preload on the shim stack. The piston that the shim stack sits on must be dished out to accommodate the deflection of the shim stack from the preload

There are many different varieties of monotube dampers but they all operate under the same principles. Some of these different varieties are shown below in Figure 2.12.

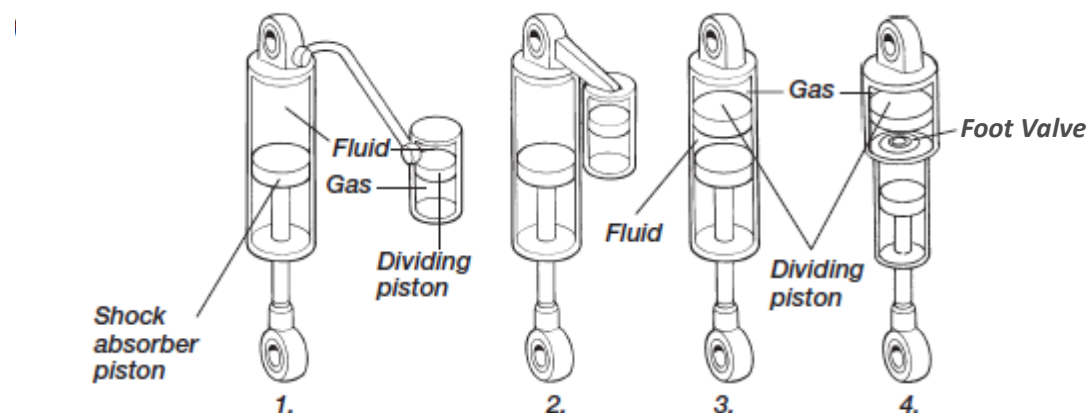


Figure 2.12: Monotube Damper Varieties [11]

The first two dampers have external reservoirs to house the floating gas piston. The primary reason for this is to make the damper more compact. The third damper is identical to the one described above. The fourth damper incorporates a foot valve into the

rebound chamber. This is a fixed valve that minimizes pressure changes in the gas chamber and increases the pressure in the compression and rebound chambers during compression to prevent cavitation. Often a foot valve is incorporated into the top of the external reservoirs. The foot valve allows for a convenient place for external adjustments.

## 2.2 Twin Tube Damper

Modern twin tube dampers produced for motorsports applications are not the same as traditional twin tube dampers. Traditional twin tube dampers are similar to a monotube damper with a foot valve as shown above. The difference is that the gas chamber and the chamber between the floating gas piston and the foot valve are located circumferentially around the damper body [9]. This is shown below in Figure 2.13.

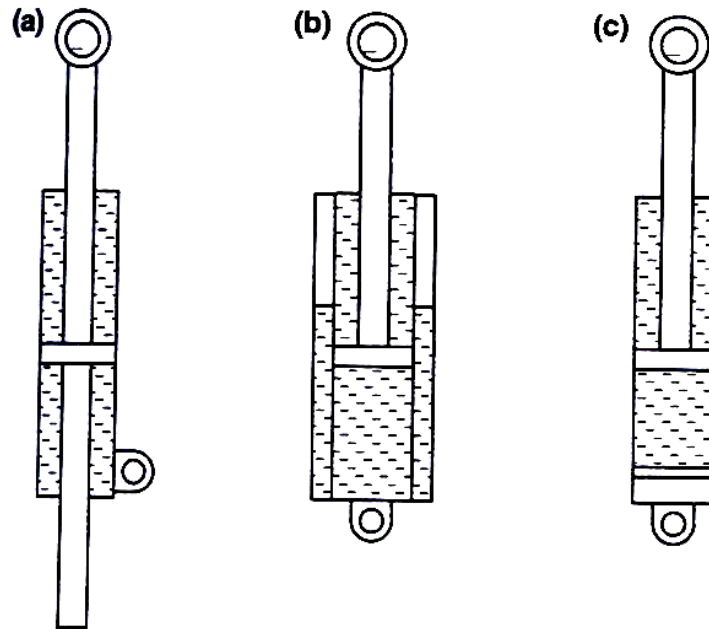


Figure 2.13: Twin Tube and Monotube Dampers [9]

Damper (c) is a regular monotube damper and damper (b) is a traditional twin tube damper. Damper (a) is a through rod monotube damper. Through rod dampers can be either of the twin tube or monotube variety. The main benefit of them is that the gas chamber is not necessary to compensate for the volume change caused by rod insertion. However, they generally still have a small gas chamber to compensate for the volume changes caused by temperature variations and damper compliance. Also the area of the compression and rebound side of the piston are equal. This eliminates the static force produced by the pressure of the gas chamber acting on unequal areas.

A modern twin tube damper uses the circumferential tube as an external passage for the damper fluid. This passage connects the rebound and compression chambers. The majority of these dampers have solid pistons without any orifices or valves. These pistons instead move through the fluid, forcing the fluid through the external passage. This is shown below in Figure 2.14. The orifices and shim stacks on the damper piston in the figure are to control extremely high velocity inputs and are not commonly used in motorsports applications.

As can be seen in the figure the orifices and valves are located in the external passages to provide the flow restrictions. These orifices and valves are similar to those located on a monotube damper piston. For control of the low speed damping a small bleed orifice with an adjustable needle is generally used. For control of high speed damping a shim stack, coil spring, or combination thereof along with a larger orifice is often used.

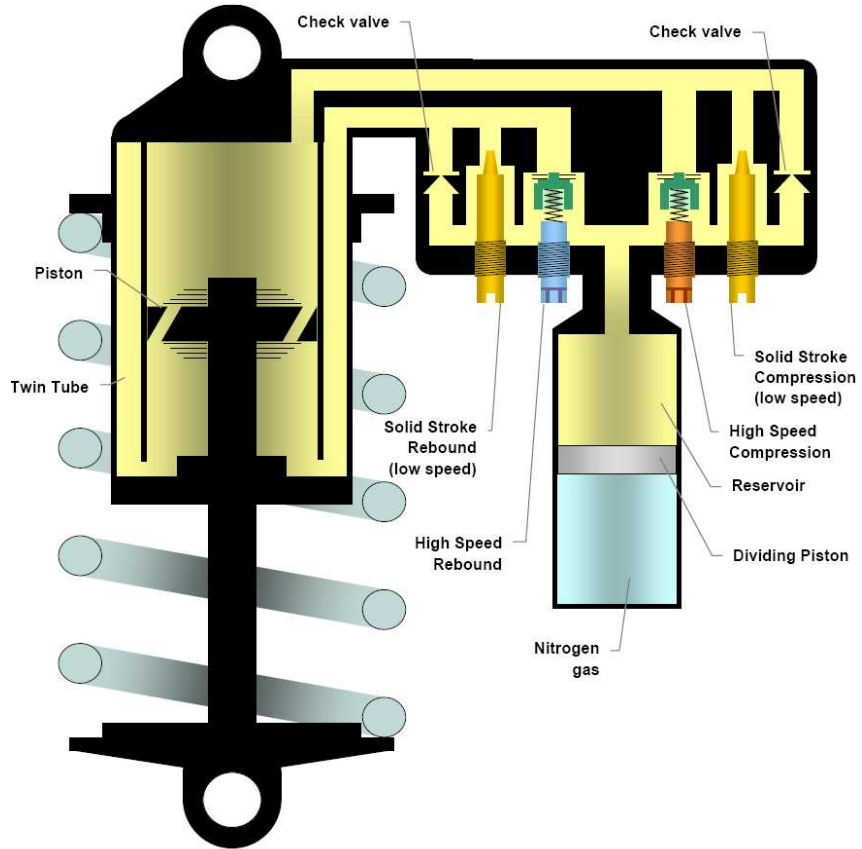


Figure 2.14: Modern Twin Tube Damper [12]

Figure 2.15, on the next page, shows the damper compressing at low speed. Fluid is flowing through the bleed orifice and needle valve only because of the preload on the high speed valve. Once the damper velocity is high enough the preload force will be overcome and fluid will flow through both orifices. The gas chamber is acting on the rebound chamber under these conditions. Therefore to generate damping force the pressure in the compression chamber must increase. This eliminates the risk of rebound chamber cavitation that is found in a monotube damper. However, local cavitation in areas of low pressure is still possible.

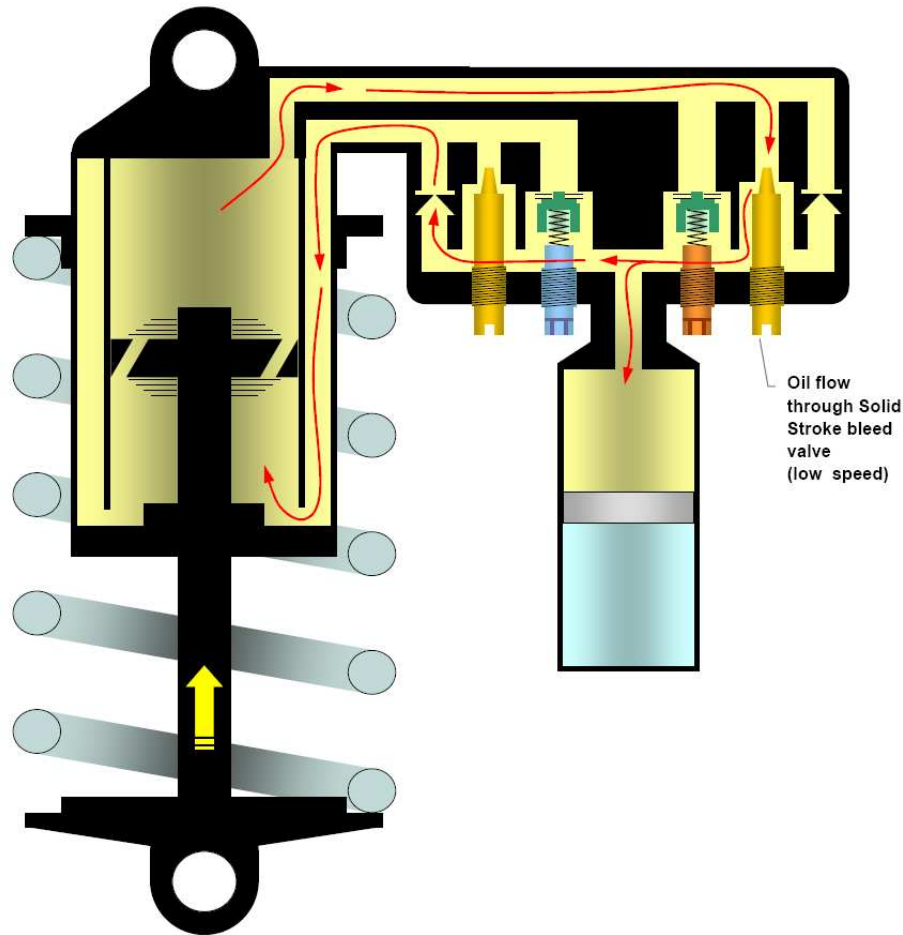


Figure 2.15: Modern Twin Tube Damper in Low Speed Compression [12]

In rebound the direction of flow is reversed. The check valve on the left will close and the fluid will flow through the valves on the left. Then it will exit through the check valve on the right. Therefore the gas chamber is now acting on the compression chamber like in a monotube damper. A small amount of fluid will also leak between the piston seals and the damper body.

Many aspects of the monotube damper and the modern twin tube damper are similar. The damping force is generated by restricting fluid flow through orifices and valves. A gas chamber is used to compensate for volume changes and prevent cavitation.

There are three main flow paths of the fluid; flow through the low speed bleed orifice, flow through the high speed orifice and valve, and leakage around the piston.

There are also major differences in the operation of these types of damper. The gas chamber pressure in the monotube damper always acts on the compression chamber. In the twin tube damper the gas chamber acts on different sides of the piston. This allows twin tube dampers to run much lower gas pressure without the risk of rebound chamber cavitation. The lower gas pressure decreases the stress on the damper and rod seal and reduces the gas spring effect of the damper [13]. The other major difference is that in the twin tube damper there is much more fluid flow as was mentioned previously.

Relationships defining the flow through the damper, the deflection of the valve springs, and the pressures will be developed for both styles of dampers. These relationships are the basis for the models developed and will also give further insight to the operation of the damper.

### **2.3 Damper Characterization**

Characterization of dampers is generally done through experimental testing. A damper dynamometer is used to perform this testing. Figure 2.16 shows a Roehrig Engineering 5VS damper dynamometer. This is a commercially available dynamometer that is used in many types of motorsports [14]. The damper is held securely at both ends and forced to compress and extend in a sinusoidal motion by a motor in the base of the dynamometer. The force outputted by the damper is measured throughout the testing.



Figure 2.16: Roehrig Engineering 5VS Damper Dynamometer [14]

The equations below give the resulting displacement, velocity, and acceleration of the damper during testing. The velocity and acceleration are the first and second derivatives of the displacement. As can be seen in these equations the motion profile is defined by the amplitude and frequency. Figure 2.17 shows the motion profile for a typical damper test with amplitude of .013 meters and a frequency of 1.6 hertz.

$$x(t) = Amp * \sin(2\pi ft) \quad (2.7)$$

$$\dot{x}(t) = (2\pi f)Amp * \cos(2\pi ft) \quad (2.8)$$

$$\ddot{x}(t) = (2\pi f)^2Amp * \sin(2\pi ft + \pi/2) \quad (2.9)$$

$$\ddot{x}(t) = -(2\pi f)^2Amp * \sin(2\pi ft) \quad (2.10)$$

$$\ddot{x}(t) = (2\pi f)^2Amp * \sin(2\pi ft + \pi) \quad (2.11)$$

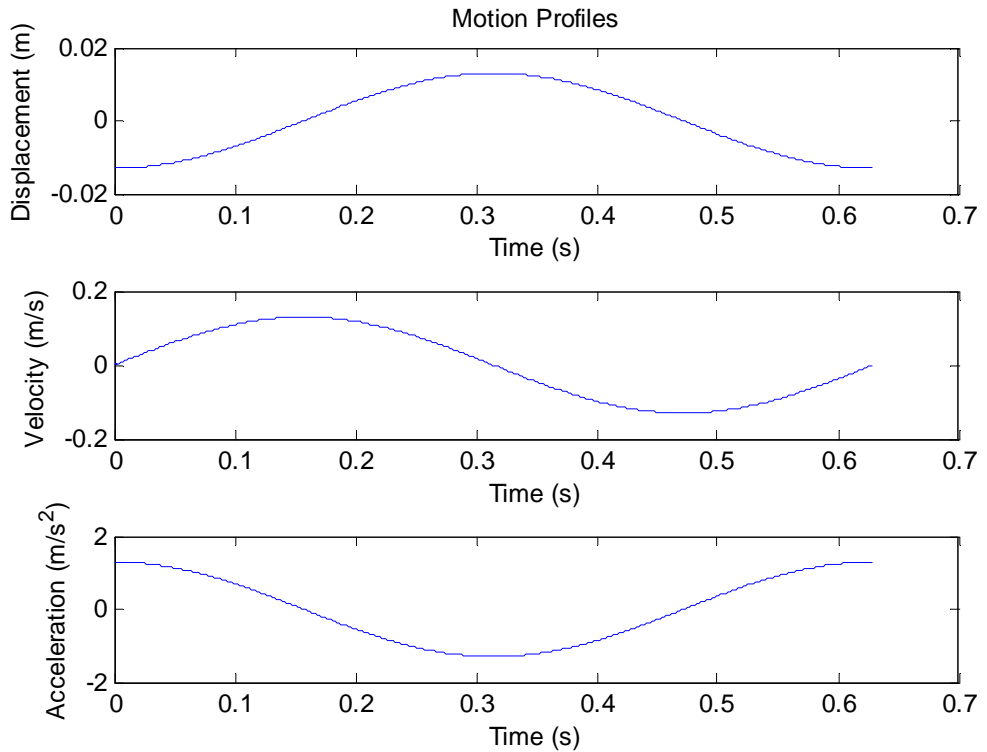


Figure 2.17: Damper Test Motion Profile

In the above equations  $Amp$  is the amplitude which is half of the stroke,  $f$  is the frequency, and  $t$  is the time. As can be seen in equations (2.8) and (2.9) the velocity is  $\pi/2$  radians out of phase with the displacement. Therefore the maximum velocity will occur one quarter of a revolution before the damper displacement reaches its maximum. In equations (2.10) and (2.11) the acceleration of the damper caused by the dynamometer increases as a function of the frequency squared. Therefore at a frequency of 1.6 Hz the max acceleration will be approximately 1.3 m/s compared to 5.2 m/s at 3.2 Hz. Therefore, significantly more hysteresis can be seen in the characteristic and work diagrams as the frequency is increased since it is strongly dependent on the acceleration of the damper. The maximum acceleration lags the displacement by  $\pi$  radians. Therefore

the peak acceleration will occur at one half of a revolution after the damper displacement reaches its maximum. The displacement, velocity, and acceleration are all directly proportional to the amplitude of the motion.

Throughout this motion the force exerted by the damper onto the dynamometer is recorded. From this the characteristic and work diagrams can be generated. A characteristic diagram is a plot of the damper force as a function of the velocity. A work diagram is a plot of the damper force as a function of the displacement. A characteristic diagram is the primary method for expressing the force of a damper, but a work diagram is used occasionally.

Two different styles of characteristic diagrams are shown in Figures 2.18 and 2.19. The velocity for the compression stroke is positive, while for the rebound stroke it is negative. Velocity is often expressed as an absolute value so that both ends of the plot are right of the y-axis. Forces produced under compression are considered positive while forces produced during rebound are considered negative. This sign convention is consistent throughout this work, but may be different in other literature.

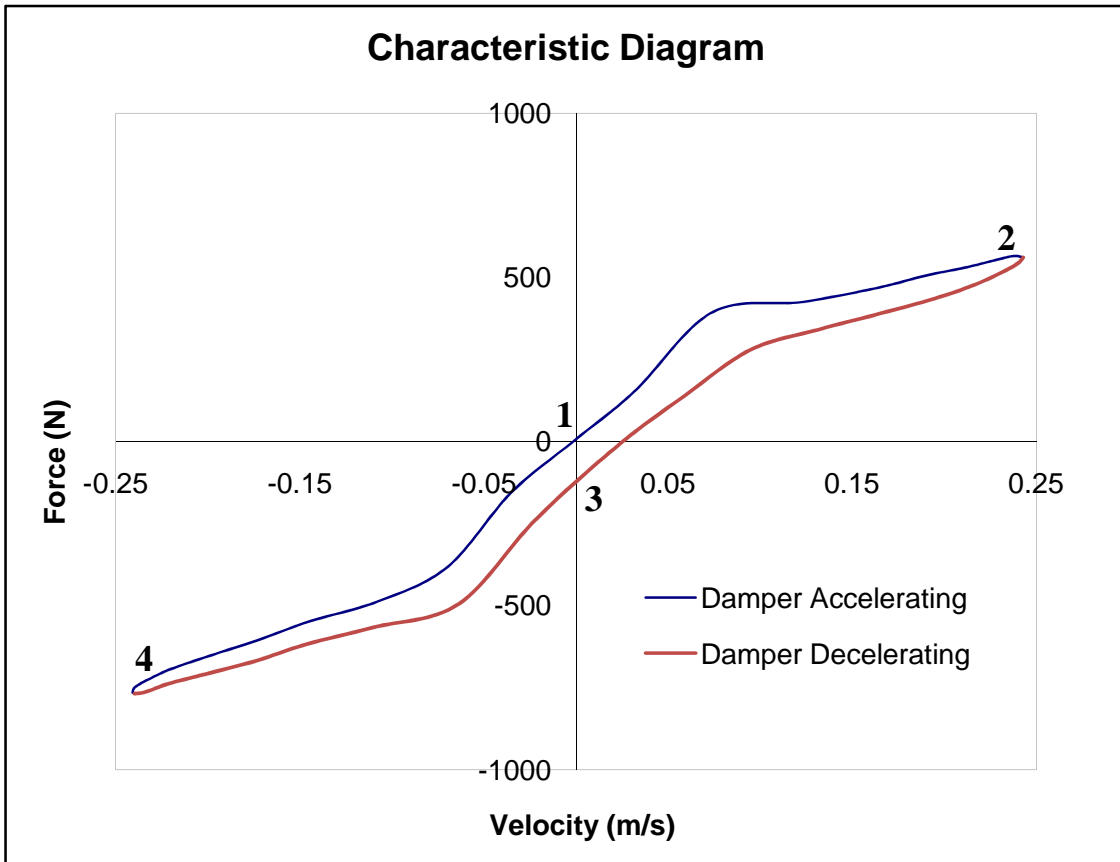


Figure 2.18: Continuous Velocity Characteristic Diagram

The plot in Figure 2.18 is a continuous velocity plot (CVP). Velocity and force are recorded throughout one whole cycle, and then all of the data is plotted. This plot is useful because it gives more detailed information about the damper force. At 1 in the figure the damper is at the beginning of the sine wave and is fully extended. Therefore it has zero velocity and the maximum positive acceleration it will achieve. In the figure from 1 to 2 the compression velocity of the damper is increasing and the acceleration is positive. At 2 the damper displacement is zero since it is at the middle of the stroke. T this point the maximum compression velocity occurs while the acceleration is zero. After

this point the damper begins to decelerate. From 2 to 3 the compression velocity is decreasing to zero velocity at point 3. At this point the damper is fully compressed and the maximum negative deceleration occurs. After point 3 the rebound stroke begins and from 3 to 4 the damper is decelerating until the maximum negative velocity is reached at 4. At this point the damper displacement is back to zero and the acceleration is also zero. Then the damper accelerates to full extension at point 1 to finish the cycle. The difference between the force generated when the damper is accelerating and decelerating is the hysteresis.

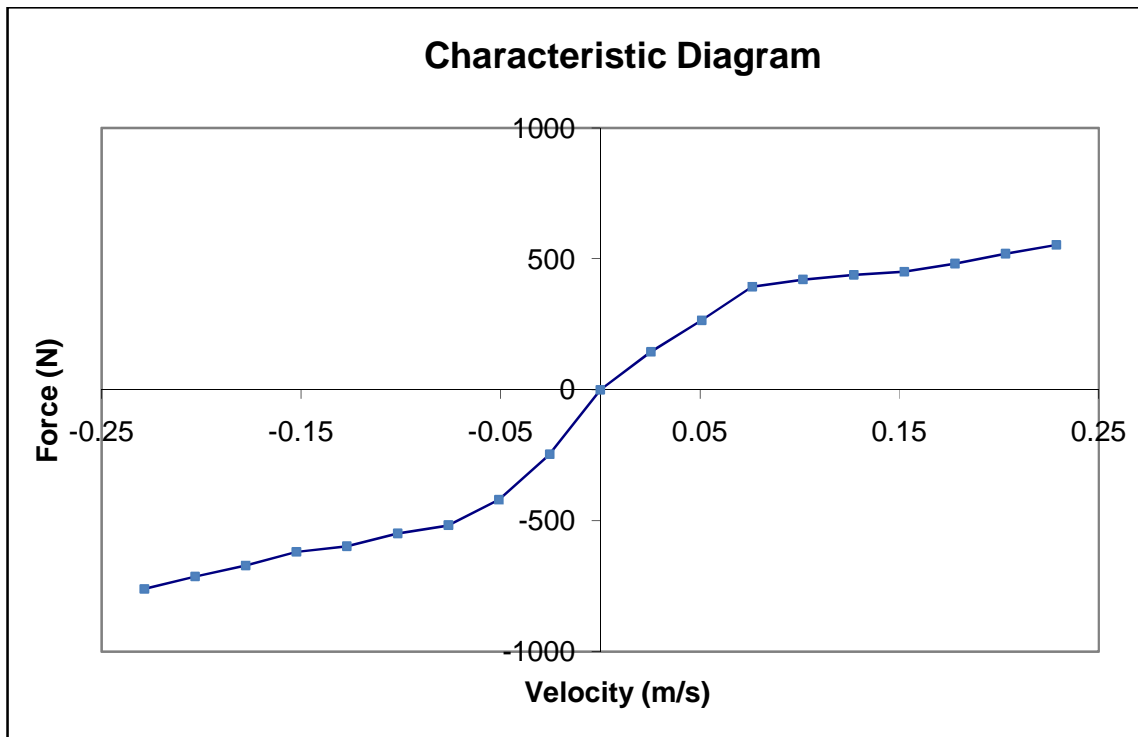


Figure 2.19: Peak Velocity Characteristic Diagram

The plot in Figure 2.19 is a peak velocity plot (PVP). When many different dampers or adjustments are being compared against each other a CVP becomes very

difficult to read. Therefore a PVP plot is often used. A PVP plot is generated by running tests at different frequencies or amplitudes to get different peak velocities. Then the force only at the peak velocities is used. The maximum force values from the multiple tests are plotted against their velocity. Then these points are connected to form the characteristic diagram. Therefore there will only be one line and the hysteresis will not be displayed.

The markers in the figure represent the points at which the data was collected.

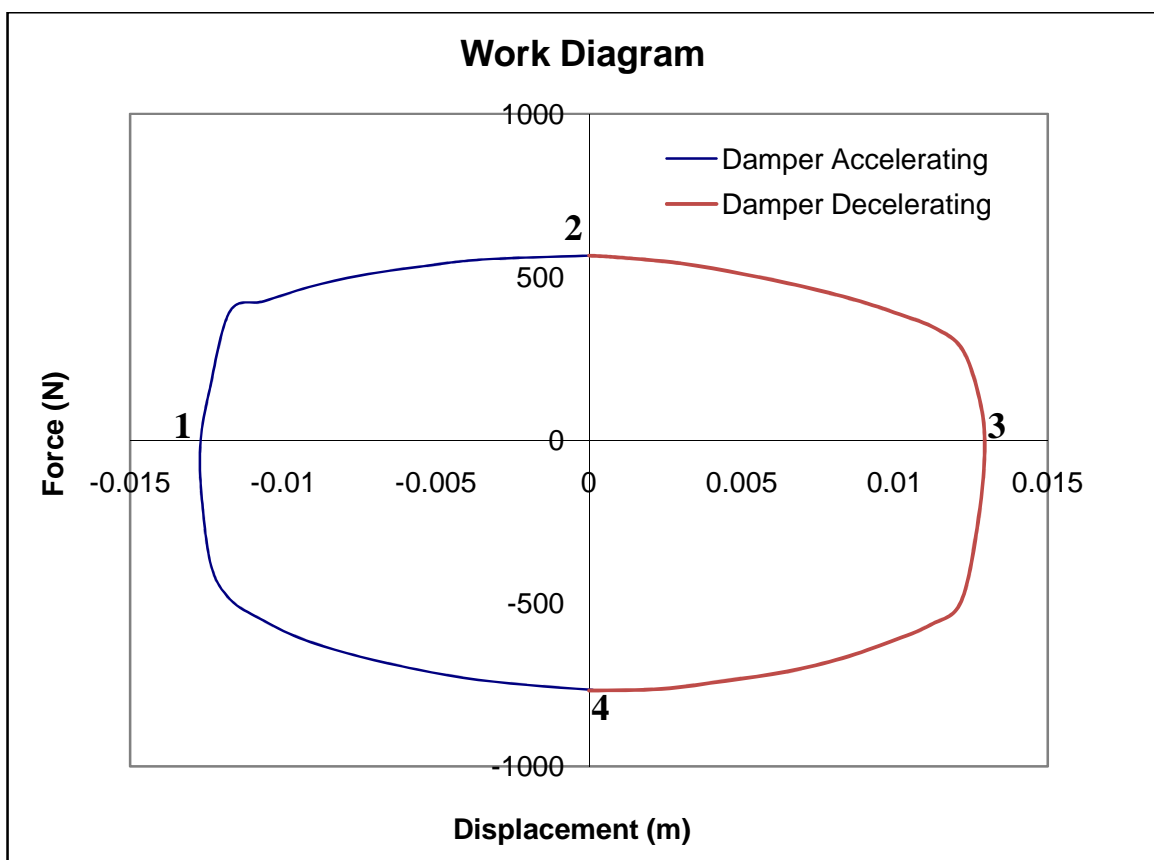


Figure 2.20: Work Diagram

Figure 2.20, above, displays a work diagram. The sign convention used for the force is positive in compression and negative in rebound. This style of plot is not as

useful as a characteristic diagram because the damper force is much more dependent on velocity than displacement. However, it is still used occasionally because it was the original style of displaying data when testing dampers. This originated when damper testing was performed with only mechanical equipment.

The numbers in the figure represent the same states as were described for the characteristic diagram in Figure 2.18. At point 1 the damper is fully extended and has zero velocity. The damper accelerates to point 2 where it reaches zero displacement and its maximum compression velocity. It then decelerates to point 3. At this point the damper is fully compressed and at zero velocity. It continues to decelerate to point 4 where it again reaches zero displacement but is at its maximum rebound velocity. It then accelerates to point 4 to complete the cycle. The lack of symmetry about the vertical axis is a result of the hysteresis in the damper.

### **3. LITERATURE REVIEW**

The improvement of ride and handling has always been one of the main focuses in automotive engineering. The development of automotive dampers began in the early 1900's and still continues today. In 1901 Horock was the first to patent an automotive damper. It was a telescopic hydraulic damper. However, until about 1925 most vehicles were either not equipped with dampers or came with dry friction dampers that used only coulomb friction to dissipate energy [9].

Since 1925 the telescopic, hydraulic damper as discussed in the section 2.2 has become almost universally used throughout the automotive industry. Also at this time the first papers addressing dampers were published. These publications focused on the different types of dampers available at the time and used work diagrams to characterize the dampers [9]. In 1958 Hoffmann published some of the first analytical work on dampers. He predicted that for the damper he was working on that the force was solely dependent on the piston velocity. He contributed the difference between the predicted and experimental values to hysteresis due to rubber mounts, the pressure required to open the check valves, the delay for the check valves to close, and the cavitation of the fluid [9, 15].

The earliest and still one of the most comprehensive papers on damper modeling was that of Segel and Lang published in 1981 [15]. This work was based on Lang's Ph.D.

dissertation from 1977 [16]. In this dissertation an 82 parameter analogue computer model of a conventional twin tube damper was developed. The main goals of the model were to characterize the damper forces in the frequency range of 1 to 10 Hz and explain the frequency dependence of these forces [15, 16].

The model examined the physical effects of the fluid and valves interaction to determine the forces produced by the damper. The chamber pressures and the fluid flow based on pressure differentials were modeled analytically. The forces on the valves were determined experimentally. It also included the compressibility of the damper fluid and the compliance of the damper body to examine the resulting hysteresis from these effects [15, 16].

In this model an attempt was made to relate the discharge coefficient to the velocity and acceleration of the fluid. Therefore, the steady state discharge coefficient, which is a function of the Reynolds number and the diameter to length ratio, was replaced with a dynamic discharge coefficient for flow through an orifice. This coefficient is a function of the acceleration number, Reynolds number, Cauchy number, and diameter to length ratio. The dynamic discharge coefficients were determined experimentally to improve the analytical model of the fluid flow [16].

The model was validated with experimental testing of the damper. After the validation, parameter studies exploring the effects of fluid compressibility, fluid vapor pressure, input frequency, and temperature were performed. However, since the model was executed on an analog computer and the average run time was seven hours the usefulness of the model was limited [16].

Understanding the shortcomings of the particular damper being tested, Lang suggested separation of the gas and fluid as well as pressurization of the gas chamber to minimize cavitation. These principles are now used in all modern high performance dampers. Lang also suggested a through rod damper to completely eliminate the need for a gas chamber.

Reybrouck developed a parametric model of a monotube damper [17]. However, empirical relations were used to model flow restrictions and determine the total damping force. These empirical relations were based on physical characteristics of the damper but still had to be determined experimentally. Therefore implementation of this model would be very difficult. This model compared very accurately to experimental testing over a wide frequency range.

Later this model was developed further for a conventional twin tube damper and included fluid compressibility and compressibility of gas entrained in the fluid [18]. This resulted in a model showing significant hysteresis.

Audendino and Belingardi developed a model for a conventional twin tube motorcycle damper [19]. The effect of various damper properties on the accuracy of the model was investigated. It was determined that modeling fluid compressibility and entrained air in the fluid was very important when investigating hysteresis. Fluid and valve inertia were found to be negligible to the results of the model. Also friction was found to be a secondary effect and could be neglected without significant error. However if it was to be included a more complex model then pure coulomb friction would be required to improve the results. This is especially important at low velocity and force output.

Mollica and Youcef-Tuomi presented a very comprehensive monotube damper model [20]. This was based on Mollica's M.S. thesis [21]. It looked in detail into the causes of hysteresis in characteristic diagrams. It was found that fluid compressibility, gas chamber compressibility, and resistive fluid damping through piston orifices contributed to hysteresis in the characteristic diagram. Minimizing air entrained in the damper fluid can also have a significant effect on the hysteresis, because it contributes to the compressibility of the fluid.

Also the friction of the floating piston and the compliance due to the piston valve preloads contributed to hysteresis near zero velocity. The compliance due to the piston valve preloads was caused because the specific damper modeled did not have bleed orifices. So at low speed before the pressure on piston valve overcame the preload force the only flow path for the fluid is leakage around the piston.

It was also found that fluid inertia and gas piston inertia were both negligible. As mentioned previously the gas piston friction was much more significant. The fluid inertia was negligible because the amount of fluid being accelerated at any given time is equal to the volume of the piston orifices. This volume is generally very small and thus has little mass. It was also determined that laminar flow through orifices only occurs at very low velocities. Assuming turbulent flow and constant discharge coefficients when modeling orifice flow gave accurate results.

Talbot and Starkey an experimentally validated damper model for a high performance Ohlin's NASCAR damper [1]. This paper, published by the Society of Automotive Engineers (SAE), was based on Talbot's M.S. thesis. One of the main goals

of this model was to develop a physical model that applied to all dampers of similar style. Therefore the use of empirical or experimental factors had to be minimized.

Similarly to Lang flow resistance through the piston orifice, bleed orifice, and piston valve were calculated from the pressure drop across the orifices. The pressure in the gas chamber and compression chamber were also related. The result was a parametric physical model similar to that done by Lang, but applied to a high performance monotube damper. However the fluid was assumed to be incompressible, thus the model did not accurately predict hysteresis.

One of the most significant parts of this work though was the modeling of the shim stack. An analytical model was developed to predict the stiffness of the shim stack. It used equations for bending of uniform thickness circular plates and superposition. The stiffness could be determined for stacks of 3 to 10 shims of different thicknesses and diameters.

The dynamic discharge coefficients and the damper friction were determined through testing of the damper on a standard damper dynamometer. The model showed good correlation to experimental testing especially at high velocities where hysteresis was less significant.

Parametric studies on the shim stack stiffness, piston orifice area, bleed orifice area, and shim stack preload were also performed. These studies provided insight to how the damper worked. They also provide guidelines for tuning the damper to achieve desired characteristics.

Rhoades developed a model similar to Talbot's for a Tanner damper [2]. This damper is the same type as that modeled by Talbot but is significantly smaller. The other

significant difference between these models is that Rhoades used Finite Element Analysis (FEA) to determine the shim stack stiffness. This was necessitated by the fact that the shims had holes in them to allow fluid flow through the piston. It was determined that these holes only had a small effect on the stiffness.

This model also accurately predicted the performance of the damper, since the hysteresis of the damper was relatively small. Additional parameter studies were also performed to examine the affects of the bleed orifice or low speed adjustment, the fluid density, and the number of piston orifices. The effect of the damper body compliance was also found to be negligible in comparison to the fluid compressibility.

*The Shock Absorber Handbook* by Dixon is the only book devoted to dampers in the English language [9]. While it does not provide a direct damper model, it does contain information regarding fluid dynamics, valve modeling, and flow paths in the damper that are very valid and could be applied to a damper model. It also covers many aspects in the design, testing, and specification of dampers.

The fundamental principles and findings from the research presented will be applied to develop a mathematical model of a modern twin tube damper. Specifically the fluid dynamic relationships developed in Lang's Ph.D. dissertation and Talbot and Starkey's SAE paper will be used in the development of the monotube damper model. These relationships will then be adapted to represent the physical operation of a modern twin tube damper. Dixon's *The Shock Absorber Handbook* also provides fluid dynamic principles and other relationships necessary to describe the moonotube and twin tube damper.

The findings in some of the other research will also be used. In Audendino and Belingardi's paper and Mollica's thesis it was found that effect of fluid inertia was negligible for a monotube damper [19, 21]. This effect will be adapted to and reexamined with the twin tube damper model. The damper body compliance and valve inertia will be assumed to be negligible for both models based on the findings of Rhoades and Mollica, respectively [2, 21]. Constant discharge coefficients will be used since this was found to be accurate in the research of Talbot and Starkey, Rhoades, and Lang [1, 2, 16].

A similar methodology and solution method to that used by Talbot and Starkey will be used to develop and solve the twin tube damper model. Through this previous research it is possible to accurately model and evaluate the performance of a modern twin tube damper. The characteristic of monotube and twin tube dampers will be compared and the effect of fluid inertia and viscous effects will be examined.

## **4. MODEL DEVELOPMENT**

An explanation of the static forces present in a damper is first presented to improve the understanding of the operation of dampers. Next, development of the model for a monotube damper is explained in detail. This is followed by the adaptation of this model to represent a modern twin tube damper. Then the effects of fluid inertia are modeled in this section. A detailed description of the solution method and execution of the model follows. Finally the spring mass damper model used to analyze the affects of the damper characteristics on the vehicle is described.

### **4.1 Static Damper Properties**

Figure 4.1 below shows the layout for a very basic damper. However this damper has a major problem. Since the damper fluid is practically incompressible the rod and piston cannot move into or out of the damper body. Any insertion or extraction of the rod is impossible because it would cause the volume of fluid required in the damper to change. Therefore a compressible gas is used to compensate for this change of volume. Emulsification of the gas and damper fluid must be prevented to get consistent performance and avoid cavitation. Therefore the gas and damper fluid are normally separated by a floating piston.

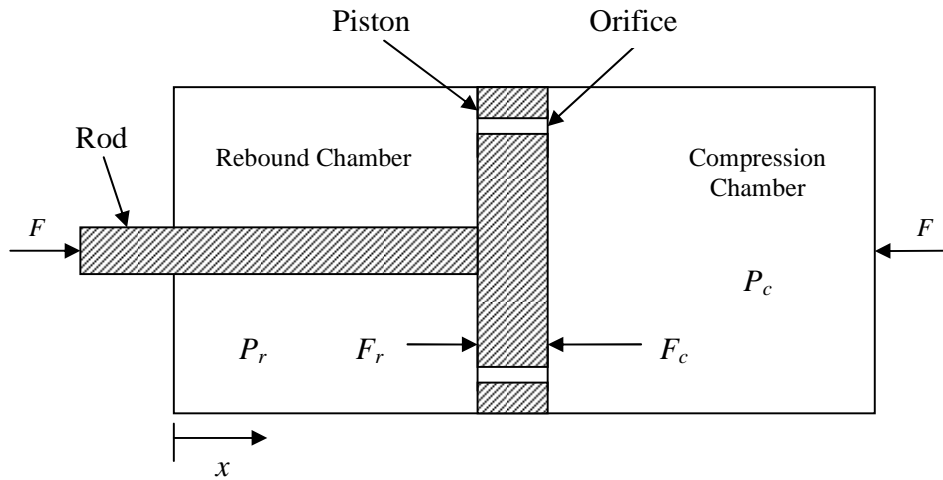


Figure 4.1: Damper at Static State

Figure 4.2, below, shows a similar damper but now a gas chamber filled with pressurized nitrogen is included. The floating piston separates the damper fluid and nitrogen. Now when the rod is inserted or extracted from the damper the compressible gas chamber will accommodate the volume change.

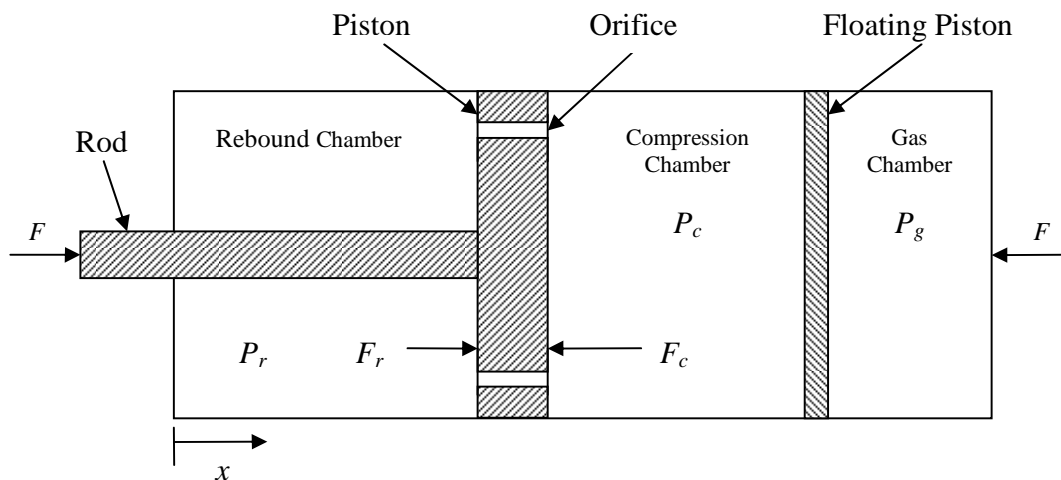


Figure 4.2: Damper with Gas Chamber at Static State

At static conditions a damper as shown in Figure 4.2 will output a force, even though dampers are primarily velocity sensitive.  $P_c$ , the compression chamber pressure, will be the same as  $P_g$ , the gas chamber pressure because they are connected by a floating piston. Since the damper is static there is no flow through the orifices. Therefore  $P_r$ , the rebound chamber pressure is equal to the compression chamber pressure. However  $A_c$ , the area on the compression chamber side of the piston is larger than  $A_r$ , the area on rebound chamber side. Equation (4.1) shows the result of this. It sums the forces on the piston and rod under static conditions.

$$F_s = F_c - F_r = P_c A_c - P_r A_r = P_g * (A_c - A_r) \quad (4.1)$$

Also since  $A_{rod}$ , the area of the rod is equal to  $A_c$  minus  $A_r$  equation (4.1) becomes:

$$F_s = P_g A_{rod} \quad (4.2)$$

This force is often referred to as the static force or gas spring force. It acts the same as a static spring preload force. It will increase with an increase in gas chamber pressure or rod diameter. This force will also increase as the rod is inserted into the damper and the gas chamber is compressed [22]. This will act like a stiffness and will be position dependent. This will be looked at in more detail in the damper model.

## 4.2 Monotube Damper Model

The force generated by the damper is caused by the pressure and area difference across the piston. This pressure difference is generated by forcing the damper fluid to flow through the orifices and valves. A physical representation of a typical damper is shown in Figure 4.3. In this figure the damper is being compressed. Thus, fluid is flowing from the rebound chamber to the compression chamber. The compression valve is open

allowing fluid flow through the piston orifice. Fluid is also flowing through the bleed orifice and there is a small amount of leakage around the piston. Assuming that the damper fluid is incompressible the displacement of the floating gas piston ( $z$ ) is proportional to the rod displacement ( $x$ ). When the damper is in rebound the flows and the displacement of the gas piston will reverse. Therefore, the compression valve will close and the rebound valve will open.

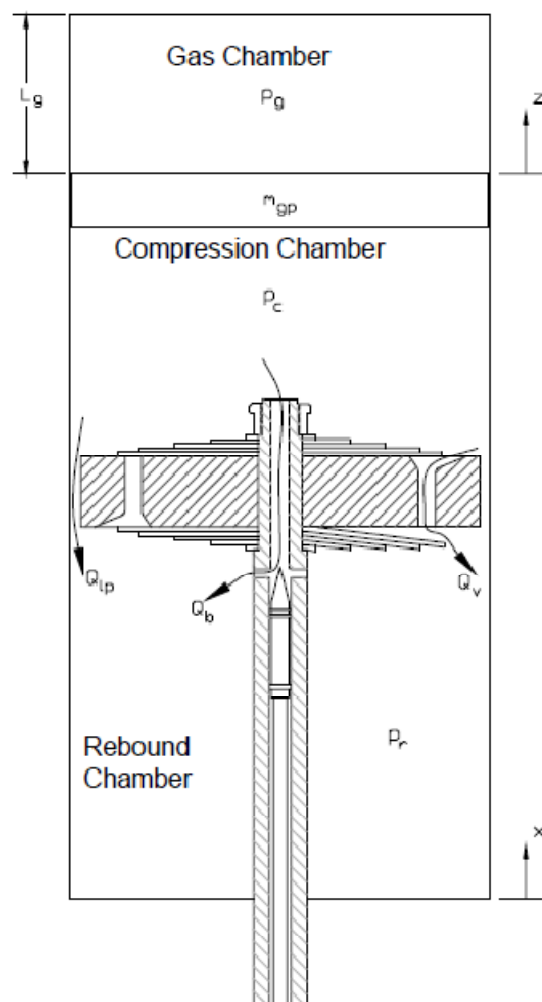


Figure 4.3: Damper during Compression [1]

The free body diagram in Figure 4.4 is used to determine the force on the piston. As can be seen the main forces on the piston are the pressure differences between the compression and rebound chambers and the friction force between the piston and the damper wall and between the rod and seal.

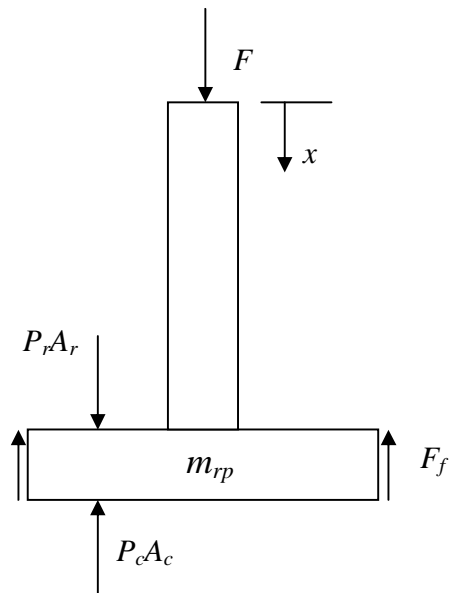


Figure 4.4: Piston and Rod Free Body Diagram

Equation (4.3) sums the forces on the damper piston. To solve this equation for  $F$ , the damper force, the pressures in the rebound and compression chambers must first be determined. This equation is similar to equation (4.1) but it also includes the friction of the piston and rod seal and the inertial force of the rod and piston.

$$F + P_r A_r - P_c A_c - F_f = m_{rp} \ddot{x} \quad (4.3)$$

Models of the fluid flow and flow resistance will be derived to determine the pressure in the rebound and compression chambers. The friction force can either be estimated or determined through experimental testing.

#### 4.2.1 Total Flow Rate

Conservation of mass requires that the fluid that flows out of the compression chamber is equal to the fluid that flows into the rebound chamber. Assuming the damper fluid is incompressible, the conservation of mass can be expressed by the flow rates. Thus, the total flow rate is the combination of the three separate flow channels through the piston. This can be seen in Figure 4.5.

$$Q_p = Q_v + Q_b + Q_{lp} \quad (4.4)$$

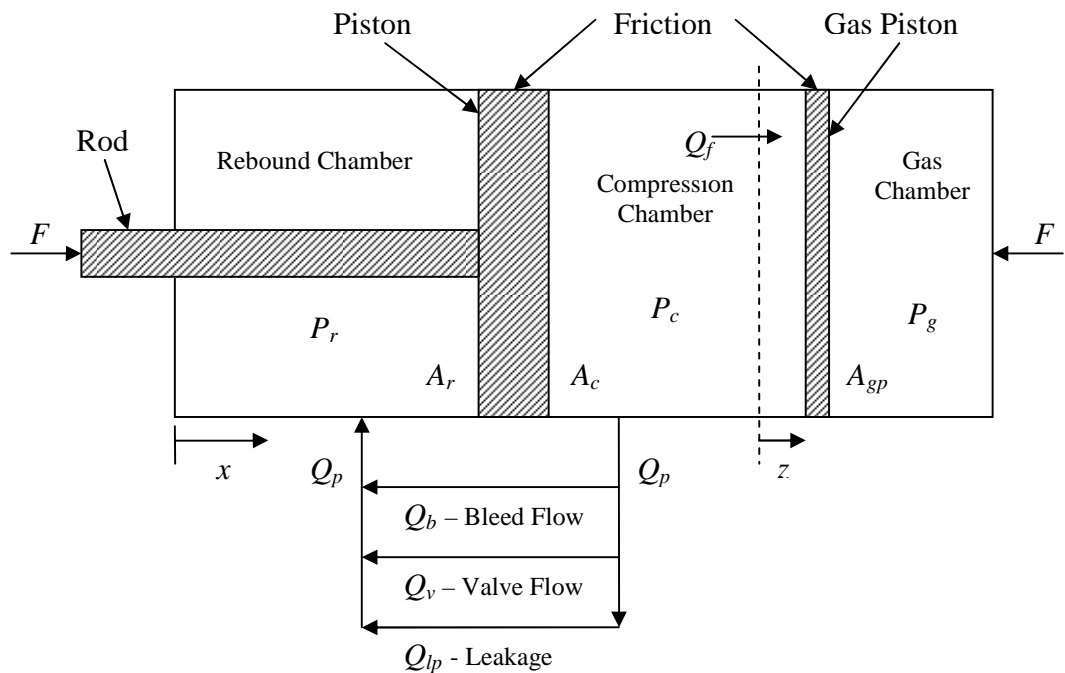


Figure 4.5: Compression Flow Diagram

Since the volume of the rod is entering the damper the gas piston is displaced. The boundary represented by the dotted line is the original position of the gas piston. Thus the flow rate,  $Q_f$ , across the boundary can be calculated.

$$Q_f = A_{rod} \dot{x} \quad (4.5)$$

Therefore the flow rate through the piston can be determined. It is the area of the rebound side of the piston times the velocity of the piston.

$$Q_p = A_r \dot{x} \quad (4.6)$$

Combining equations (4.4) and (4.6) gives a relationship between the velocity of the piston and the separate flow paths through the damper.

$$A_r \dot{x} = Q_v + Q_b + Q_{lp} \quad (4.7)$$

Equation (4.7) is the first of the system of equations that must solved to determine the damper force. Now equations for the separate flow rates need to be determined.

#### 4.2.2 Constant Area Orifice Flow

The volumetric flow rate of fluid through an orifice is given by equation (4.8).

$$Q = C_d A v_T \quad (4.8)$$

Where  $C_d$  is the steady state discharge coefficient and  $v_T$  is the theoretical fluid velocity. This coefficient is a function of the Reynolds number and the diameter to length ratio of the orifice [16]. It is the product of the area coefficient and the velocity coefficient.

As fluid flows through an orifice the flow stream will initially contract for approximately half of the diameter of the orifice and then expand again to the full area of the orifice. The point when the flow contraction is greatest is called the vena contracta.

The area coefficient is the cross sectional area of the vena contracta divided by the area of the orifice [9]. Theoretical and experimental results have shown that this coefficient is approximately .611 for sharp edged orifices at high Reynolds numbers [21]. For most damper orifices this value is slightly larger, between .7 and .8 [9]. The primary reason for this is that the orifice edges are usually chamfered or rounded to increase the area of the vena contracta. At smaller Reynolds numbers there is also a slight increase in the area of the vena contracta and subsequently the area coefficient. This is caused by the viscosity reducing the velocity of the fluid entering the orifice along the walls. This reduces the inward momentum of the fluid allowing a larger area of fluid flow.

$v_T$  is the theoretical fluid exit velocity. The actual speed is slightly less because of the viscous friction from the orifice walls and turbulence [9]. This is compensated for by the velocity coefficient which is the actual velocity divided by the theoretical velocity. This coefficient is usually assumed to be about .98 [21]. Thus, the area coefficient is the dominating factor in determining the discharge coefficient and the velocity coefficient is often treated as negligible.

The theoretical speed can be determined from Bernoulli's equation. It is assumed that the initial velocity,  $v_1$ , is equal to zero.

$$P_1 + \frac{1}{2}\rho v_1^2 = P_2 + \frac{1}{2}\rho v_2^2 \quad (4.9)$$

$$v_T = \sqrt{\frac{2(P_1 - P_2)}{\rho}} \quad (4.10)$$

Combining equations (4.7) and (4.9) gives an equation for the flow rate through an orifice as a function of the pressure differential between the entrance and exit.

$$Q = C_d A \sqrt{\frac{2\Delta P}{\rho}} \quad (4.11)$$

Lang modified this term by replacing the steady state discharge coefficient with a dynamic discharge coefficient,  $C_D$  [16]. This coefficient is a function of the fluid acceleration, Reynolds number, Cauchy number, and the orifice diameter to length ratio. This can then be applied to equation (4.11).

$$Q = C_D A \sqrt{\frac{2\Delta P}{\rho}} \quad (4.12)$$

It was found that the discharge coefficient was mainly a function of the Reynolds number and was slightly affected by the fluid acceleration [16]. However, Lang concluded that the “most significant departure from assuming a constant value of  $C_D$  occurs during flow at a low Reynolds number, and this condition occurs only during a small fraction of a cycle.” He experimentally determined the value of this coefficient.

Equation (4.12) is applicable for orifices with a length to diameter ratio up to at least 10, which makes it suitable for typical damper passages. It is also valid for turbulent or laminar fluid flow [9]. Therefore, it is can be used to determine the flow rate through both the piston and bleed orifices.

#### 4.2.3 Bleed Orifice Flow

From equation (4.12) the flow through the bleed orifice is determined. This is the second equation needed to determine the damper force.

$$Q_b = C_{Db} A_b \sqrt{\frac{2(P_c - P_r)}{\rho}} \quad (4.13)$$

$A_b$ , the area of the bleed orifice, is often externally adjustable on dampers. Thus this can be changed in the model to see how different adjustments would affect the dampers performance. The value for  $C_{Db}$ , the dynamic discharge coefficient of the bleed

orifice, was initially set to .7 according to experimental findings of Lang [16]. Talbot and Starkey experimentally found a larger coefficient of .68 for the rebound stroke than the coefficient of .61 for the compression stroke [1]. This was due to the fluid flowing in different directions through the bleed orifice and adjustable needle.

#### 4.2.4 Piston Orifice Flow

The flow through the piston valves is more complicated because it combines flow through an orifice as defined before and through the valve. These flow resistances act in series, thus they both have the same flow rate but each cause a pressure drop.  $P_v$  is the pressure as the result of the pressure drop over the orifice. This can be seen in Figure 4.6. Therefore this flow rate is determined in equation (4.14) from equation (4.12).

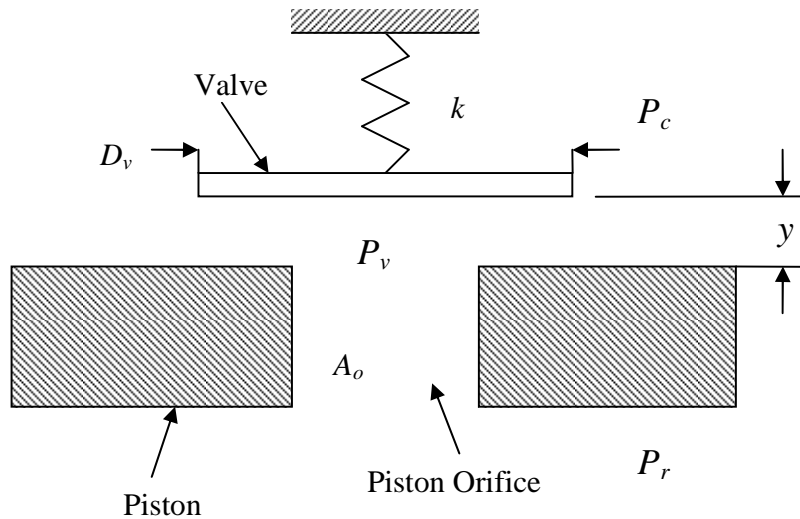


Figure 4.6: Piston Orifice and Valve

$$Q_v = C_{Do} A_o \sqrt{\frac{2(P_c - P_v)}{\rho}} \quad (4.14)$$

Unlike the bleed orifice the area of these orifices is not normally adjustable. Also  $C_{Do}$ , the dynamic discharge coefficient of the bleed orifice, is initially set to .7 according to Lang [16]. Talbot [1] and Rhoades [2] confirmed that this value correlated well with experimental data. This coefficient is generally more accurate than the one used for the bleed orifice because the geometry of the piston orifice is normally closer to the constant area assumed in equation (4.12).

In some dampers the piston orifice and bleed orifice act in series instead of in parallel. Therefore the flow rate through the piston orifice would be equal to the flow through both the valve and bleed orifice. This is expressed in equation (4.15). Depending on the layout of the damper either equation (4.14) or (4.15) is the third equation included in the system of equations.

$$Q_v + Q_b = C_{Do} A_o \sqrt{\frac{2(P_c - P_v)}{\rho}} \quad (4.15)$$

#### 4.2.5 Piston Valve Flow

For the flow through the valve the flow rate,  $Q_v$ , is the same but the pressure drop will now be  $P_v - P_c$ . Thus the total pressure drop over the piston orifice and valve will be  $P_r - P_c$ . However, this cannot be used as it was in the simpler orifice cases, because the flow contacts the valve and exits perpendicular to the initial flow. The area of the flow path also varies with the valve deflection ( $y$ ), which is an unknown.

$$A_{vf} = \alpha \pi D_v y \quad (4.16)$$

The circumference of the valve is  $\pi D_v$  and  $\alpha$  is the area flow correction factor. Therefore equation (4.12) and (4.16) are combined to determine the pressure differential

through the piston valve. Equation (4.17) is the fourth equation used to solve for the damper force.

$$Q_v = C_{Dv} \alpha \pi D_v y \sqrt{\frac{2(P_v - P_r)}{\rho}} \quad (4.17)$$

The area flow correction factor is used to adjust for valves where the whole shim stack does not deflect. Talbot used a value of .5 because the damper piston that he modeled had three equally spaced piston orifices for both the compression and rebound flow [1]. Damper pistons with differently sized or unequally spaced piston orifices might benefit from different area flow correction factors for the rebound and compression flow. Dampers with small shims that deflect all the way around their circumference would use a value of 1.

A free body diagram of the valve in Figure 4.7 shows the forces acting on the valve. The mass of the valve is assumed to be negligible.

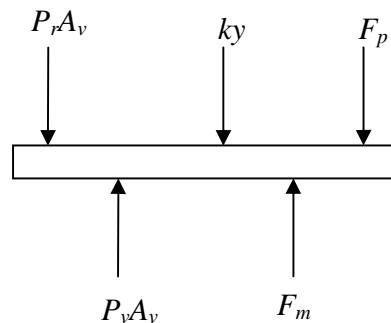


Figure 4.7: Valve Free Body Diagram

From summation of the forces in Figure 4.7 the deflection of the valve can be defined. However,  $k$ , the spring rate of the valve, must be determined either analytically or experimentally.

$$ky = (p_v - p_r)A_v + F_m - F_p \quad (4.18)$$

$A_v$  is the area on which the valve pressure acts. It is different from  $A_{vf}$  that was defined earlier.  $F_m$  is the force of the valve as a result of the momentum of the fluid having to change direction.  $F_p$  is the preload force on the valve. This force, if present, keeps the valve closed preventing flow through the piston until a certain pressure differential is reached. This preload is often adjustable externally on the damper.

The momentum force,  $F_m$ , is derived from conservation of momentum in the  $x$  direction. This assumes that all the flow exits perpendicular to the entrance flow.

$$F_m = \rho v_{x,in} Q_v - \rho v_{x,out} Q_{out} = \rho v_{x,in} Q_v \quad (4.19)$$

The velocity of the fluid entering the valve is related to the flow and the piston orifice area.

$$v_{x,in} = \frac{Q_v}{A_o} \quad (4.20)$$

Combining equations (4.19) and (4.20) gives the force from the change in fluid momentum.

$$F_m = \rho \frac{Q_v^2}{A_o} C_f \quad (4.21)$$

$C_f$  is the momentum force coefficient. This coefficient is used because the assumption that the flow exits perpendicular from the entrance is inaccurate. Lang determined this coefficient experimentally based on the predicted momentum force. A value of .3 for the coefficient correlated well to the experimental results [16]. Combining

equations (4.18) and (4.21) gives the total forces on the valve. This equation is also needed to solve for the damper force.

$$ky = (P_v - P_r)A_v + \rho \frac{Q_v^2}{A_o} C_f - F_p \quad (4.22)$$

#### 4.2.6 Leakage around the Piston

Leakage around the piston is a small contributor to the overall flow of the model. However, this is one of the few parameters that will affect the damper performance as a result of wear on the damper [16]. Therefore it will be modeled so that this affect can be explored with the model. The leakage is modeled by assuming laminar flow through parallel plates. This assumption can be used because the clearance between the cylinder wall and the piston should be very small (< .1 mm) compared to the length of the cylinder [23]. Also since this leakage is only a small portion of the total flow this assumption will not significantly affect the final results. The leakage flow can be derived from the Navier-Stokes equations which results in equation (4.23) [23].

$$\frac{Q}{L_c} = \frac{\Delta P b^3}{12\mu l} \quad (4.23)$$

$$\Delta P = P_c - P_r \quad (4.24)$$

As can be seen in Figure 4.8, the clearance between the cylinder and the piston is  $b$  and the length of the piston is  $l$ .  $L_c$  is approximated as the circumference of the leakage,  $\pi D_p$ . Combining equations (4.23) and (4.24) and substituting for  $L_c$  gives the flow caused by the pressure differential across the piston.

$$Q = \frac{(P_c - P_r)b^3}{12\mu l} \pi D_p \quad (4.25)$$

The velocity of the piston also causes additional leakage flow.

$$Q = \frac{\dot{x}b}{2}\pi D_p \quad (4.26)$$

Summing equations (4.25) and (4.26) gives the total leakage flow rate,  $Q_{lp}$ , between the piston and the cylinder wall.

$$Q_{lp} = \left( \frac{(P_c - P_r)b^3}{12\mu l} + \frac{\dot{x}b}{2} \right) \pi D_p \quad (4.27)$$

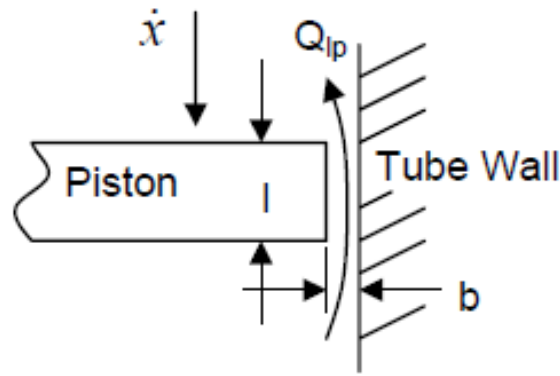


Figure 4.8: Piston Leakage [1]

#### 4.2.7 Gas Chamber Model

The gas chamber accounts for the volume change caused by the insertion of the rod. It also accounts for changes in volume of the fluid caused by the compressibility of the fluid, the compliance of the damper, and changes in temperature. However these effects are neglected in this model. Similar damper models have proven to still be accurate with these assumptions [1, 2]. This makes the gas piston displacement a function of the piston displacement.

Since it is assumed that the damper fluid and gas are maintained at a constant temperature the change in pressure of the gas chamber is inversely proportional to the change in volume.

$$\frac{P_2}{P_1} = \frac{V_1}{V_2} \quad (4.28)$$

The initial volume of the gas chamber is the area of the gas chamber times the length of the chamber. The final volume is that plus the change in volume.

$$V_1 = A_{gp}L_g \quad (4.29)$$

$$V_2 = V_1 + \Delta V = A_{gp}L_g + (-A_{rod})x \quad (4.30)$$

Using  $P_{gi}$  as the initial gas pressure and plugging equations (4.29) and (4.30) into (4.28) an expression for the gas pressure as a function of the rod displacement can be determined.

$$P_g = P_{gi} \frac{A_{gp}L_g}{A_{gp}L_g - A_{rod}x} \quad (4.31)$$

The forces on the gas piston are then summed from the free body diagram in Figure 4.9 in equation (4.32). The gas piston friction is neglected because it will be included in the total damper friction. This value will be experimentally measured.

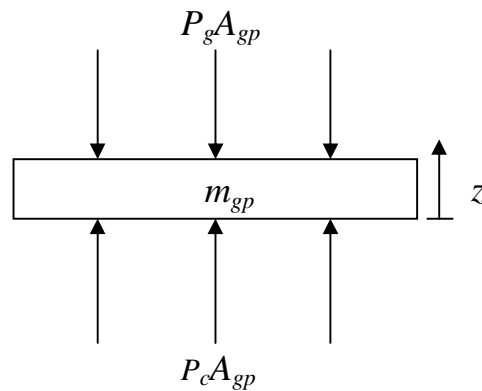


Figure 4.9: Gas Piston Free Body Diagram

$$(P_c - P_g)A_{gp} = m_{gp}\ddot{z} \quad (4.32)$$

The acceleration of the gas piston is also directly proportional to the acceleration of the rod.

$$\ddot{z} = \frac{A_{rod}}{A_{gp}}\ddot{x} \quad (4.33)$$

When equations (4.31), (4.32), and (4.33) are combined the compression chamber pressure can be determined. This is the final equation of the system of equations for the monotube damper model.

$$P_c = \frac{A_{rod}m_{gp}}{A_{gp}^2}\ddot{x} + P_{gi} \frac{A_{gp}L_g}{A_{gp}L_g - A_{rod}\dot{x}} \quad (4.34)$$

It shows that the compression chamber pressure is only a function of the piston position and acceleration. Therefore all of the velocity dependent forces produced by the damper must be generated by the pressure in the rebound chamber. Also the term in equation (4.34) that is dependent on acceleration is normally much smaller than the term dependent on the position, because the mass of the gas piston and the area of the rod are both small.

### 4.3 Twin Tube Damper Model

A modern twin tube damper is modeled using the same principles used for the monotube damper. The main physical difference between a modern twin tube damper and monotube damper is where the damping forces are generated. Damping forces are generated by fluid flow through the main piston in a monotube damper. In a modern twin

tube damper they are primarily generated by flow through the valving located externally of the main damper body.

Check valves are also used in conjunction with the valves so that the rebound and compression flow circuits are independent. This allows independent adjustment of both rebound and compression damping. Also, in a monotube damper the compression chamber pressure is nearly constant so the compression force has to be generated by a decrease in the pressure on the rebound side of the piston. This increases the chances of cavitation if the initial gas pressure is not sufficiently high. In a twin tube damper the check valves and independent circuits allow the gas chamber to act on the rebound or compression chamber depending on which direction the damper is moving. This causes the pressure to increase in the compression chamber during compression while the rebound chamber pressure is equal to the gas chamber pressure. In rebound the opposite is true. The rebound chamber pressure increases while the compression chamber pressure is equivalent to the gas chamber pressure. This greatly reduces the need for high gas pressure to avoid cavitation [13]. However, cavitation in local areas of low pressure is still possible.

A diagram of the flow of fluid through the damper is shown below in Figure 4.10. This diagram represents the damper undergoing compression. This damper has a solid main piston and a separate fixed valve in the external flow path to provide flow restrictions and allow adjustability. This external flow path is located concentrically around the damper body hence the name twin tube. Therefore all of the damper fluid except the very small amount that leaks past the main piston flows through the reservoir

chamber and the fixed valve. This enables the adjustments to be as effective as possible since they restrict the flow of practically all of the damper fluid.

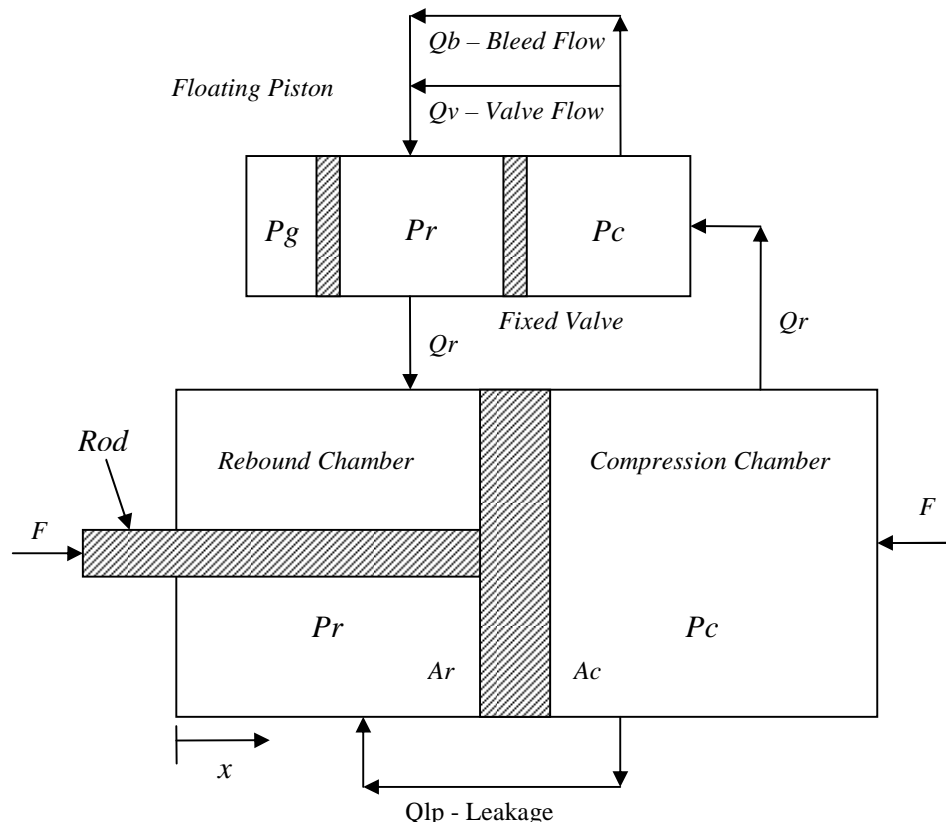


Figure 4.10: Modern Twin Tube Damper Compression Flow Diagram

Another diagram of the fluid flow through the damper is shown below in Figure 4.11. This diagram represents the damper rebounding. As can be seen from the figure the flow and force directions are reversed from Figure 4.10. Also the gas chamber is now acting on the compression chamber. This is achieved by the check valves and independent circuits in the damper.

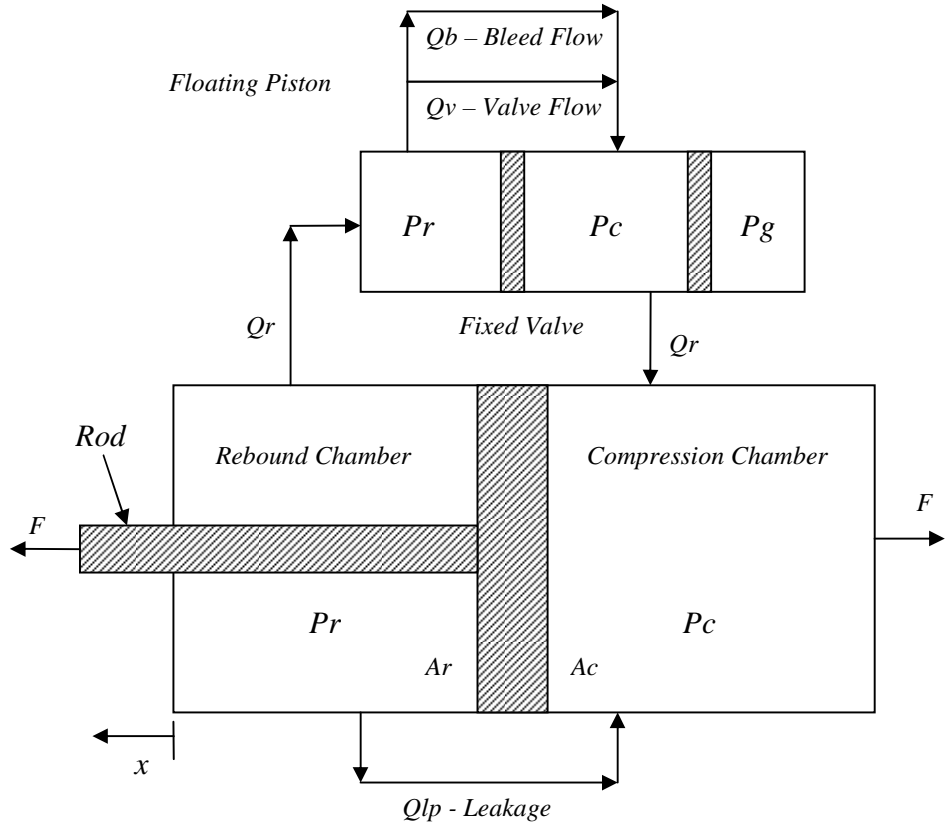


Figure 4.11: Modern Twin Tube Damper Rebound Flow Diagram

The model for this damper is surprisingly similar to the one for the monotube damper. The main difference is that the compression chamber pressure is only equal to the gas chamber pressure during rebound. In compression the rebound chamber pressure is equal to the gas pressure. These changes make equation (4.34), restated below, only valid for the rebound stroke. Equation (4.35) is then valid for the compression stroke.

$$P_c = \frac{A_{rod}m_{gp}}{A_{gp}^2} \ddot{x} + P_{gi} \frac{A_{gp}L_g}{A_{gp}L_g - A_{rod}x} \quad (4.34)$$

$$P_r = \frac{A_{rod}m_{gp}}{A_{gp}^2} \ddot{x} + P_{gi} \frac{A_{gp}L_g}{A_{gp}L_g - A_{rod}x} \quad (4.35)$$

Unlike the monotube damper model the rebound pressure is known during compression of the damper. The system of equations that are solved to determine the damper pressures will have to be altered to solve for the compression chamber pressure instead of the rebound chamber pressure during compression.

Since the damper valves operate under the same principles the other primary equations are not changed. However, since the fluid flow through the valve and bleed orifice go through the external valving and the leakage flow goes around the main piston care must be taken that the restrictions are modeled accordingly. Basically leakage is the same since it still occurs across the main piston but the flow through the bleed orifices and valves goes through the external valving.

#### **4.4 Fluid Inertia and Viscous Effects**

Damper fluid is accelerated through orifices and passages in a damper at high rates. The inertial force due to the acceleration of the fluid also contributes to a pressure drop. It has been shown by Audendino and Belingardi, and Mollica that the inertial forces of the fluid are negligible for a monotube damper and for a traditional twin tube damper [19, 21]. This is logical because even though the fluid may experience very large accelerations the volume of fluid in the orifices is very small. Subsequently the mass will also be very small. However, in a modern twin tube damper the mass of fluid being accelerated is significantly greater. Therefore the effect of the fluid inertia will be modeled.

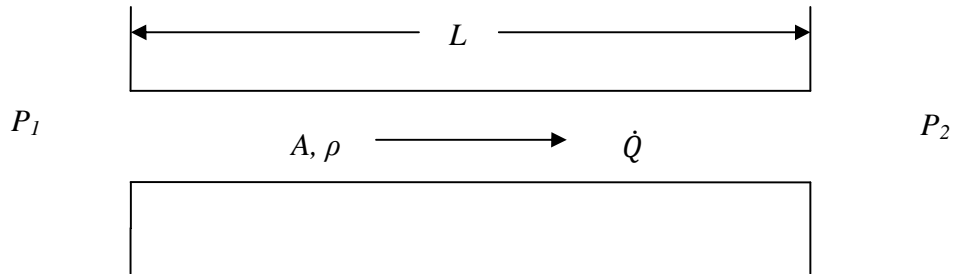


Figure 4.12: Fluid Inertia

A simple pipe with fluid accelerating through it is shown in Figure 4.12. The inertial force of the fluid is the product of its mass and acceleration. For the fluid the mass is equal to the product of the density,  $\rho$ , the cross sectional area of the pipe,  $A$ , and the length of the pipe,  $L$ . The volumetric flow acceleration,  $\dot{Q}$ , is the rate of change of the volumetric flow rate,  $Q$ . The fluid acceleration is equal to the volumetric flow acceleration divided by the area,  $A$ . This is shown in equation (4.36).

$$F = ma = \rho L A \frac{d}{dt} \frac{Q}{A} = \rho L \dot{Q} \quad (4.36)$$

$F$  is the force required to accelerate the fluid through the pipe. As can be seen the area of the pipe does not affect the force required to accelerate the fluid. Dividing equation (4.36) by the cross sectional area of the pipe the change in pressure required for the acceleration of the fluid can be determined.

$$\frac{F}{A} = P_2 - P_1 = \frac{\rho L}{A} \dot{Q} \quad (4.37)$$

This shows that when determining the change in pressure caused by the inertial force the effective “mass” of the fluid is equal to  $\frac{\rho L}{A}$  [24]. Therefore if fluid in a pipe with

a small area has the same volumetric flow acceleration as fluid in a pipe with a large area, the fluid in the small pipe will have more of an effect on the pressure drop in the system.

Applying this effect to the damper model requires careful treatment of the pressures and flow rates. Accurate modeling requires knowledge of the layout and direction of operation of the damper. A model of the damper under compression with the flow path immediately after the external valves will be described. For this case  $P_2$  is equal to the rebound chamber pressure,  $P_r$ , and  $P_1$  is equal to the pressure of the fluid immediately after it exits the valves. This will be referred to as  $P_t$ .

$Q$  is the sum of the flow rates through the bleed orifice and the piston valve,  $Q_v$  and  $Q_b$ . Since the damper model only solves for the volumetric flow rates, an approximation must be used to determine the volumetric flow acceleration. This is shown below in equation (4.38).

$$\dot{Q} = \frac{Q_i - Q_{i-1}}{t} \quad (4.38)$$

The solution method which will be discussed in more detail in section 4.6 determines all of the unknown pressures and flow rates at multiple time steps. The duration of each time step is  $t$ .  $Q_i$  is the flow rate at the current time step and therefore is the sum of  $Q_v$  and  $Q_b$  which are both unknowns solved by the model.  $Q_{i-1}$  is equal to the sum of the flow rates,  $Q_v$  and  $Q_b$ , of the previous time step and is therefore known. Since the time steps are typically very small this approximation is accurate. Combining this information with equations (4.37) and (4.38) an equation can be derived that expresses the current, unknown flow rates as a function of the pressure differential and the flow rates of the previous time step. This equation can be used in the damper model to examine the effects of the fluid inertia.

$$Q_v + Q_b = (P_t - P_r) \frac{At}{\rho L} + Q_{v(i-1)} + Q_{b(i-1)} \quad (4.39)$$

The viscous effects of the fluid flowing through the external damper passages can also be examined. These effects are caused by the shear force developed between the moving fluid and stationary wall. Fox, McDonald, and Pritchard give the equation for the flow rate as a function of the pressure differential for a circular pipe [23]. It is derived from the Hagen-Poiseuille equation. This equation is only valid for laminar flow, which is defined as having a Reynolds number less than 2300 [23]. The Reynolds number can be calculated from equation (4.41).

$$Q = \frac{\pi \Delta P D^4}{128 \mu L} \quad (4.40)$$

$$Re = \frac{\rho V D}{\mu} \quad (4.41)$$

In equation (4.40) and (4.41)  $D$  is the diameter of the pipe. However, in most dampers the passages are not circular. Therefore we must define the hydraulic diameter,  $D_H$  [9]. This acts as an effective diameter to be used in equations (4.40) and (4.41).

$$D_H = \frac{4A}{C_w} \quad (4.42)$$

$A$  is the cross sectional area of the fluid and  $C_w$  is the wetted circumference. For a modern twin tube damper with a circumferentially located passage the hydraulic diameter can be calculated as shown below in equation (4.43). In the following equation  $D_o$  is the outer diameter of the passage,  $D_i$  is the inner diameter, and  $b_t$  is the width of the gap between the two.

$$D_H = \frac{4A}{C_w} = \frac{(D_o^2 - D_i^2)}{D_o + D_i} = D_o - D_i = 2b_t \quad (4.43)$$

Now the diameter in equation (4.41) can be replaced by the hydraulic diameter to determine the flow rate.

$$Q = \frac{\pi \Delta P b_t^4}{8\mu L} \quad (4.44)$$

$$Q_v + Q_b = \frac{\pi(P_t - P_r)b_t^4}{8\mu L} \quad (4.45)$$

In equation (4.45) the flow rates and pressures are expressed as they were when the effects of fluid inertia were examined. This is suitable because both of these effects occur over the same section of the damper. Equation (4.45) can be individually added to the system of equations being solved or it can be combined with equation (4.39) and they can be solved simultaneously. Combining these equations first requires solving each equation for the pressure differential. Then the equations can be combined by adding the terms as shown in equation (4.46). Equation (4.47) is derived from this equation and put in the same format as the other equations used in the model.

$$(P_t - P_r) = \frac{(Q_v - Q_{v(i-1)}) + (Q_b - Q_{b(i-1)})}{(P_t - P_r) \frac{At}{\rho L}} + \frac{(Q_v + Q_b)}{\frac{\pi b_t^4}{8\mu L}} \quad (4.46)$$

$$Q_v + Q_b = \frac{(P_t - P_r) \left[ \frac{\pi b_t^4}{8\mu L} * \frac{At}{\rho L} \right] + (Q_{v(i-1)} + Q_{b(i-1)}) \left[ \frac{\pi b_t^4}{8\mu L} \right]}{\left[ \frac{\pi b_t^4}{8\mu L} + \frac{At}{\rho L} \right]} \quad (4.47)$$

## 4.5 Model Execution

First equations (4.6) and (4.34) are solved independently to determine the total flow rate and the compression chamber pressure. Then the system of equations (4.7), (4.13), (4.14) or (4.15), (4.17), (4.22) and (4.27) can be solved. Newton's method for solving nonlinear equations was used to solve the system iteratively. This method will be

covered in more detail in the next section. Six unknowns are solved for from the six equations mentioned previously:

1. Flow rate through the piston valve ( $Q_v$ )
2. Flow rate through the bleed orifice ( $Q_b$ )
3. Leakage past the piston ( $Q_{lp}$ )
4. Valve deflection ( $y$ )
5. Rebound chamber pressure ( $P_r$ )
6. Pressure in the valve ( $P_v$ ).

Solving this system of equations requires initial guesses of the unknown values so that initial calculation can be made. Then these equations are solved iteratively in one of two loops until the convergence criteria are satisfied. The first loop is for when the valve deflection is zero because of the preload on the valve spring or shim stack. Thus equations (4.14) or (4.15), (4.17), and (4.22) are equal to zero. However once the spring deflection becomes greater than zero an alternate loop with all six of the equations is used to solve for the unknowns. This process is then repeated for the rebound stroke of the damper. The force of the damper is solved for by equation (4.3).

If fluid inertia and viscous effects are to be included then equation (4.47) can be added to the system of equations along with the seventh unknown,  $P_t$ . Alternatively the effects of fluid inertia or viscous flow can be examined independently by adding equation (4.39) or (4.45), respectively, to the system of equations.  $P_t$  would still be the additional unknown but the pressure differential between  $P_t$  and  $P_r$  would only represent the pressure drop caused by the fluid inertia or the viscous effects.

This system of equations was solved over a complete sine wave of motion so that the rebound and compression stroke would be independently calculated. The sine wave is split into a user defined number of time steps. Each time step is solved individually and then the results are combined to show the characteristics of the damper over the whole cycle.

#### 4.6 Solution Method

Newton's iterative method of solving nonlinear equations was used to solve this system of equations because it always converges as long as the initial guess is close to the solution and it converges quadratically [25]. This ensures that the model will be reliable and will come to a solution quickly.

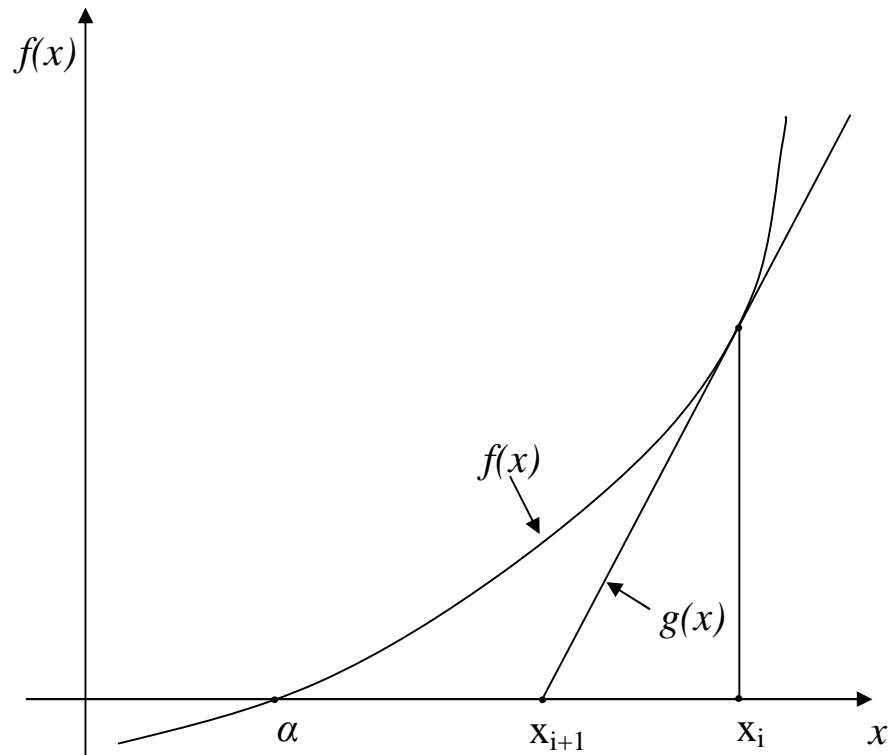


Figure 4.13: Newton's Method

This method, represented in figure 4.13, approximates the actual nonlinear function,  $f(x)$ , with the linear function,  $g(x)$ , which is tangent to  $f(x)$ . First  $g(x) = 0$  is computed where  $x_i$  is the initial guess. The solution to this,  $x_{i+1}$ , is then used to solve the system of equations. Then  $g(x)$  is recalculated for  $x_{i+1}$ . This is repeated through multiple iterations until  $g(x) = 0$  becomes close enough to the solution that the convergence criteria are satisfied. Equation (4.48), given by Hoffman [25], expresses this mathematically.

$$f'(x_i) = \text{Slope of } f(x) = \frac{f(\alpha) - f(x_i)}{x_{i+1} - x_i} \quad (4.48)$$

Equation (4.49) is then determined by solving for  $x_{i+1}$ .  $f(\alpha)$  is set to zero since the equations to be solved will also be set equal to zero.

$$x_{i+1} = x_i + \frac{-f(x_i)}{f'(x_i)} \quad (4.49)$$

This equation iterates until either one of the convergence criteria in equations (4.50) or (4.51) are satisfied. In these equations  $\epsilon$  and  $\delta$  are the user defined convergence criterion.

$$|x_{i+1} - x_i| \leq \epsilon \quad (4.50)$$

$$|f(x_{i+1}) - f(x_i)| \leq \delta \quad (4.51)$$

For a system of equations this method is the same except for  $x_i$  is a matrix of the initial values for the six or seven unknown variables and  $f(x_i)$  is a matrix of the solutions to the system of equations.  $f'(x)$  is the Jacobian matrix of the system of equations. The Jacobian matrix consists of the partial derivative of the equations being solved with respect to the unknown variable. Therefore  $x_{i+1}$  is a vector representing the new values for the original unknown variables. When the convergence criteria are met the

corresponding elements of  $x_{i+1}$  are saved as the solutions for that time step. Using these solutions as initial guesses for the next step the program begins to solve for the next set of unknowns.

## **5. EXPERIMENTAL PROCEDURE**

Experimental testing of the damper modeled was performed to verify the model. A damper dynamometer was used to collect force and displacement data on the damper modeled. The physical parameters of the damper were carefully measured. Specific tests were used to isolate certain parameters of the damper so that the accuracy of the model could be evaluated.

### **5.1 Experimental Apparatus**

The dynamometer used was an Instron 8501 servo-hydraulic dynamic testing machine. This is shown below in Figure 5.1. An Instron FastTrack 8800 controls the dynamometer. This is connected to a Labview interface in a computer so that the amplitude and frequency of the sine wave can be specified by the user. Other motion profiles can be executed by the dynamometer, but using a sine wave is the standard for damper testing.

The force produced by the damper is measured by a load cell and the displacement of the dynamometer by a linear variable differential transformer (LVDT). The computer collects this force and displacement data and then it is inputted into Excel for analysis. The velocity is calculated from the displacement and time data. Then characteristic and work diagrams can be created.



Figure 5.1: Instron 8501 Damper Dynamometer

As discussed in section 2.1 the displacement of the dynamometer can be calculated from the amplitude and frequency. Then the velocity and acceleration can be determined by taking the first and second derivatives of the displacement. These equations are restated on the next page.

$$x(t) = Amp * \sin(2\pi ft) \quad (5.1)$$

$$\dot{x}(t) = (2\pi f)Amp * \cos(2\pi ft) \quad (5.2)$$

$$\ddot{x}(t) = -(2\pi f)^2 Amp * \sin(2\pi ft) \quad (5.3)$$

Typical test values are .013 or .026 m for the amplitude and .8, 1.6, or 3.2 Hz for the frequency. These frequencies are often used because they convert to round radian frequencies of 5, 10, or 20 radians/s. Also sometimes the damper is tested at the sprung and unsprung frequencies of the vehicle it will be used on. Then the amplitude is determined from the maximum speed that the damper is required to be tested at. Typical maximum speeds that motorsports dampers are tested at are .13 and .26 m/s.

Plots of the displacement and velocity from the Instron dynamometer are shown below in Figures 5.2 and 5.3. This shows the damper being tested at frequencies of .8, 1.6, and 3.2 Hz with an amplitude of .013 m. The data was logged at 500 Hz.

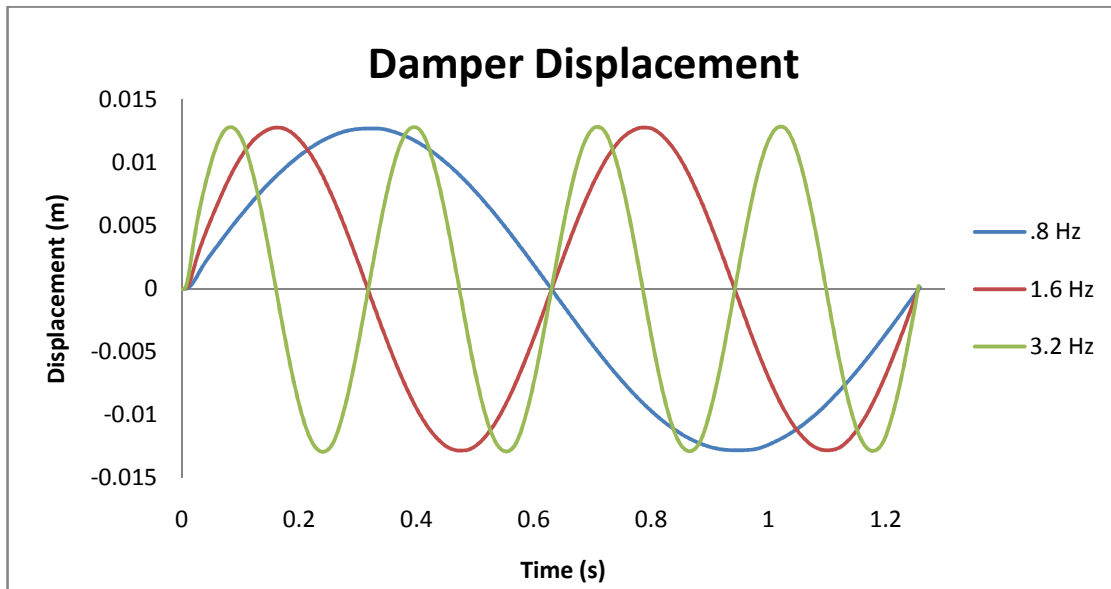


Figure 5.2: Damper Displacement

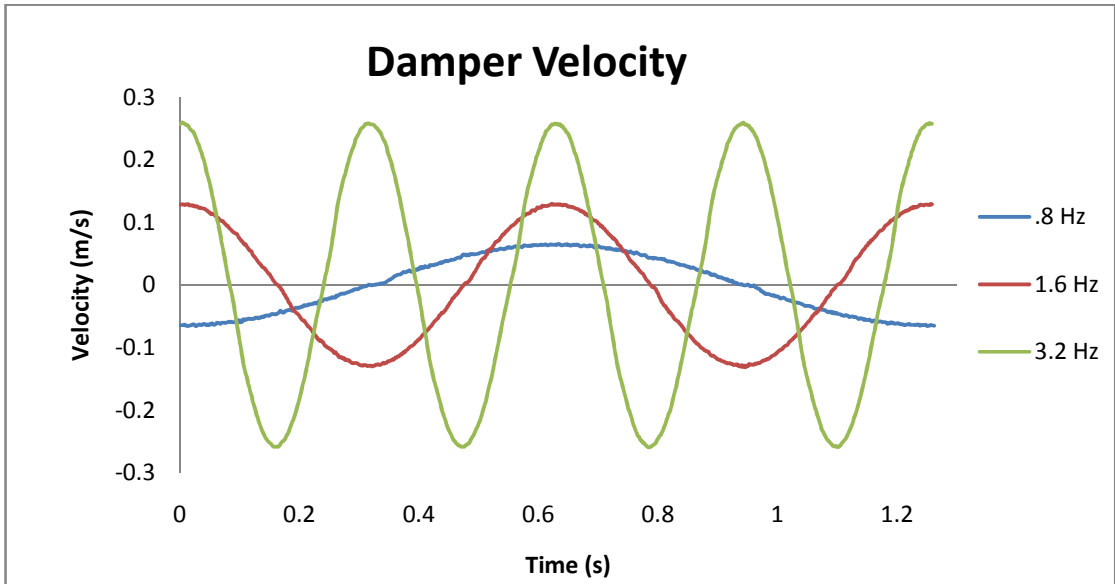


Figure 5.3: Damper Velocity

The energy and power dissipated by the damper throughout these tests can be calculated. The energy dissipated per cycle is given below in equation (5.4) and the mean power dissipation is given in equation (5.5) [9]. The damping coefficient is represented as  $c$  and the maximum damper velocity is  $\dot{x}_{max}$ .

$$E = 2\pi^2(Amp)^2 * cf \quad (5.4)$$

$$P = 2\pi^2(Amp)^2 * cf^2 = \frac{1}{2}c * (\dot{x}_{max})^2 \quad (5.5)$$

## 5.2 Damper Parameters

The damper that has been modeled and tested is the Cane Creek Double Barrel damper. This damper was originally designed as a bicycle damper, but was revalved to meet the needs of a Formula SAE car. This damper was chosen because it uses the Ohlins Twin Tube technology. This technology is also used in Ohlins top of the line

dampers, including the TTX40 which has been successfully used in the Indy Racing League and the Champ Car World Series.

In Figure 5.4 the Cane Creek Double Barrel damper can be seen. This is a very compact damper. The outer diameter of the main cylinder is approximately 30 mm and the rod diameter is 8 mm. The fully extended length of the damper is 200 mm and it has a total stroke of 57 mm. The main piston is 25 mm in diameter and has no orifices or valves. It is solely used to force damper fluid through the external valves so that the adjustments have as much effect as possible [26].



Figure 5.4: Cane Creek Double Barrel Damper

The valves and adjusters are located where “CANE CREEK” is printed on the damper. The main cylinder houses the damper piston and an internal cylinder to create a flow path from the rebound and compression chamber to the external valving. The

cylinder at the top houses the gas chamber and floating piston. It also includes the valving and adjusters.

A close up of the adjusters is shown in Figure 5.5. The adjusters on the left control the compression force and those on the right control the rebound force. Turning the adjusters clockwise restricts makes the damper stiffer. The smaller slotted adjusters are used to control the force at low speeds. They change the size of the bleed orifice by moving a small angled needle into or out of the orifice as they are turned. They each have 24 clicks of adjustment. Each click is one-sixth of a revolution. The larger hexagonal adjusters affect the force of the damper at high speeds by preloading the valve spring. Increasing this moves the transition in the slope of the characteristic diagrams from low to high speed damping force to higher velocities. More pressure and subsequently higher velocities are required to overcome the preload in the spring and deflect the valve. Both the compression and rebound adjusters have 4 full revolutions of adjustment.



Figure 5.5: Cane Creek Double Barrel Adjusters

The adjusters, springs, and valves are shown in more detail in Figure 5.6. As can be seen the spring is a typical coil spring with a diameter of 9.8 mm. The bleed orifice and needle are contained in the adjuster on the left. The orifice is only 1.5 mm in diameter and this area is partially reduced by the needle at all times. The valve and bleed orifice operate in series in this damper. The small hole in the center of valve on the far right allows fluid to flow to the bleed orifice. The diameter of the valve is approximately 10 mm.



Figure 5.6: Cane Creek Double Barrel Internal Valve

### 5.3 Validation Procedure

Correlation of the damper model with experimental testing is very important. A test procedure was developed to collect accurate data that could be compared to the damper model. Five different tests were performed. All tests were performed with an amplitude of .013 m. Before each test the damper was warmed up so that when each test was performed the damper temperature was  $22^{\circ}\text{C} \pm 2^{\circ}\text{C}$ . This temperature was chosen

because it was easily repeatable and the properties of the damper fluid used in the model were taken at 20° C.

First the damper pressure was checked by measuring the static damper force. The recommended gas pressure for the Cane Creek dampers is 5 bar. It was measured by calibrating the load cell of the damper dynamometer to zero without the damper installed. Then once the damper was installed the static force could be determined. The gas pressure in the damper can now be determined by dividing the static force by the rod area as can be seen below. This gas pressure was used to confirm the value directly measured and check to make sure the dampers were still adequately pressurized.

$$P_g = \frac{F_s}{A_{rod}} \quad (5.6)$$

For the rest of the tests the static force was subtracted from both the experimental data and the model. Since this force is position dependent and not a function of the damper velocity it should be removed [13]. The additional stiffness caused by the compression of the gas chamber is still included in the data but it is extremely small.

Then the friction in the damper was determined by testing the damper at extremely low velocities. It was tested at a frequency of .016 Hz which resulted in a maximum velocity of .0013 m/s. The force outputted by the damper at zero displacement will be recorded and used as the friction force in the damper model.

Next data will be collected to correlate the bleed orifices to the damper model. For this test the damper was run at frequencies of .8 and 1.6 Hz since the low speed region is of the most significance. The low frequency used also isolated the effects of the bleed orifice. Testing at lower frequencies was attempted but the damper hysteresis and friction effects rendered the results inconclusive. Tests were performed with the bleed

orifices at different adjustments to allow different fluid flow and force output to be compared. The high speed adjusters were set to full stiff to maximize flow through the bleed orifices. However with the bleed adjustments at stiff settings, the preload on the valve spring was overcome allowing flow through the valve. This limited the usefulness of these results to very low speeds.

The next test was to correlate the location of the knee to that observed in the damper model. This test was run at 1.6 Hz to ensure sufficient pressure would overcome the valve spring preload to produce the knee. This test was run with the bleed orifices set to their medium setting. This setting was chosen because at soft settings the slope transition was not very well defined because the curves were of similar slope. At stiff settings significant hysteresis caused difficulty in determining the location of the transition. The high speed adjusters were adjusted to different settings throughout the test.

Then correlation of the valve and orifice were performed. The damper was run at a frequency of 3.2 Hz since the high speed region of the damper curve is of importance. The bleed orifices were set also set to a medium setting to prevent excessive hysteresis and provide a clear slope transition. The high speed adjusters were set to various settings to compare against the data produced by the model. This test was to correlate the slope and curvature of the high speed portion of the characteristic diagram with the damper model.

The best correlation was determined by calculating the sum of the square and the mean squares within samples of the data. This value was primarily used to compare the quality of correlation for different settings in the model. The mean was used since a different number of data points were collected for different tests. The number of points

collected depended on the test frequency and logging frequency. The number of time steps in the model was then adjusted so that the same number of data was calculated at the same time intervals. Ott and Longnecker give formulas for the within sample sum of the squares and the within sample mean squares. These are given below in equations (5.7) and (5.8), respectively [27].

$$SSW = \sum_i (y_{1i} - y_{2i}) = \sum_i (F_{exp}(i) - F_{model}(i)) \quad (5.7)$$

$$S_w^2 = \frac{SSW}{n_T - 1} \quad (5.8)$$

In the above equations  $F_{model}$  is the data collected from the computer model,  $F_{exp}$  is the data from the experimental testing, and  $n_T$  is the number of samples collected. The variance is the difference between these values. This was plotted against velocity so that it could be clearly seen at what velocities the most significant error between the experimental and predicted data occurred.

## **6. RESULTS**

The results of the model validation will be given first. The effects of fluid inertia and its impact on the damper characteristics will then be examined. Then using the twin tube and monotube damper models a comparison of these two types of dampers will be presented. This will focus primarily on the forces generated by the dampers and the pressures in the rebound and compression chambers. Parameter studies will be performed to compare the effects of external adjustments and changing the physical parameters of the damper. The twin tube damper model will be used for this analysis. Finally the effect of a linear, asymmetric damper on the spring mass damper model will be examined.

### **6.1 Model Validation**

The results of the separate tests to validate the damper model are in the following sections. The determination of the friction and static forces, and the correlation of the bleed orifice, knee, and valve are included. The goal of the validation was not to accurately predict exact forces produced by the damper. The presence of hysteresis and the compressibility of the actual damper fluid prevent this. The goal of the validation was to predict general trends in the force with changes in the damper adjustments.

### 6.1.1 Static and Friction Forces

The static force was measured directly with the load cell on the dynamometer. It was then compared to the predicted value determined by measuring the gas chamber pressure. These values differed slightly because the static force was measured with the damper at midstroke, where the gas chamber pressure was measured with the damper at full extension.

The measured static force was 23.4 N. Dividing this value by the area of the rod gives a gas chamber pressure of 4.6 bar at the midstroke of the damper. The measured gas pressure was approximately 4.3 bar. The difference of these values is partly due to the compression of the gas chamber due to rod insertion and the limited accuracy of measuring the gas chamber pressure. Since the static force is subtracted from the data this small pressure difference will have negligible results on the results. Most importantly these tests confirm that the damper is properly pressurized. Therefore an initial gas pressure of 4.6 bar at midstroke will be inputted into the damper model.

Next the friction forces generated by the damper were determined. For this test the damper dynamometer was run at .016 Hz giving a maximum velocity of less than .0013 m/s at midstroke. Figure 6.1 below shows the data collected from this test. This is a work diagram with the compression stroke above the x-axis and the rebound stroke below the x-axis. The friction force in both rebound and compression at zero displacement will be inputted into the damper model because this is also where the static force was measured. Therefore a compression friction force of 38 N and a rebound force of 30 N were inputted into the model.

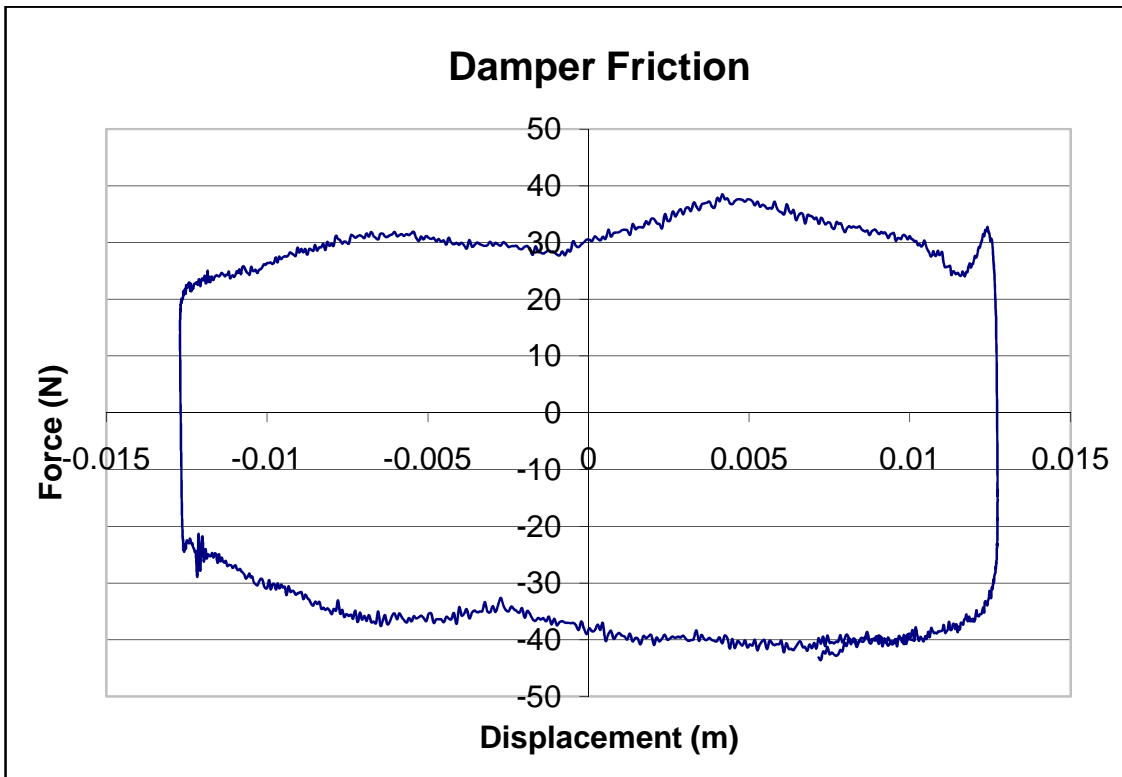


Figure 6.1: Damper Friction

The asymmetry of the friction is most likely due to the rod or piston seals. A similar effect was also observed by Talbot and Starkey [1]. The slight upwards slope towards positive displacement indicates the stiffness of the damper provided by the compression of the gas chamber.

#### 6.1.2 Bleed Orifice Correlation

The accuracy of the bleed orifice flow is very important since they are always open and are the primary mechanisms generating the force of the damper at low speeds. The piston leakage only has a small effect at low speeds because of the relatively small pressure differential and low velocity.

Figures 6.2 and 6.3 below are characteristic diagrams comparing the experimental data and the model data. These results are from tests at .8 Hz and 1.6 Hz, respectively, with the low speed rebound and compression adjusters set to full soft. The blue line is the data from the model and the pink line is the experimentally collected data. For these tests the high speed valves did not open at all. This is apparent since there is no abrupt change in the slope of the lines of the experimental data.

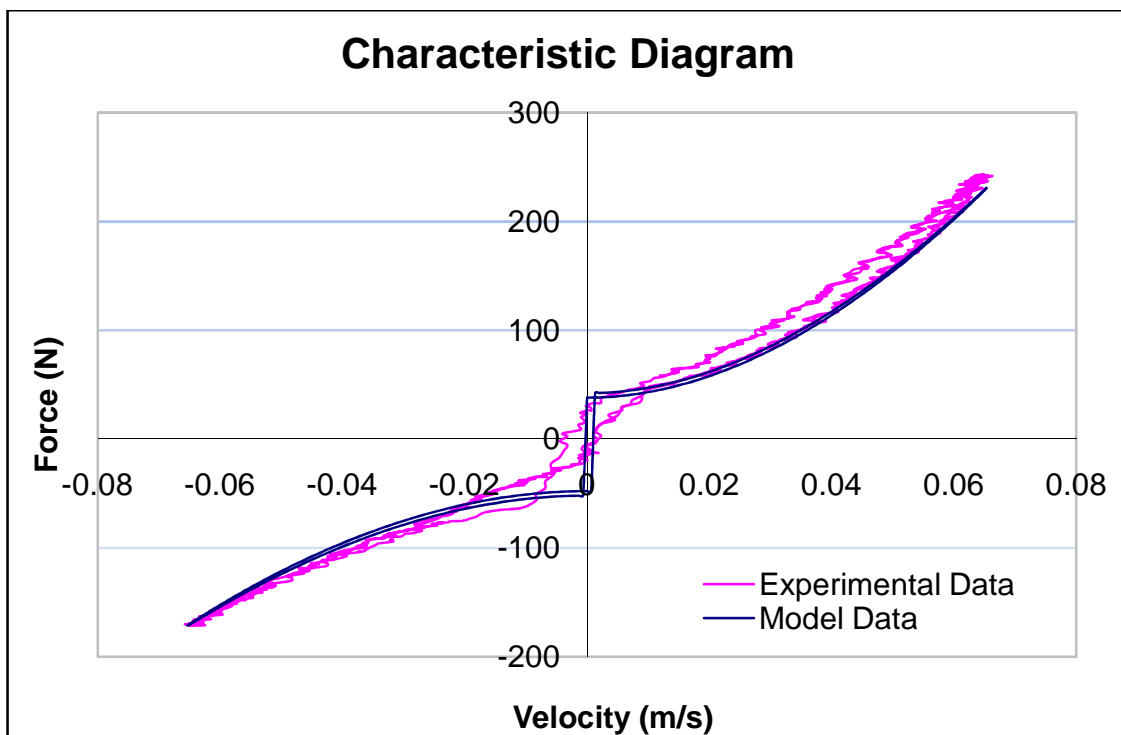


Figure 6.2: Bleed Correlation at Soft Low Speed Adjustment and .8 Hz

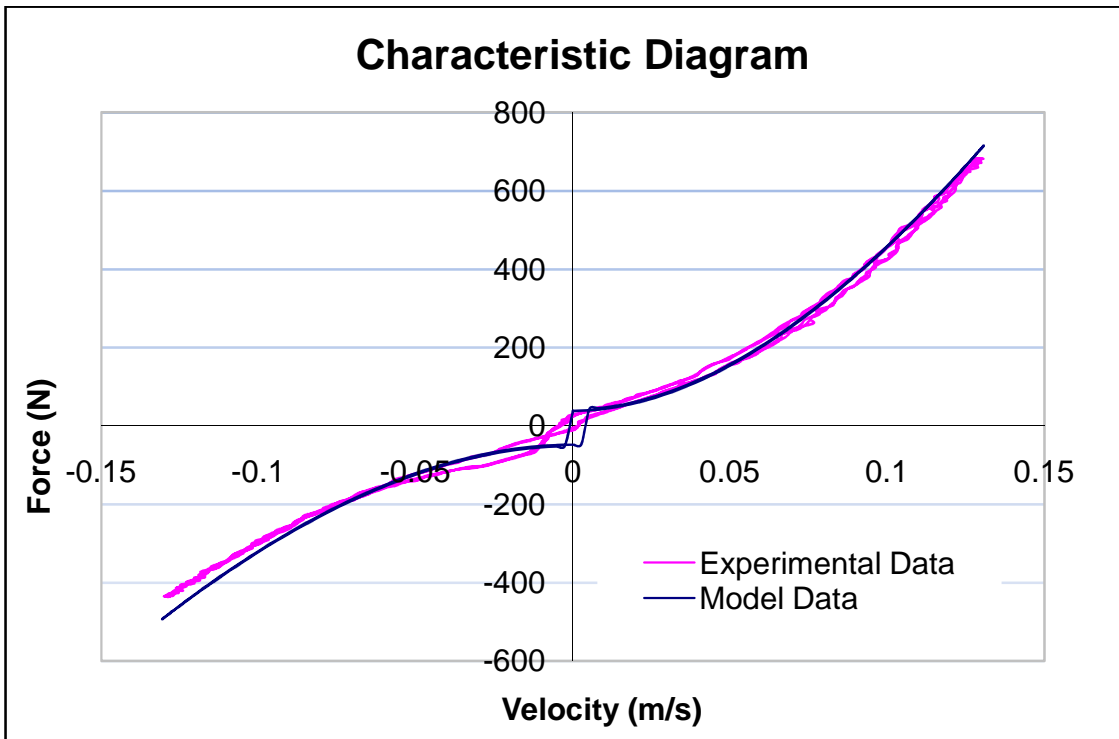


Figure 6.3: Bleed Correlation at Soft Low Speed Adjustment and 1.6 Hz

For this setting the dynamic discharge coefficient was initially set to .70. However the best correlation between the experimental data and the model data occurred with a coefficient of .68 for the compression orifice and .70 for the rebound orifice. Typically, the desired knee location is at velocities less than .1 m/s. Therefore the correlation focused on the low speed region of the curve. The force at velocities above the knee is primarily dependent on the valve properties not the bleed orifice. At high velocities it can be seen that the error increases. This is most likely because the discharge coefficient in the model is constant but in actuality it is dependent on velocity and acceleration of the fluid. Greater accuracy could probably be achieved if a variable discharge coefficient was implemented into the model. However, since the high speed region is not of primary importance this would be unnecessary for this model.

The values of the mean square for this correlation are 200 for the test at .8 Hz and 584 for the test at 1.6 Hz. These values may seem very high but they are mainly from the error at very low velocities from friction and pressure lag. The pressure lag is caused by the compressibility of the fluid and compliance of the damper. These factors cause the pressure buildup in the damper to happen over a finite amount of time and consequently delay the force buildup of the damper. The hysteresis of the damper also causes the mean squares to be large because the model does not predict the significant hysteresis in the damper. The effect of both of these factors would increase as the test frequency and damper velocity are increased.

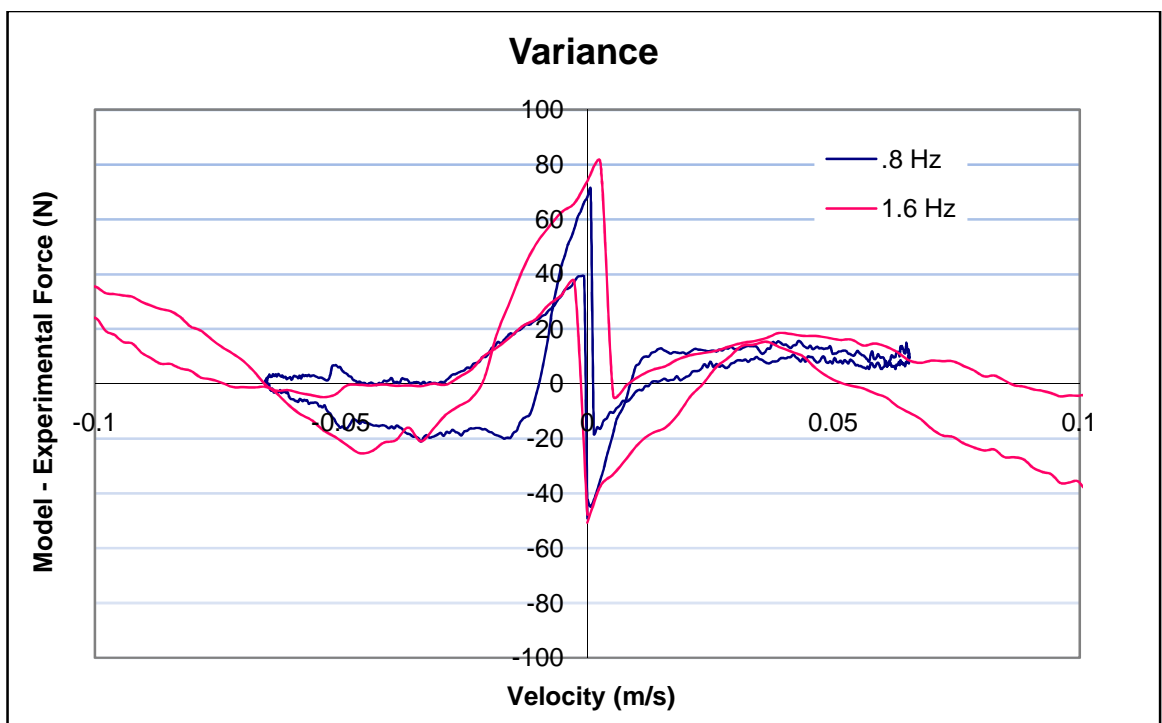


Figure 6.4: Variance at Soft Low Speed Adjustment and .8 Hz

The location and magnitude of the error between the model and experimental data can be seen above in Figure 6.4. This is a plot of the variance between the two data sets as a function of the damper velocity. The range of the velocity plotted is between -.1 and .1 m/s because this is the range the correlation focused on. As can be seen the most significant variance is at low velocities. Above .01 m/s the variance is less than 20 N for the test at .8 Hz and less than 40 N for the test at 1.6 Hz. Again the trend of increasing variance could most likely be improved through the use of a variable discharge coefficient. It can be seen that in compression and rebound the model is initially under predicting the force but above .075 m/s is over predicting the force.

For the next test the low speed compression and rebound adjusters were set to medium. The characteristic diagrams comparing the experimental and the model data from these tests are shown below in Figures 6.5 and 6.6. These results are from tests at .8 Hz and 1.6 Hz, respectively. For the test at 1.6 Hz the high speed valves began to open at about .09 m/s in compression and .11 m/s in rebound. This is apparent in Figure 6.6. Therefore data above .09 m/s was omitted from the statistical analysis.

The best correlation between the experimental data and the model data occurred with a discharge coefficient of .66 for the compression orifice and .68 for the rebound orifice. These coefficients are smaller than those found for the previous test. This is potentially a result of the increased velocity of the fluid. The greater inward momentum of the fluid could cause a slightly smaller vena contracta reducing this coefficient and increasing the force produced by the damper.

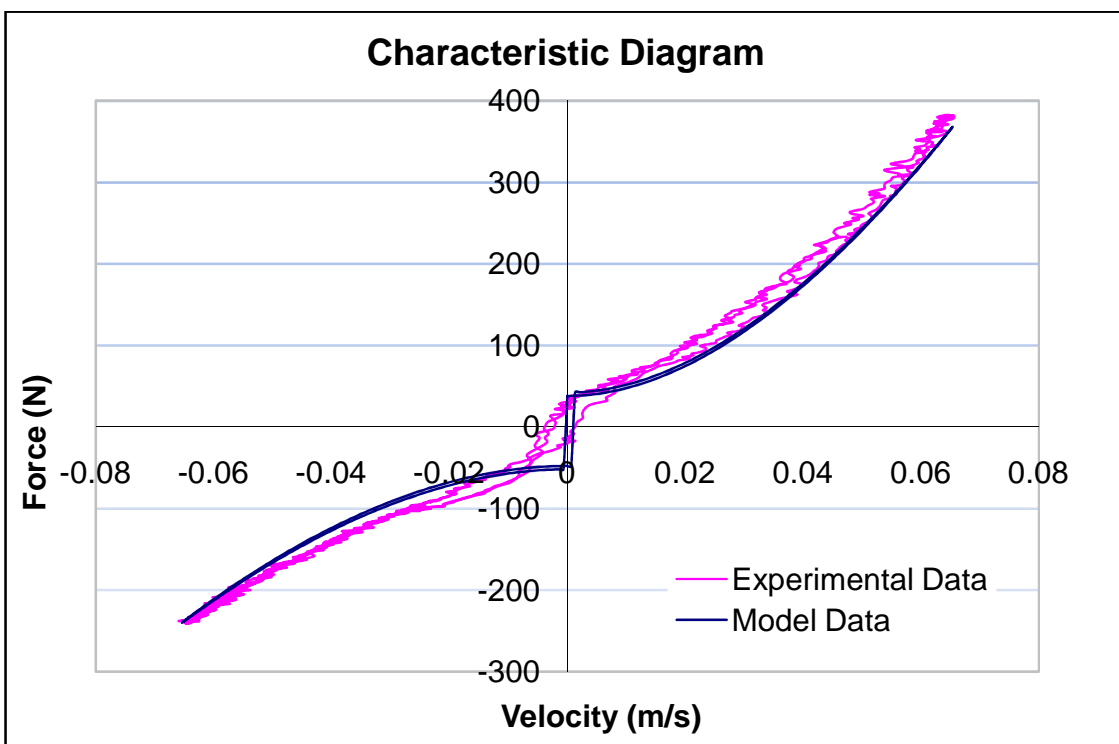


Figure 6.5: Bleed Correlation at Medium Low Speed Adjustment and .8 Hz

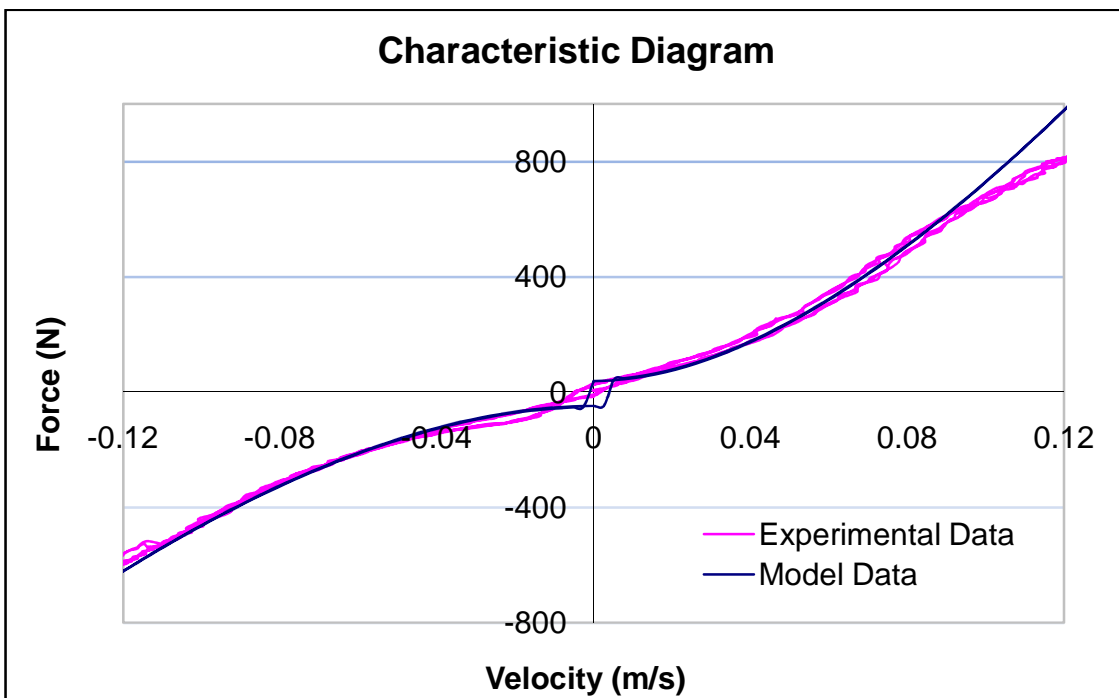


Figure 6.6: Bleed Correlation at Medium Low Speed Adjustment and 1.6 Hz

The values of the mean square for this correlation are 297 for the test at .8 Hz and 424 for the data collected at velocities below .09 m/s for the test at 1.6 Hz. As can be seen in Figure 6.7 these values are due mainly to the error at very low velocities from friction and pressure lag. Since the damper is producing more force than the previous test the fluid pressure will also be greater. This causes the effects from the fluid compressibility and hysteresis to be more significant. As can be seen the plots of variance show very similar trends for the two tests. Above .01 m/s the variance is less than 20 N for the test at .8 Hz and less than 40 N for the test at 1.6 Hz until the high speed valve opens at approximately .09 m/s. Also the model is initially under predicting the force and then at above .075 m/s it over predicts the force.

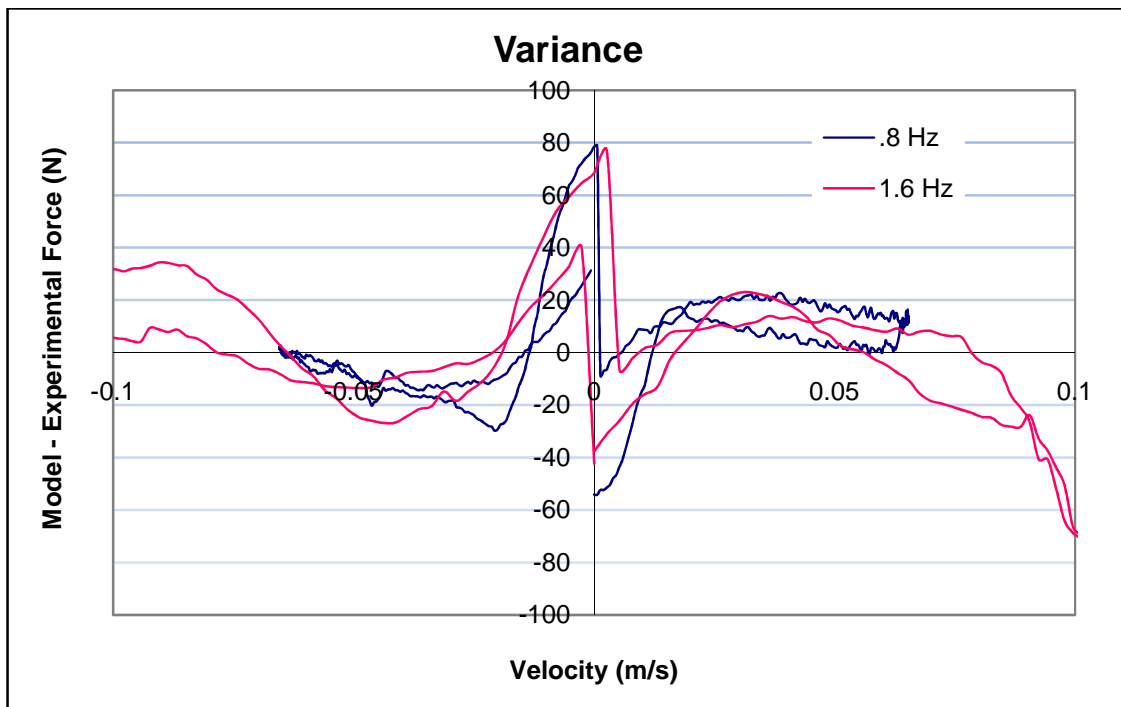


Figure 6.7: Variance at Medium Low Speed Adjustment and .8 Hz

Figure 6.8 below shows the effect of various discharge coefficients on the force predicted by the model. The coefficients displayed in the figure represent the typical range for damper orifices [9]. For simplicity in the model coefficients of .66 for the compression orifice and .68 for the rebound orifice could be used regardless of the adjustment setting. With these settings good correlation could still be achieved across the whole adjustment range. This is especially true depending on the knee location. If the knee occurs at low velocities the inaccuracy from the coefficient is very small. This coefficient has negligible effect on the high speed region of the curve because the majority of fluid flows through the valve and not the bleed orifice.

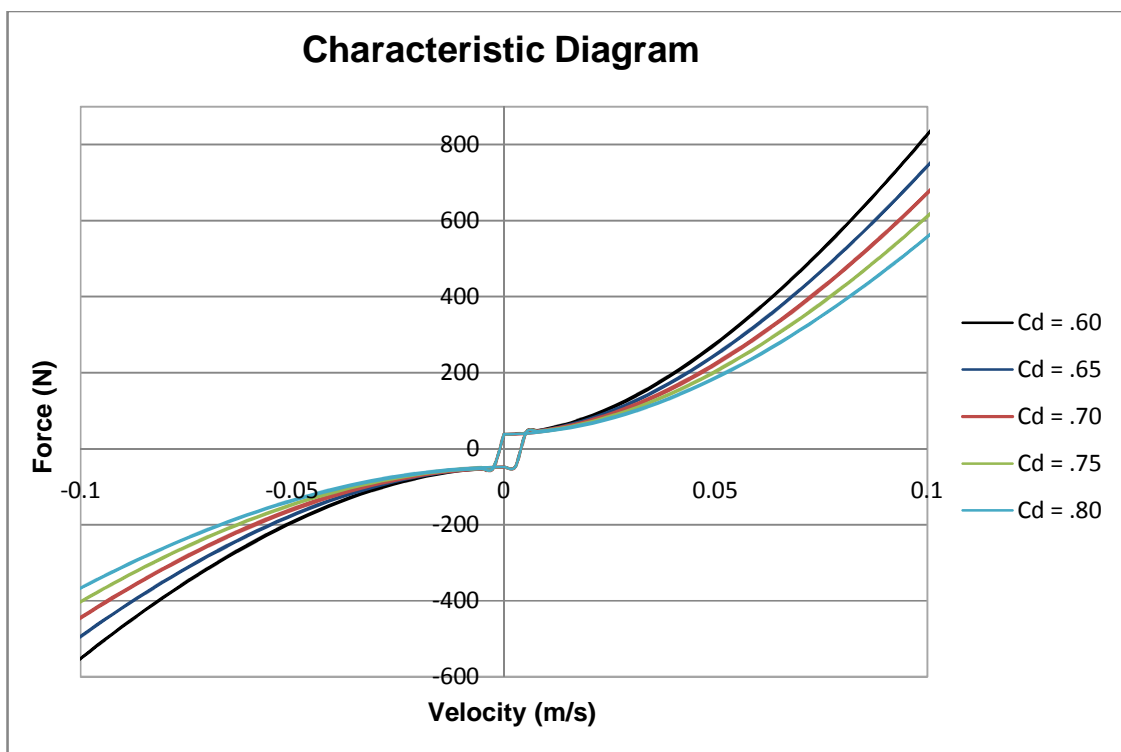


Figure 6.8: Model Sensitivity to the Discharge Coefficient

### 6.1.3 Knee Location Correlation

The correlation of the knee consisted of three separate tests with different settings for the high speed adjusters. All tests were run at 1.6 Hz with the low speed adjusters set to medium. The goal of these tests was to determine the initial preload force on the valves. The valve spring stiffness of both the rebound and compression valve is known to be 20 N/mm [26]. Therefore the damper will be tested at different settings and compared to the model. From this the initial preload force can be determined.

The results of the tests are shown below in Figures 6.8, 6.9 and 6.10. The first figure shows the results with the high speed adjusters set to soft. This setting would provide an additional 15 N of force to the initial preload. For the next test the adjusters were set one turn stiffer, resulting in an additional 15 N of preload force. This was repeated for the final test.

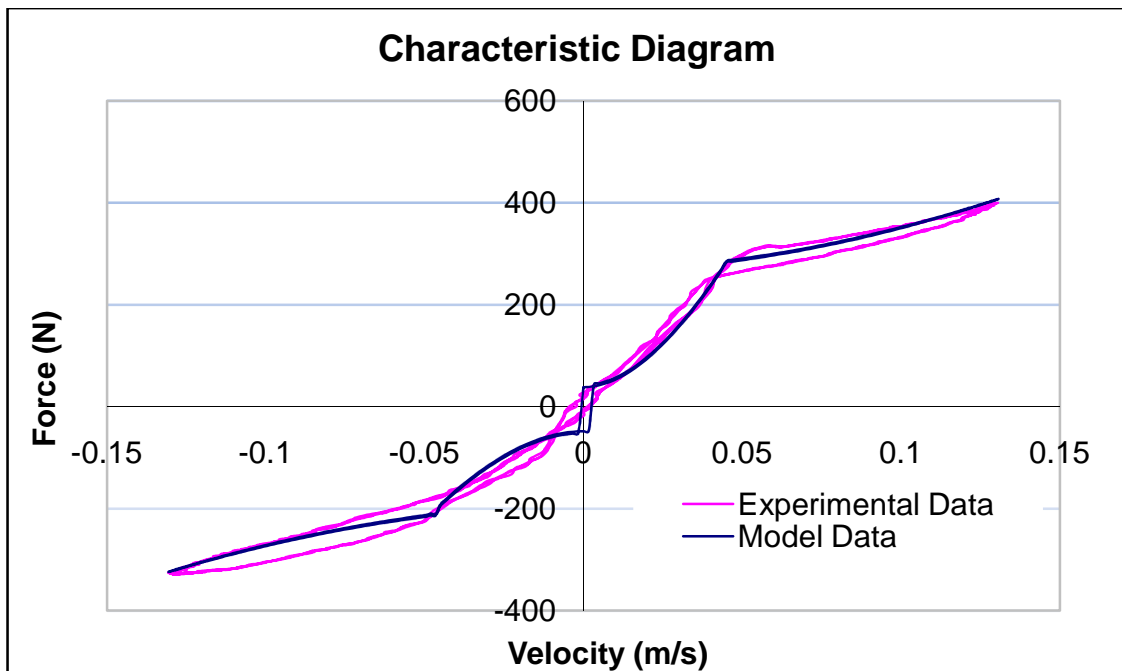


Figure 6.9: Knee Correlation at Soft High Speed Adjustment

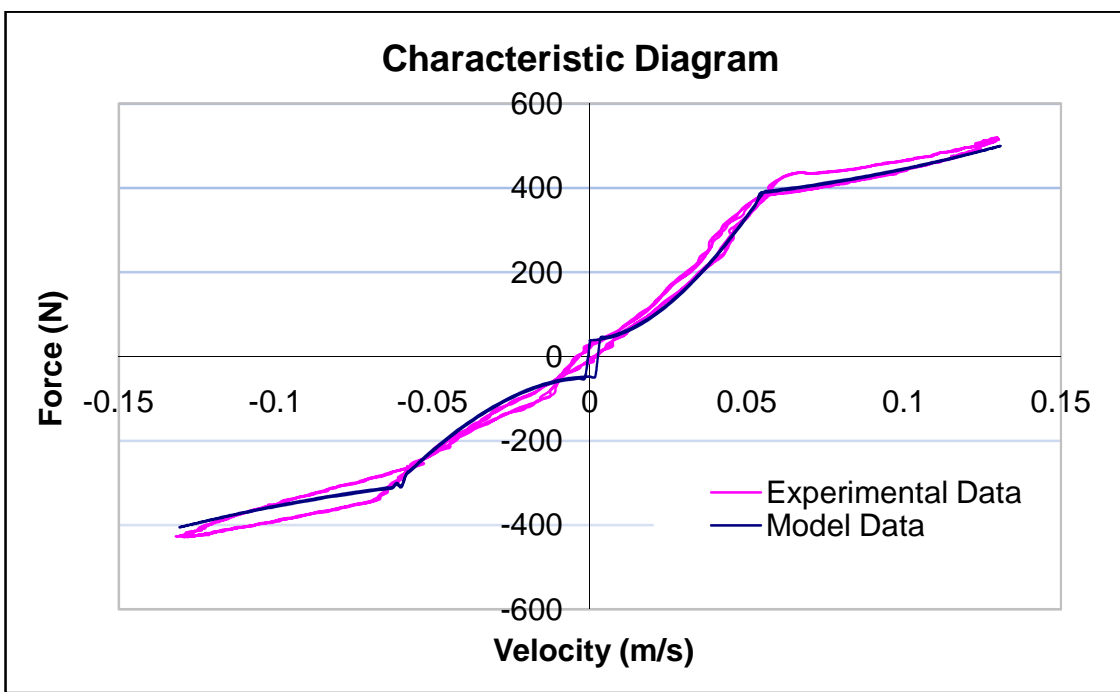


Figure 6.10: Knee Correlation at Medium High Speed Adjustment

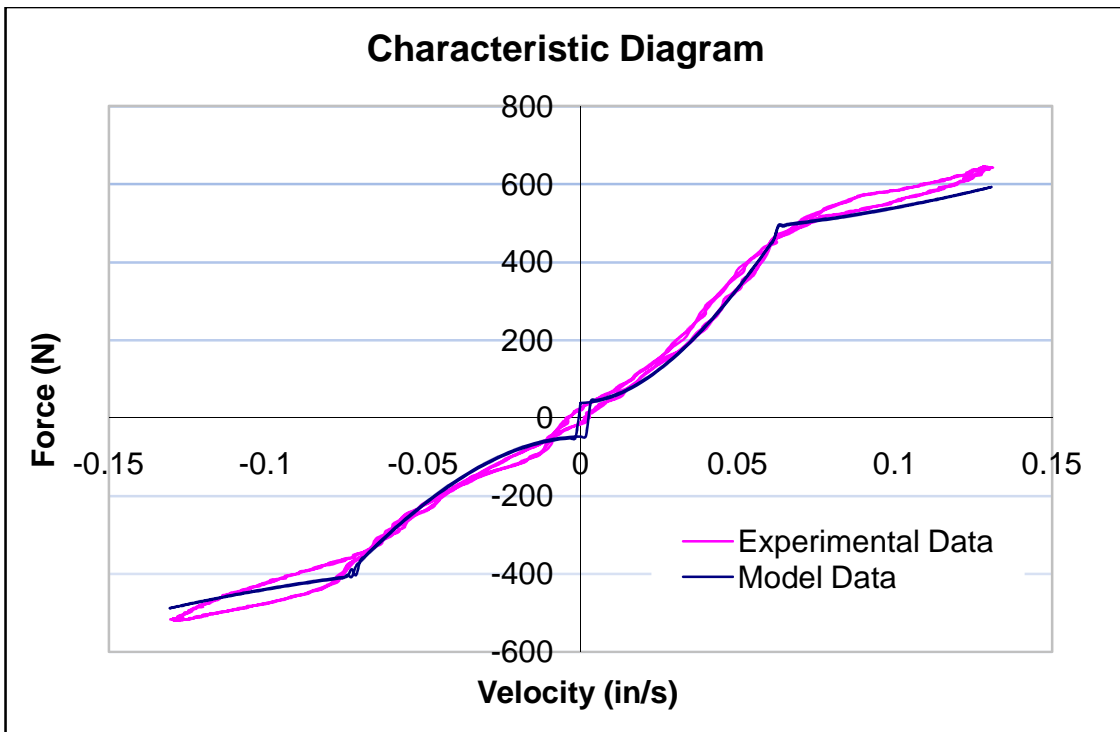


Figure 6.11: Knee Correlation at Stiff High Speed Adjustment

It was determined that the best correlation between the model and experimental data occurred with an initial preload force of 18 N on the compression valve and 10 N on the rebound valve. For the soft setting shown in Figure 6.8 this results in total preload forces of 33 N on the compression valve and 25 N on the rebound valve. For the medium setting in Figure 6.9 the total forces were 48 N on the compression valve and 40 N on the rebound valve. For the stiff setting in Figure 6.10 the total forces were 63 N on the compression valve and 55 N on the rebound valve.

The difference in the initial valve preload is most likely an effect of small differences in the springs or the adjusters. The difference of 8 N between the preload of the compression and rebound valve is representative of slightly more than half of a turn on the adjusters. The thread pitch of the adjusters is .75 mm [26]. Therefore to achieve 8 N more preload force the compression spring would be compressed only .4 mm more than the rebound spring.

#### 6.1.4 Valve Correlation

The valve correlation is very important to the accuracy of the high speed region of the characteristic diagram. The slope and curvature of this region of the plot is primarily controlled by the valve and orifice size, and the valve spring stiffness. These values can be measured easily. In order to adjust the model to achieve the optimum correlation the dynamic discharge coefficients of the piston orifices will be adjusted. The discharge coefficient was initially set to .70. However, a value of .68 was found to give the best overall correlation for the tests.

All of the tests were run at 3.2 Hz with the low speed adjusters set to medium. At 3.2 Hz significant hysteresis and pressure lag results from the compressibility of the fluid and compliance of the damper. This contributes to inaccuracy in the data, but the trends of the data are still very apparent.

The first test was run with the high speed adjusters set to soft. Figure 6.11 below is the characteristic diagram comparing the experimental and model data for this test. It can be seen that the main areas of error are at extremely low and high speeds. The error at low speeds is caused by the damper friction and pressure lag while the force at high speeds is affected by the discharge coefficient and the fluid compressibility. The mean square value for this test is 959.

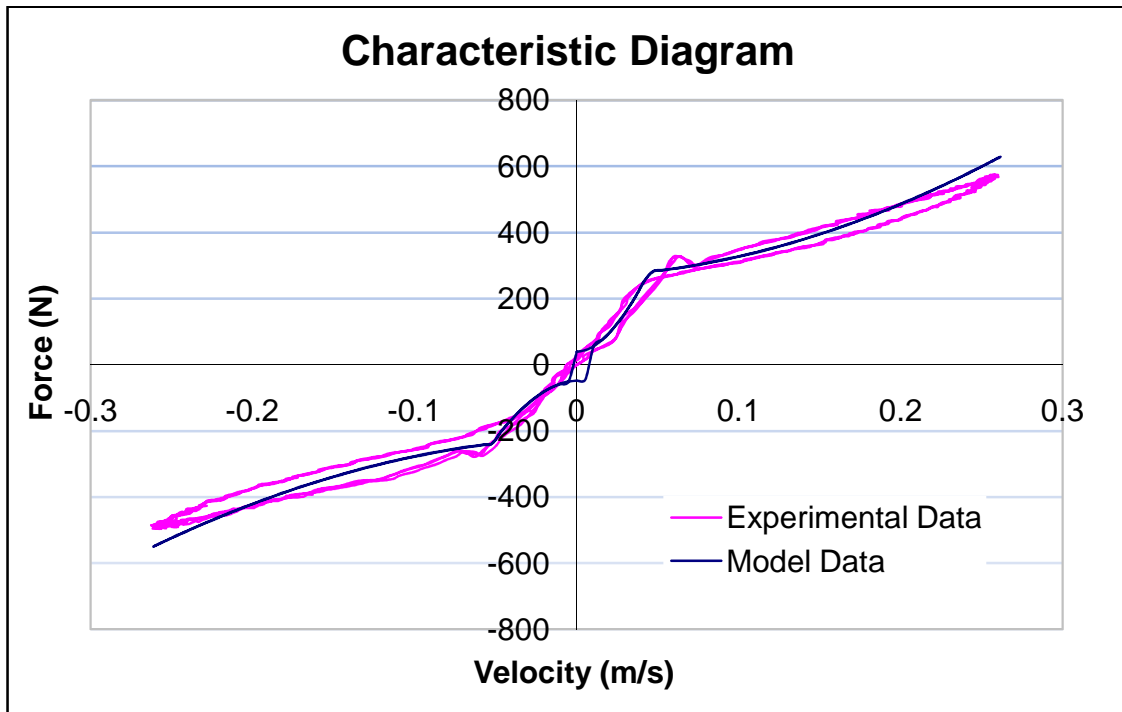


Figure 6.12: Valve Correlation at Soft High Speed Adjustment

Figure 6.12 shows the variance between the model and experimental data. The large difference in variance at velocities greater than .01 m/s is caused by the hysteresis of the damper. Large error also occurred near the knee location. The more gradual slope transition of the damper is most likely caused by leakage around the valve at high damper velocities and pressures.

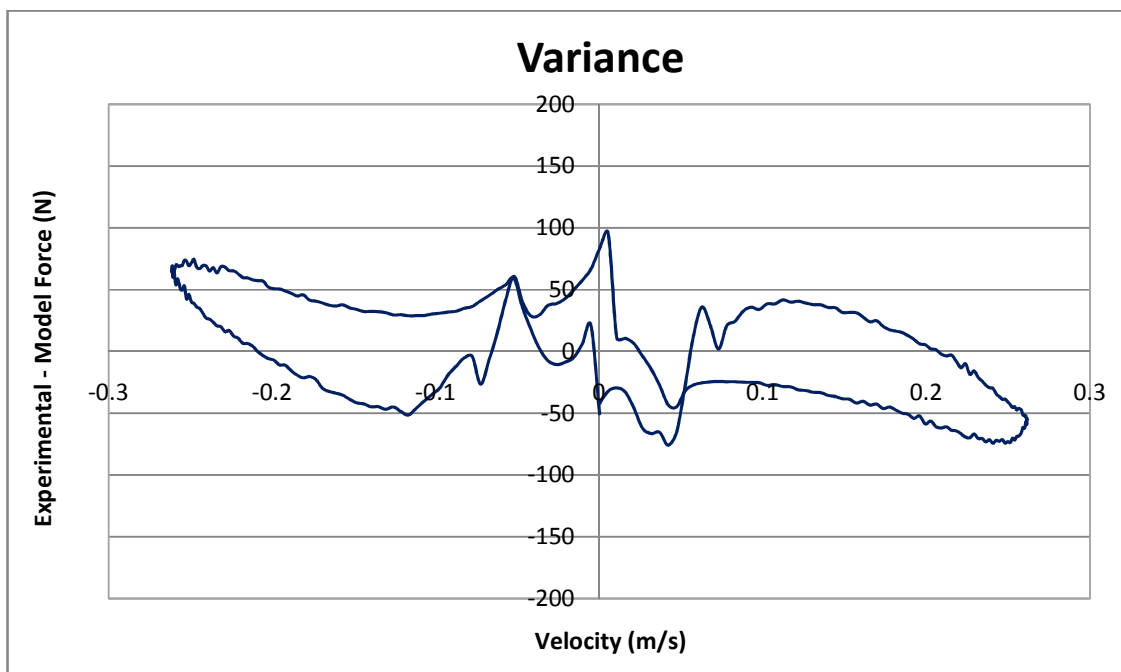


Figure 6.13: Variance at Soft High Speed Adjustment and 3.2 Hz

The next test was run with the high speed adjusters set to medium. Figure 6.13 below is the characteristic diagram comparing the experimental and model data for this test and Figure 6.14 shows the variance between the model and experimental data. This data is very similar to the previous test. There is significant variance caused by the friction at low speeds and the hysteresis at high speeds.

The variance at the knee locations is significantly greater than in the previous test. Since the valve spring has more preload at this setting greater pressure is required to open the valve. Therefore this larger pressure differential across the valve probably contributes to more leakage around the valve. This would make the transition from the low to high speed regions of the curve more gradual. The mean square value for this test is 941.

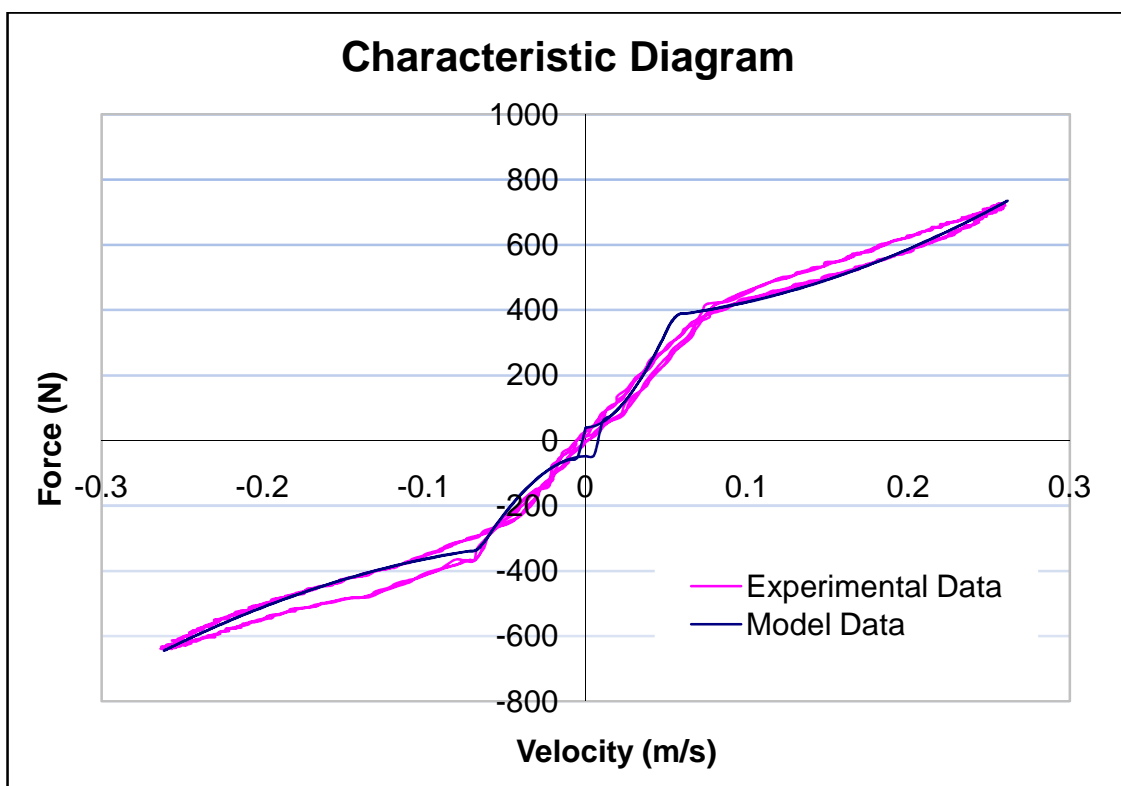


Figure 6.14: Valve Correlation at Medium High Speed Adjustment

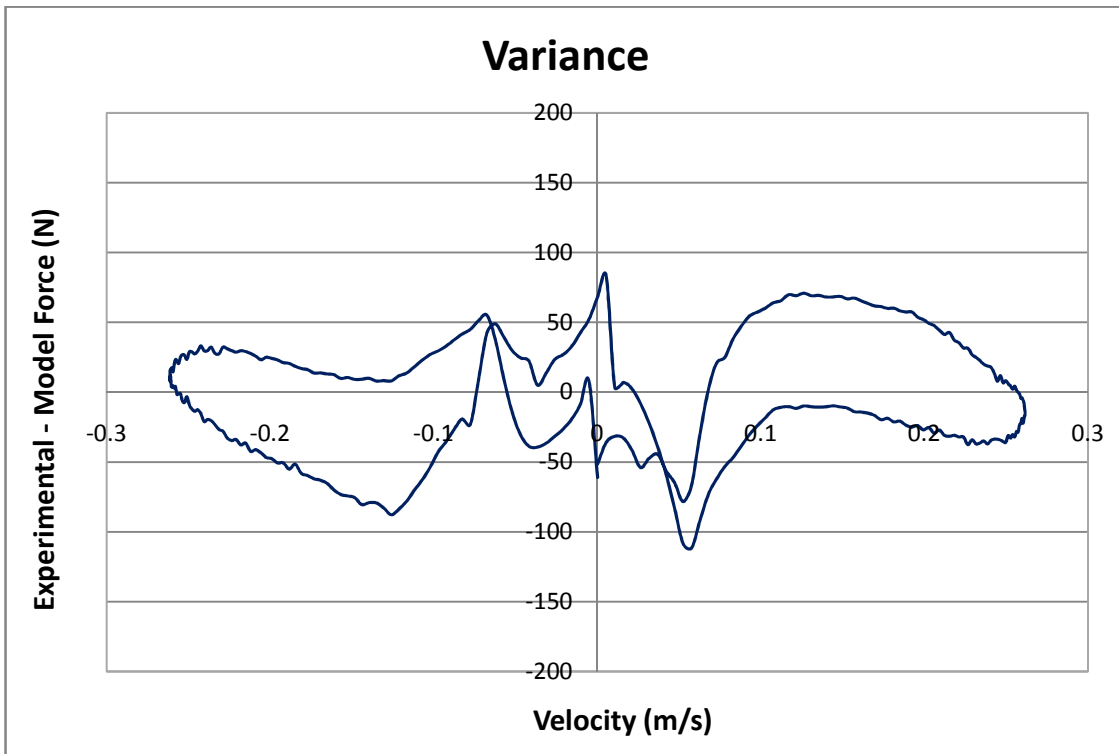


Figure 6.15: Variance at Medium High Speed Adjustment and 3.2 Hz

The next test was run with the high speed adjusters set to stiff. Figure 6.15 below is the characteristic diagram comparing the experimental and model data for this test. Figure 6.16 shows the variance between the model and experimental data. This data follows the same trends as the previous tests. The mean square value for this test is 1053.

Slightly better accuracy could have been achieved for this correlation by determining different discharge coefficients for each adjustment setting like was done in the bleed orifice correlation. However the physical meaning of this is not clear since the fluid velocity through the orifice and valve should not change significantly with this adjustment as it does in with the low speed adjustment.

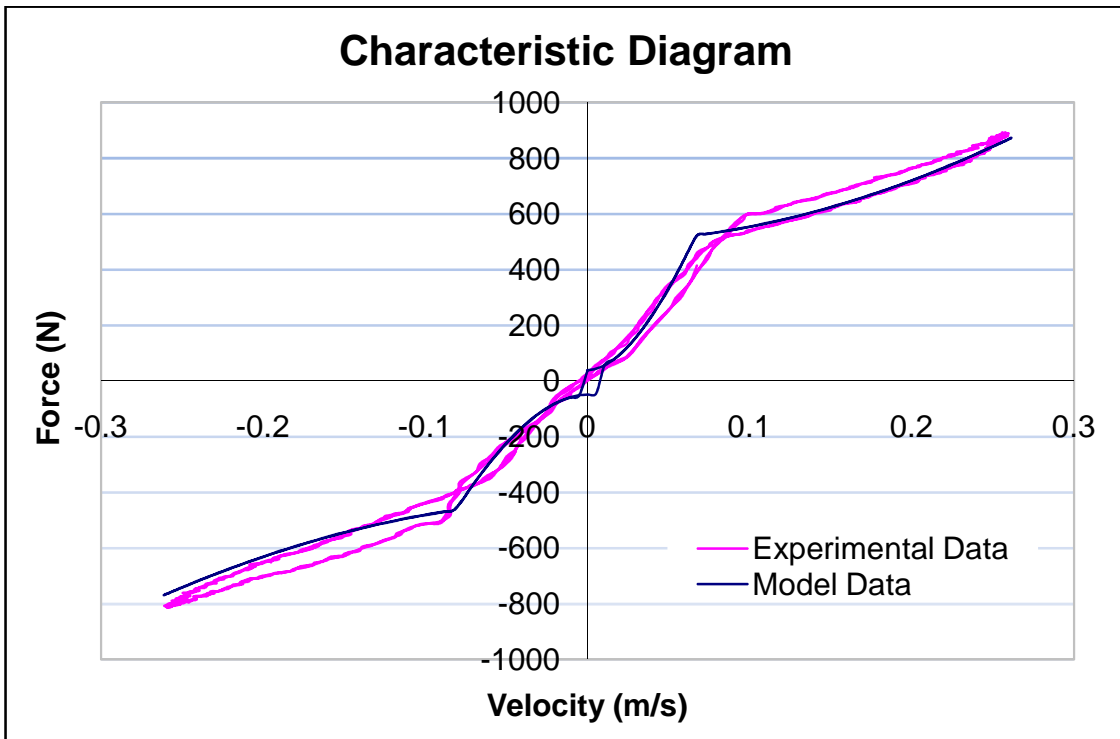


Figure 6.16: Valve Correlation at Stiff High Speed Adjustment

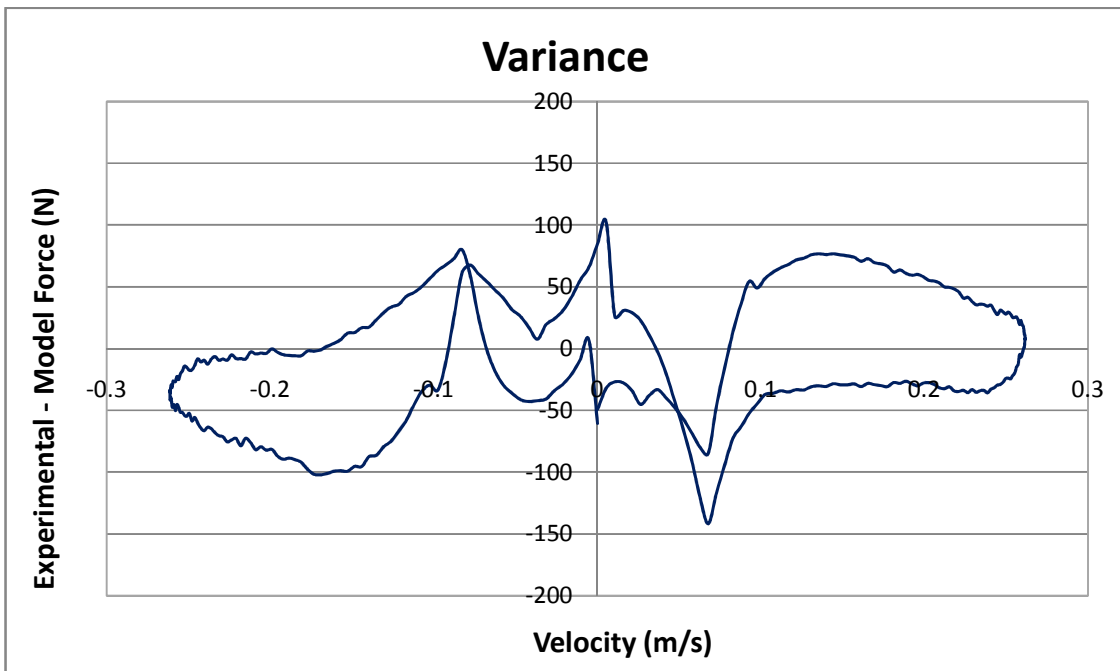


Figure 6.17: Variance at Stiff High Speed Adjustment and 3.2 Hz

In the previous tests it was shown that the model can predict the trends of the experimental data. This would be very useful for predicting the behavior of the damper if it is revalved or the adjustments are changed. This was the goal of the model because without accounting for the fluid compressibility and damper compliance exact correlation of the model data to the experimental data is not possible.

## 6.2 Fluid Inertia Effects

The effect of fluid inertia and viscous effects in the external flow passages of the twin tube damper will now be examined. This will be done by comparing the results from the twin tube with and without the effects included in the calculations. The significance of both of these effects combined will first be evaluated. Then each one will be examined separately to reveal their specific characteristics.

The combined fluid inertia and viscous effects are shown in Figure 6.18 below. As can be seen these effects have a significant influence on the damper performance. The maximum additional force from these effects is 63.7 N which is a 20.5% increase over the model which omits these effects. When comparing the high speed region of the curve it can be seen that this effect has more influence on the performance of the Cane Creek Double Barrel Damper than the restriction provided by the main orifice and valve. In the figure it can be seen that the additional force is present throughout the damper stroke and increases with the damper speed.

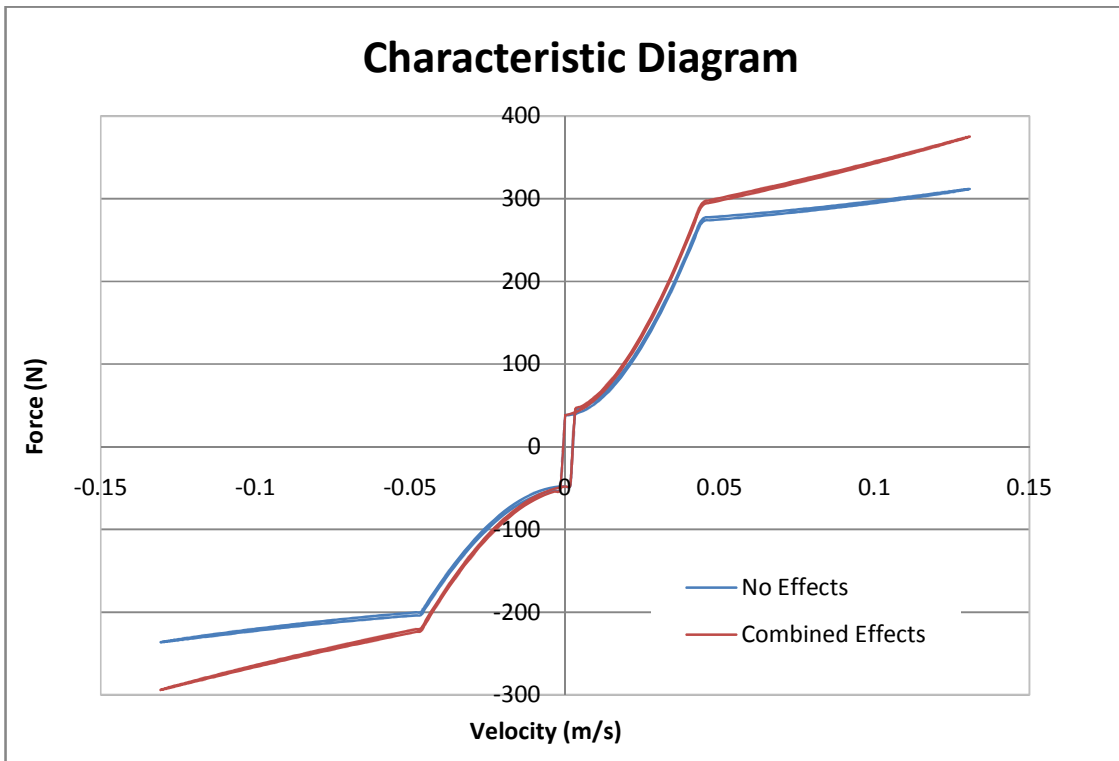


Figure 6.18: Characteristic Diagram with Combined Inertia and Viscous Effects

Figure 6.19 below displays the pressures at different locations in the damper. The blue and red lines represent the pressures in the rebound and compression chambers, respectively. The difference in these lines is the pressure differential across the piston which is the primary factor influencing the damper force. The green line is the pressure immediately after the damper valves and before the circumferential fluid passage. Therefore the difference between this and the rebound chamber pressure, the blue line, is the pressure drop that occurs from the fluid flowing through the circumferential passage. The maximum pressure drop is 1.28 bar at the maximum velocity. This corresponds to the location of the maximum difference in force.

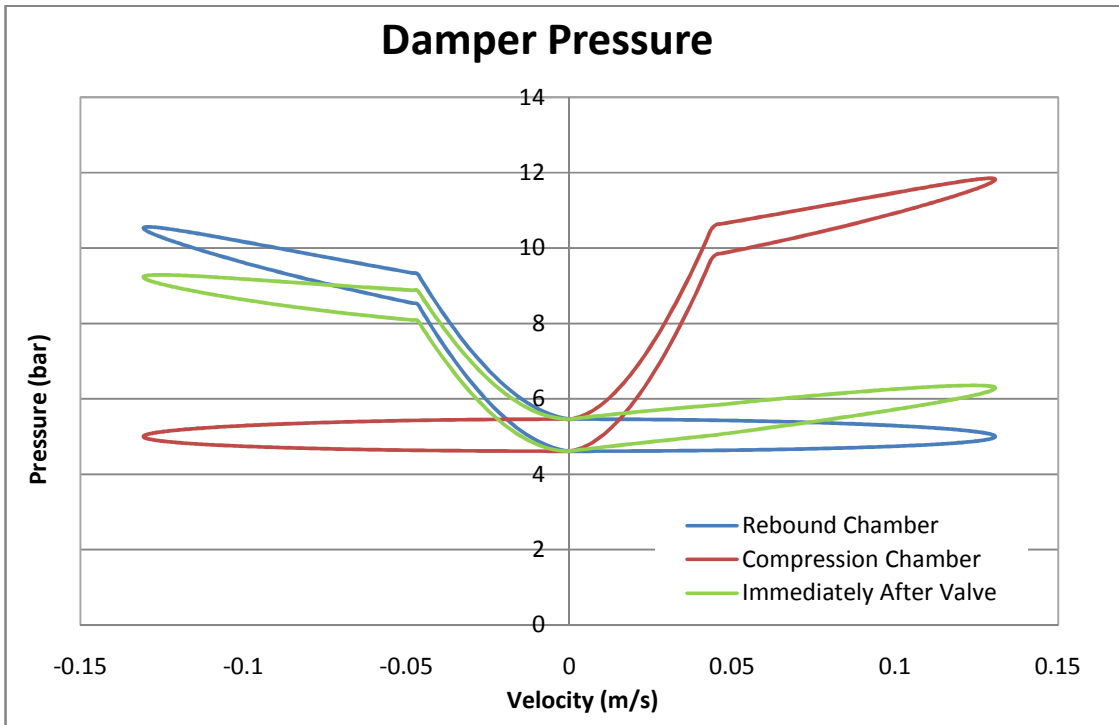


Figure 6.19: Damper Pressure with Combined Inertia and Viscous Effects

It was shown in section 4.4 that the force from fluid inertia is a function of fluid acceleration and the force from viscous effects is a function of fluid velocity. In section 2.4 it was shown that the maximum velocity of a sinusoidal wave occurs at zero displacement and the maximum acceleration occurs at the maximum amplitude when the velocity is zero. Since the maximum force difference occurs at maximum velocity it is from the viscous effects.

Figures 6.20 and 6.21 show similar plots as above but the effect of the fluid inertia is not included. Only the viscous effects of the fluid are included. The maximum force and pressure differences are the same as in the previous example because they

occur at the maximum velocity. At this velocity the fluid acceleration would be at a minimum negating the fluid inertia effects. It is still obvious that the viscous effect is the main contributor to the additional force and is not negligible in modern twin tube dampers.

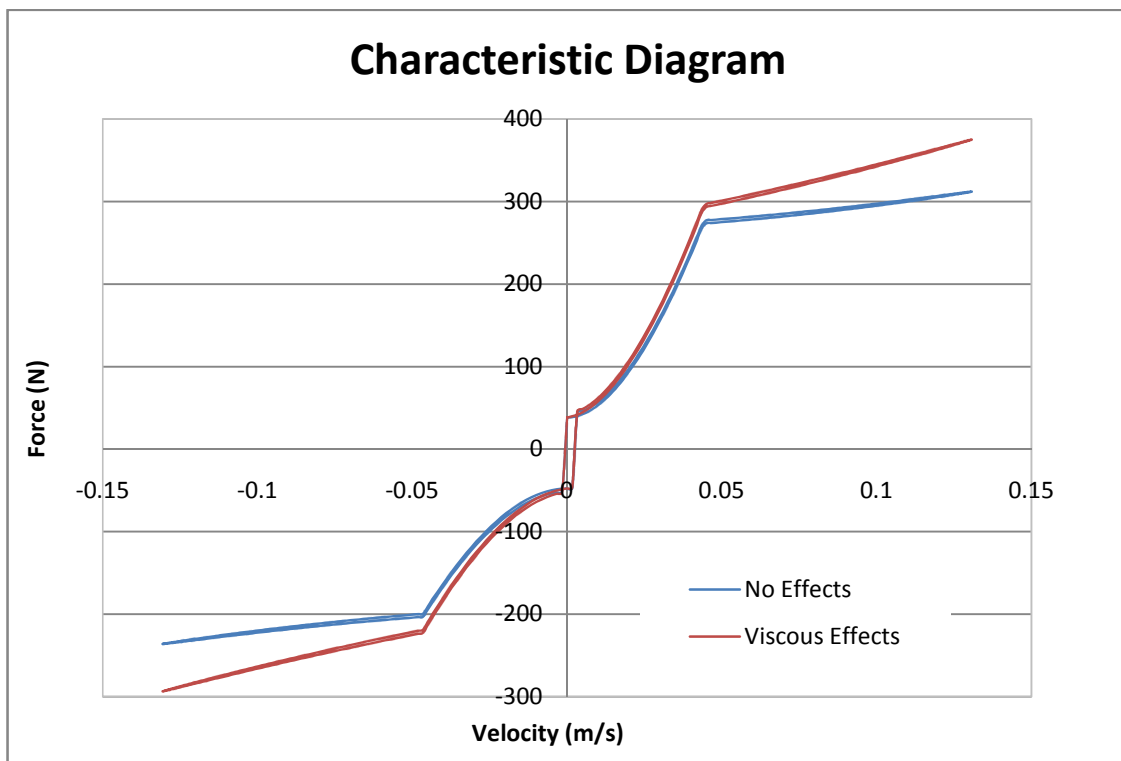


Figure 6.20: Characteristic Diagram with Viscous Effects

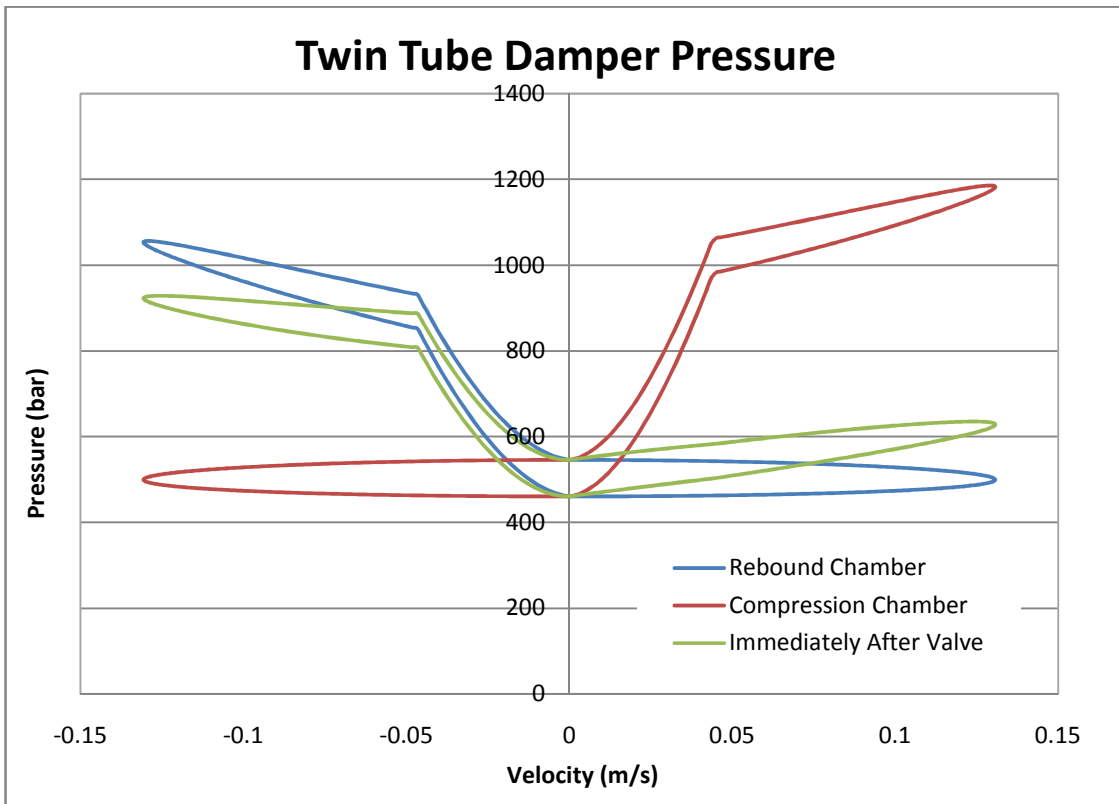


Figure 6.21: Damper Pressure with Viscous Effects

Figures 6.22 and 6.23 show plots with only the fluid inertia effects included. Not visible in the figures is the maximum force difference of .21 N at zero velocity. This force is significantly less than the friction forces that are dominant at low velocities. The maximum pressure drop caused by the fluid inertia is .0042 bar. This effect is very small and many other factors have a much larger affect on the damper performance. Therefore for this style of damper the effect of fluid inertia can be considered negligible in standard sinusoidal testing.

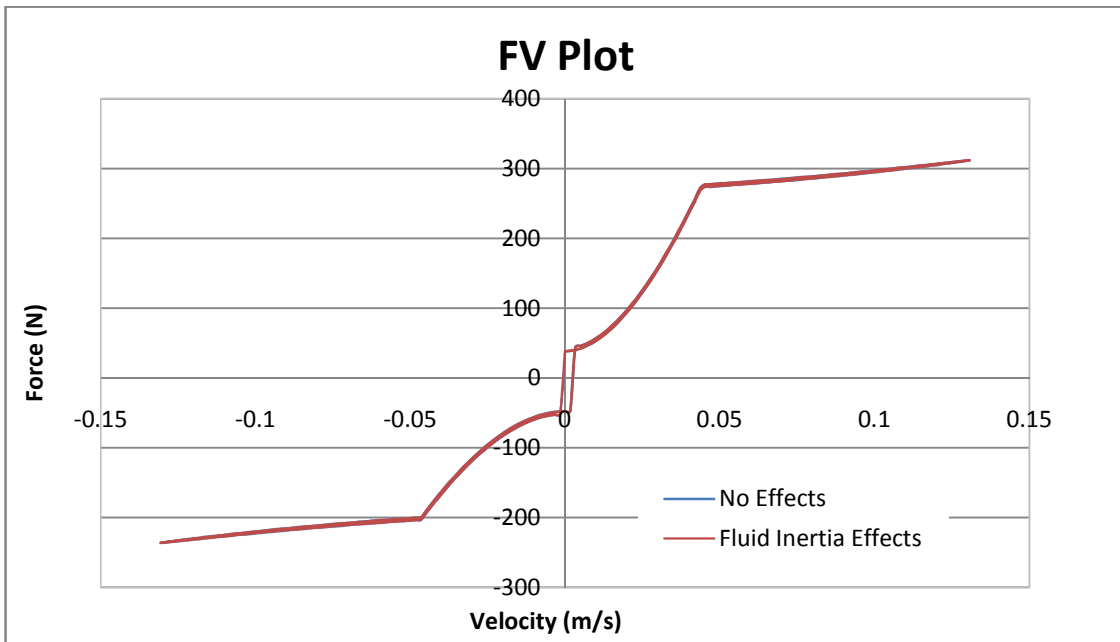


Figure 6.22: Characteristic Diagram with Fluid Inertia Effects

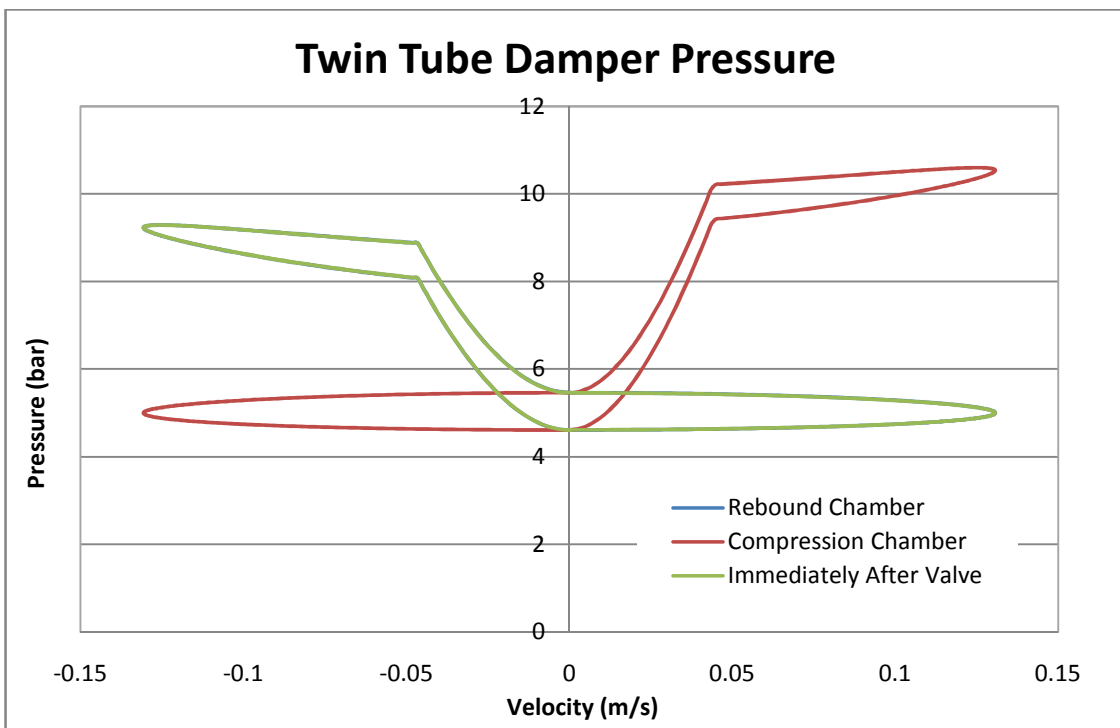


Figure 6.23: Damper Pressure with Fluid Inertia Effects

### **6.3 Twin Tube and Monotube Damper Comparison**

As mentioned previously one of the primary differences in the operation of a twin tube and monotube damper is the side of the piston that the gas chamber is connected to during compression. The effect of these differences will be explored using the twin tube damper model of the Cane Creek Double Barrel damper. It will be compared to a monotube damper model that has same input parameters. Basically it represents the Cane Creek Twin Tube damper as a monotube damper. Since the fluid inertia and viscous effects were explored in the previous section they will be omitted here.

Figure 6.24 shows the characteristic diagrams from the twin tube and monotube models. As can be seen the force generated by the dampers in rebound is the same. This is logical because the operation of the dampers in rebound is practically the same since the gas chamber is acting on the compression chamber in both cases. However it can clearly be seen that there is a significant difference in the force generated in compression.

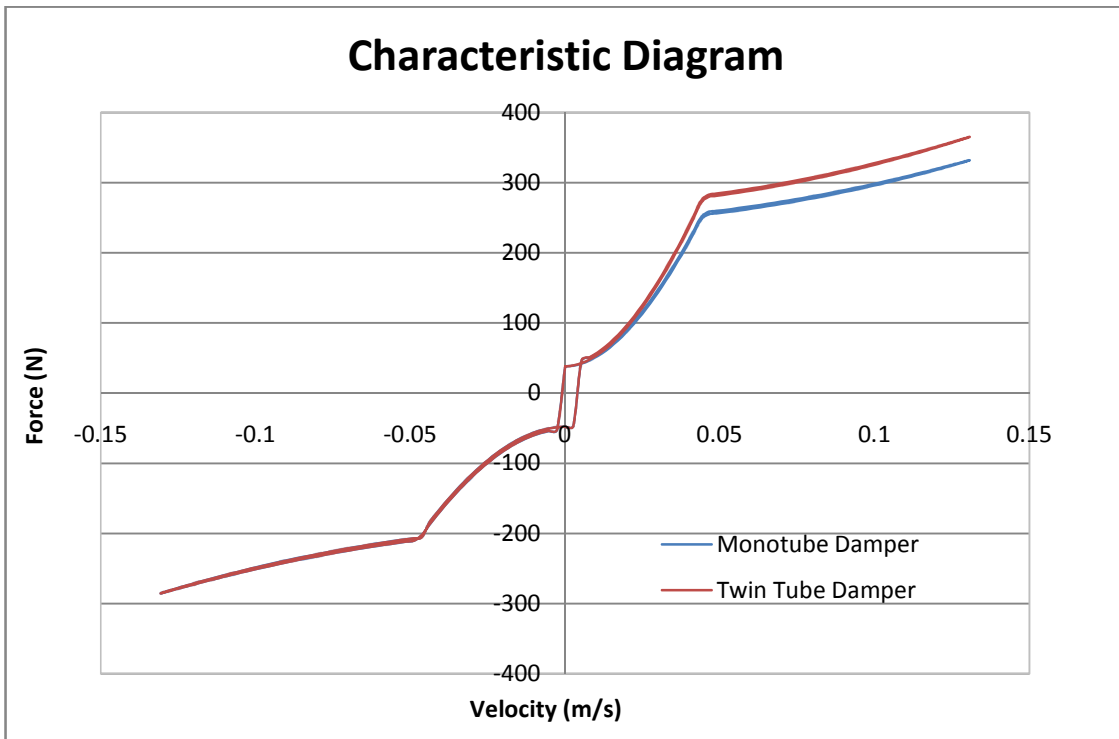


Figure 6.24: Characteristic Diagram of Twin Tube and Monotube Damper

The force of the twin tube damper in compression is greater throughout the full stroke and the maximum difference is at 33.3 N at the maximum velocity. The cause of this is that in the twin tube damper the pressure in the compression chamber increases during rebound. In a monotube damper the gas chamber is always connected to the compression chamber. Therefore to generate force in compression the pressure in the rebound chamber must decrease. Since the pressure differential in each damper is the same this by itself is not the cause of the force difference. The force difference is caused by the different areas on the rebound and compression side of the piston because of the rod and the different pressure distribution.

A simplified example will be used to explain this effect. The maximum pressures on the compression side of the piston for the twin tube and monotube damper are 10 bar

and 5 bar. The product of these pressures and the compression side piston area of 490 mm<sup>2</sup> results in forces of 490 N for the twin tube damper and 245 N for the monotube damper. The maximum pressures on the rebound side of the piston for the twin tube and monotube damper are 5 bar and 0 bar. The product of these pressures and the rebound side piston area of 440 mm<sup>2</sup> results in forces of 220 N for the twin tube damper and 0 N for the monotube damper. Subtracting the compression force from the rebound force gives the damper force from the pressure differential. The force for the twin tube damper is 270 N while the monotube damper is only 245 N. Thus even though the pressure differential across the piston is 5 bar for both dampers the force output is different.

Figure 6.25 below shows the compression and rebound chamber pressures for the twin tube damper. As can be seen the compression chamber in rebound has little variation. Since this chamber is connected to the gas chamber the variation is caused by the insertion of the rod and the subsequent compression of the gas chamber. The increase of pressure in the rebound chamber generates the force. In compression the opposite occurs. The rebound chamber pressure stays relatively constant and the force is generated by the increase in compression chamber pressure. Therefore the pressure in the compression and rebound chamber is always equal to or greater than the gas chamber pressure. Therefore cavitation will not occur as long as the initial gas pressure is greater than the fluid vaporization pressure.

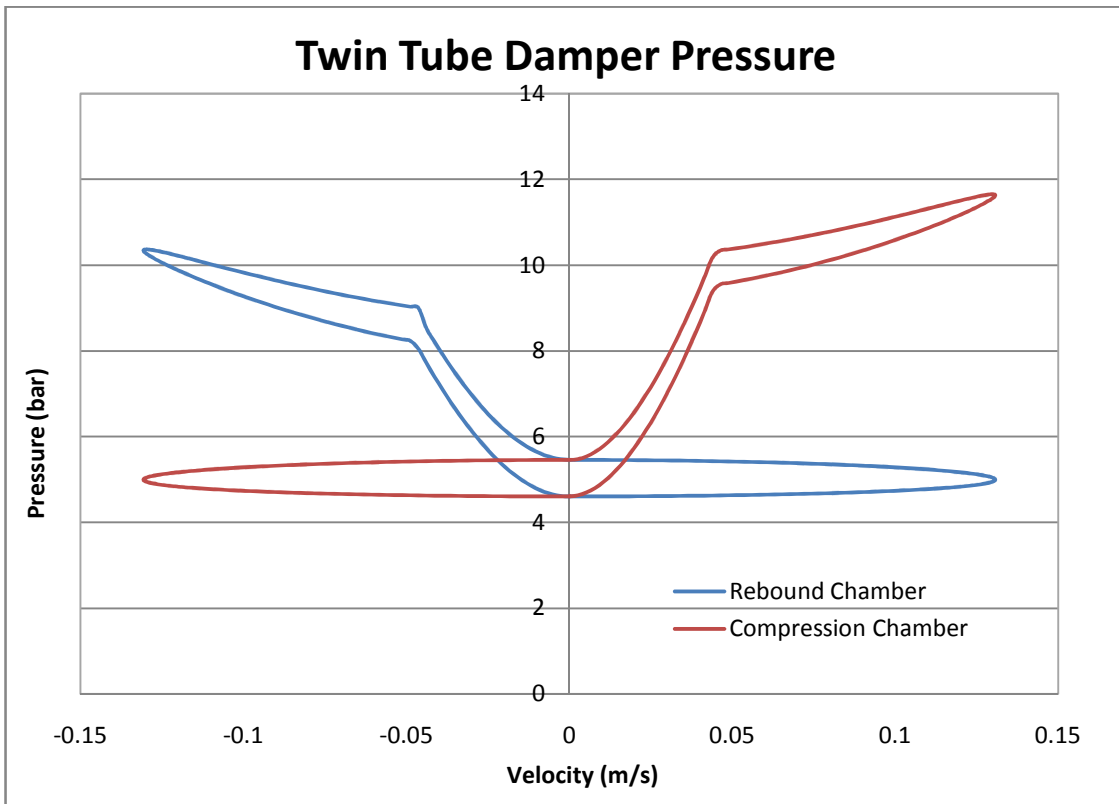


Figure 6.25: Twin Tube Damper Chamber Pressures at 5 bar

Figure 6.26 below shows the compression and rebound chamber pressures for the monotube damper. As can be seen the compression chamber pressure has little variation compared to the rebound chamber. In rebound the pressure increase in the rebound chamber generates force and in compression the pressure decrease generates force. In this specific plot the rebound chamber pressure has dropped below zero. This would cause cavitation in the rebound chamber significantly affecting the performance of the damper. Therefore a higher initial gas pressure is required to prevent cavitation in this chamber.

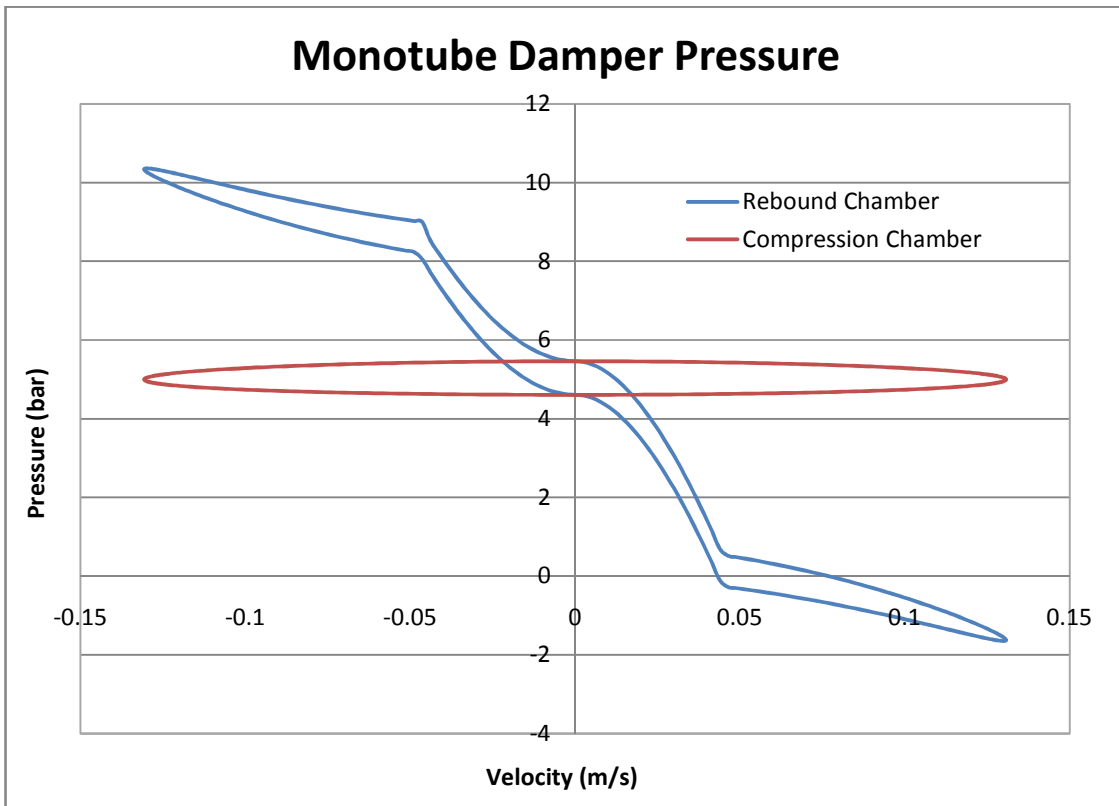


Figure 6.26: Monotube Damper Chamber Pressures at 5 bar

A higher initial gas pressure of 10 bar has been inputted into the model to prevent cavitation in the rebound chamber. Figure 6.27 below shows the chamber pressures for this test. They are significantly higher than the previous example and the variation of the gas and rebound chamber caused by the rod insertion is much greater. The variation of pressure is 1.7 bar at zero velocity for this test compared to .85 bar for the previous examples.

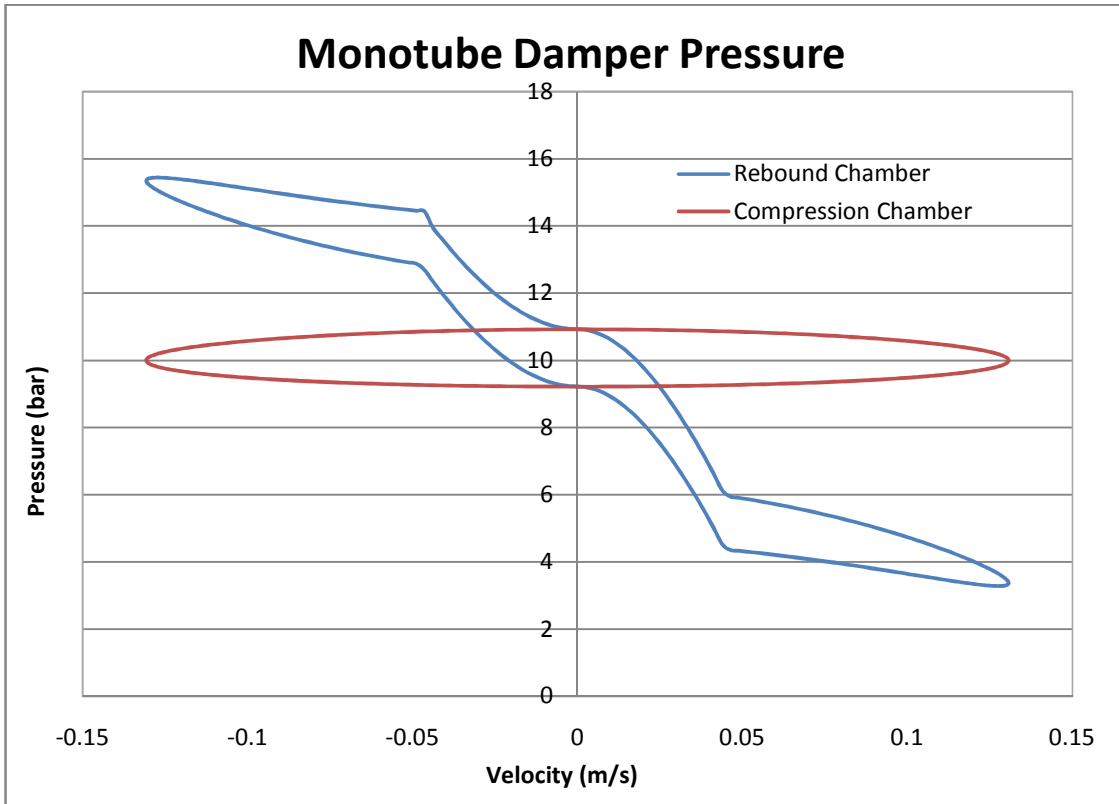


Figure 6.27: Monotube Damper Chamber Pressures at 10 bar

The characteristic diagram is not significantly affected by this increase in pressure. The most apparent effect that this pressure increase has is it increases the static gas force. This is subtracted from the data so it cannot be seen in the characteristic diagrams but can easily be determined from equation (4.2) which is restated below.

$$F_s = P_g A_{rod} \quad (4.2)$$

The other main effect is that the increased variation in the gas chamber pressure as a result of rod insertion contributes to additional hysteresis in the characteristic diagram. This is shown below in Figure 6.28. This figure is only shows the high speed region of the curve so that the increased hysteresis is clearly visible. Larger, high

performance monotube dampers have initial gas pressures of 20 bar or higher so the hysteresis produced by this can become very significant [28].

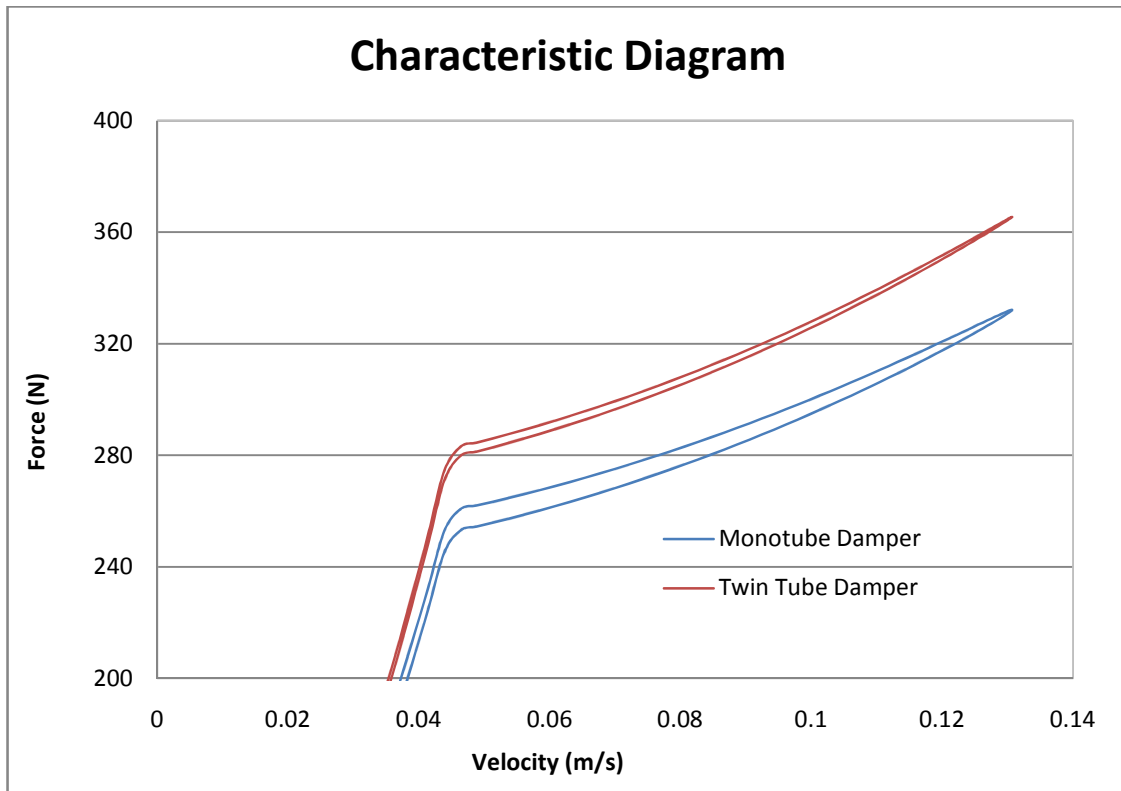


Figure 6.28: Characteristic Diagram of Twin Tube and Monotube Damper with Different Initial Gas Pressures

The higher pressures necessary in the monotube damper to prevent cavitation also puts more stress on the damper and seals. This can lead to more hysteresis from the fluid compressibility and damper compliance. Since the piston and rod seals are required to withstand higher internal pressures they often have more friction [13].

## **6.4 Parameter Studies**

With a validated model it is possible to evaluate quickly and easily the effect of many different parameters on the model. The value of these parameters will be varied and the resulting effects will be compared. This will aid in the understanding of the physics of the damper and could also be useful for damper design. The parameters to be varied are the bleed orifice area, the valve orifice area, the valve spring stiffness, the piston leakage gap, and the width of the circumferential fluid passage.

### 6.4.1 Bleed Orifice Area

In the Cane Creek Double Barrel damper the low speed adjustment changes the area of the bleed orifice by using a needle that restricts the orifice. The magnitude of this area is very important to the damper performance. It is the primary factor influencing the characteristic diagram in the low speed region of the curve. Figure 6.29 shows the affect changing the bleed orifice area has on the characteristic diagram.

The bleed orifice areas tested represent the range of adjustment of the Cane Creek Damper. The intervals of the areas are equivalent to one full turn of the low speed adjustments and are therefore not linear. These adjustments have a very large affect on the low speed performance of the damper. They also affect the location of the knee because they cause faster build up of the pressure required to overcome the valve preload. The force generated from the bleed orifice is also not linear since it is a function of the flow rate squared. The high speed region of the curve is barely affected by these changes

because the valve and valve orifice are the primary factors generating force at higher velocities.

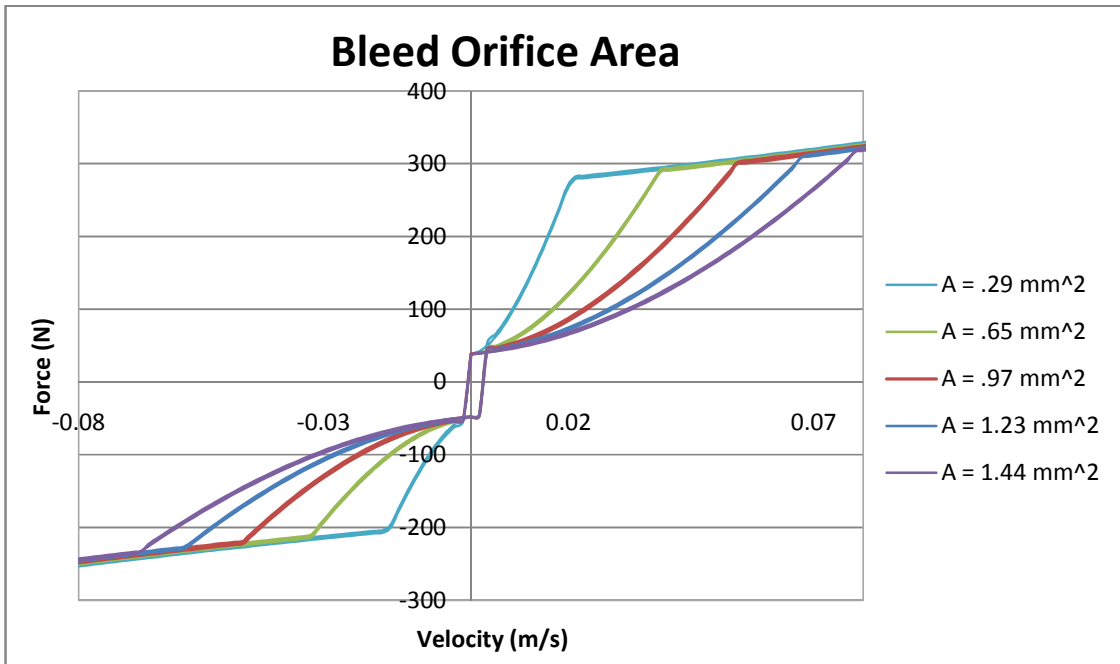


Figure 6.29: Characteristic Diagram of Bleed Orifice Area Parameter Study

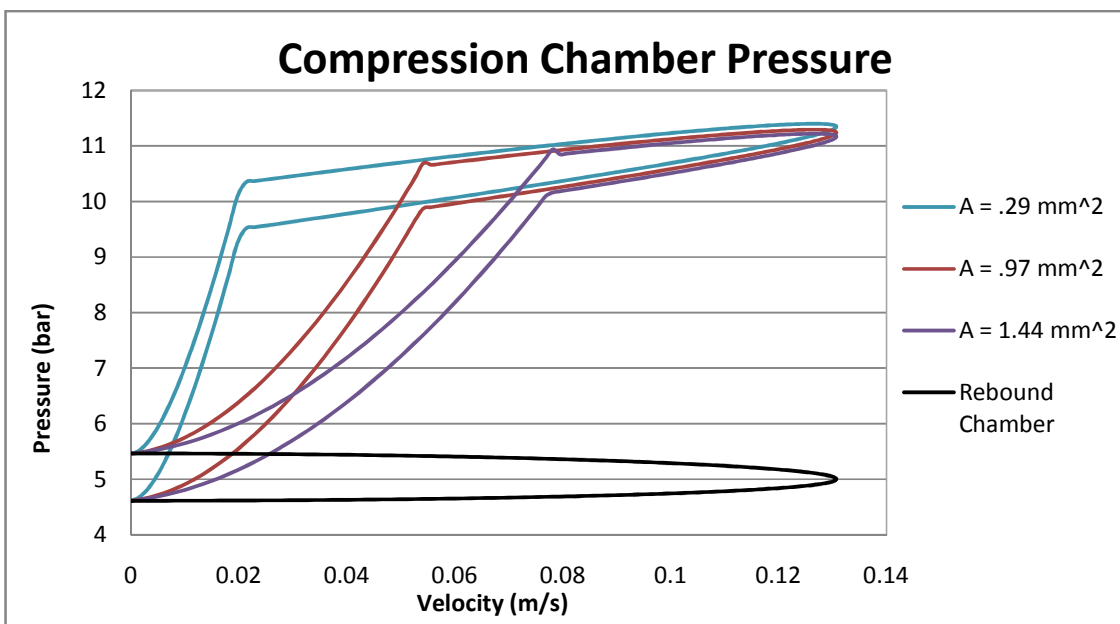


Figure 6.30: Pressure from Bleed Orifice Area Parameter Study

Figure 6.30 shows the compression chamber pressure in the damper with the various bleed orifice areas. Some of the areas tested were omitted from this figure for clarity. The black line represents the rebound chamber pressure. It is not affected by the bleed orifice area. This was included because the pressure differential between the rebound and compression chamber is directly related to the damper force. It can be seen that at higher velocities the pressure is higher for smaller bleed orifice areas.

#### 6.4.2 Valve Orifice Area

The valve orifice area is one of the primary factors influencing the slope and curvature of the high speed region of the characteristic diagram. The effect of this parameter is shown below in Figure 6.31. Only the compression of the damper is shown so that the resulting force can be seen more clearly. The trends in rebound are identical to those shown here in compression.

It can be seen that as the area is reduced the slope and curvature of the plot increase. The orifice areas used represent orifice diameters of 2.0, 2.5, 3.0, 3.5, and 4.0 mm. It can be seen that this affect like the bleed orifice is also nonlinear. However the force of the damper is not as sensitive to these changes as changes in the bleed orifice. This is a result of the orifice being significantly larger and not being the singular primary source of flow restriction. As the orifice area gets smaller the knee location increases slightly.

Figure 6.32 shows the valve deflection as a function of velocity for the different areas tested. It can be seen that less valve deflection occurs when the valve orifice area is

smaller. This is a result of the valve orifice restricting flow and reducing the pressure on the valve.

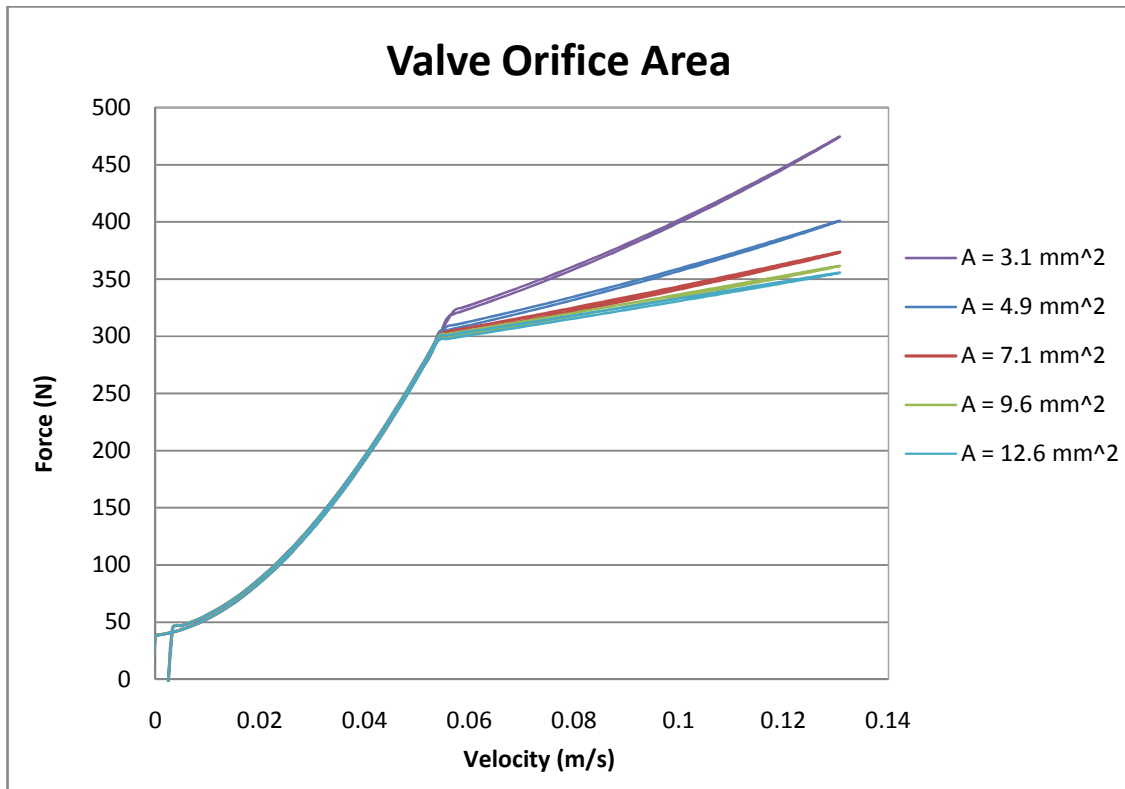


Figure 6.31: Characteristic Diagram of Valve Orifice Area Parameter Study

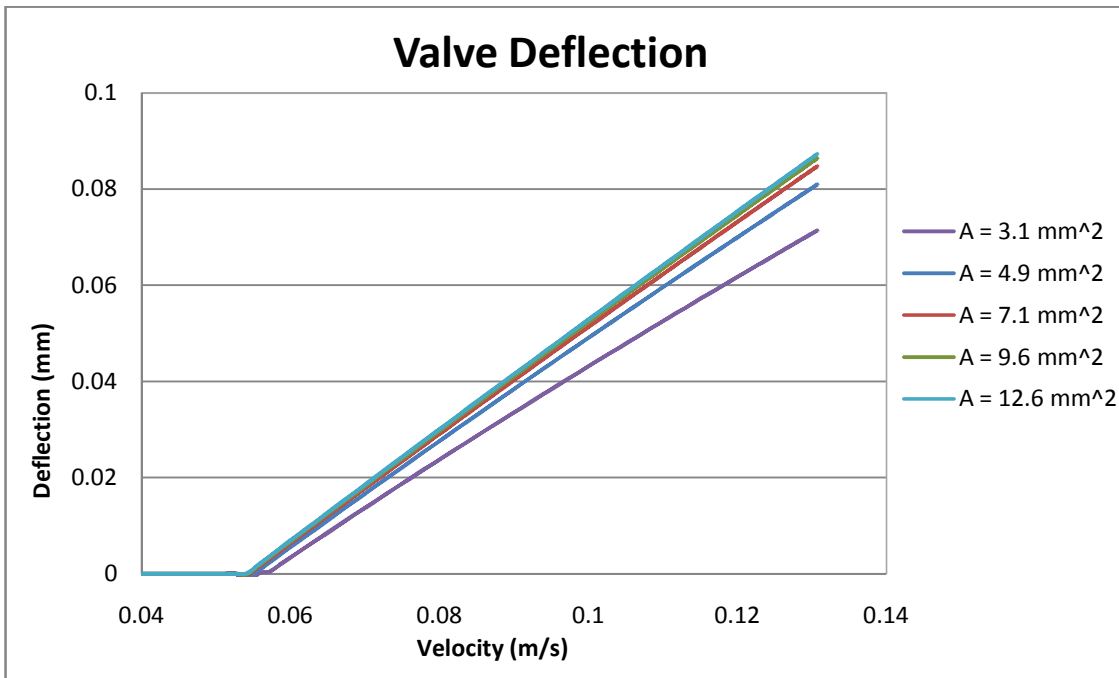


Figure 6.32: Valve Deflection from Valve Orifice Area Parameter Study

#### 6.4.3 Valve Spring Stiffness

Next the affect of the stiffness of the valve spring on the damper was examined. This parameter would also be expected to primarily influence the high speed region of the curve. The affect of this on the characteristic diagram can be seen below in Figure 6.33. Again only the compression of the damper is shown so that the resulting force can be seen more clearly.

Unlike the valve orifice the increase in damper force caused by an increase in valve stiffness is linear. The maximum damper force increased by approximately 10 N per 20 N/mm of additional valve spring stiffness. This relationship is also linear with respect to the damper velocity. Therefore the curvature of the high speed region of the plot does not change with increases in the valve stiffness. The valve stiffness also has no affect on the knee location of the damper as long as the preload force is the same.

However in many dampers shim stacks or other nonlinear springs are used. A nonlinear stiffness would introduce curvature into the high speed region. This curvature would be proportional to the instantaneous spring rate and could be easily tailored to specific requirements. Different springs could be used to achieve progressive, linear, or even digressive build up of force in the high speed region.

Figure 6.34 shows the deflection of the valve. It can be seen that the difference in deflections are linearly related. This can be compared to the nonlinear relationship of the deflections from changing the valve orifice area in Figure 6.32. Since the valve deflection is caused by the pressure of the damper fluid it is apparent that a linear change in valve stiffness will have a linear affect on the damper force.

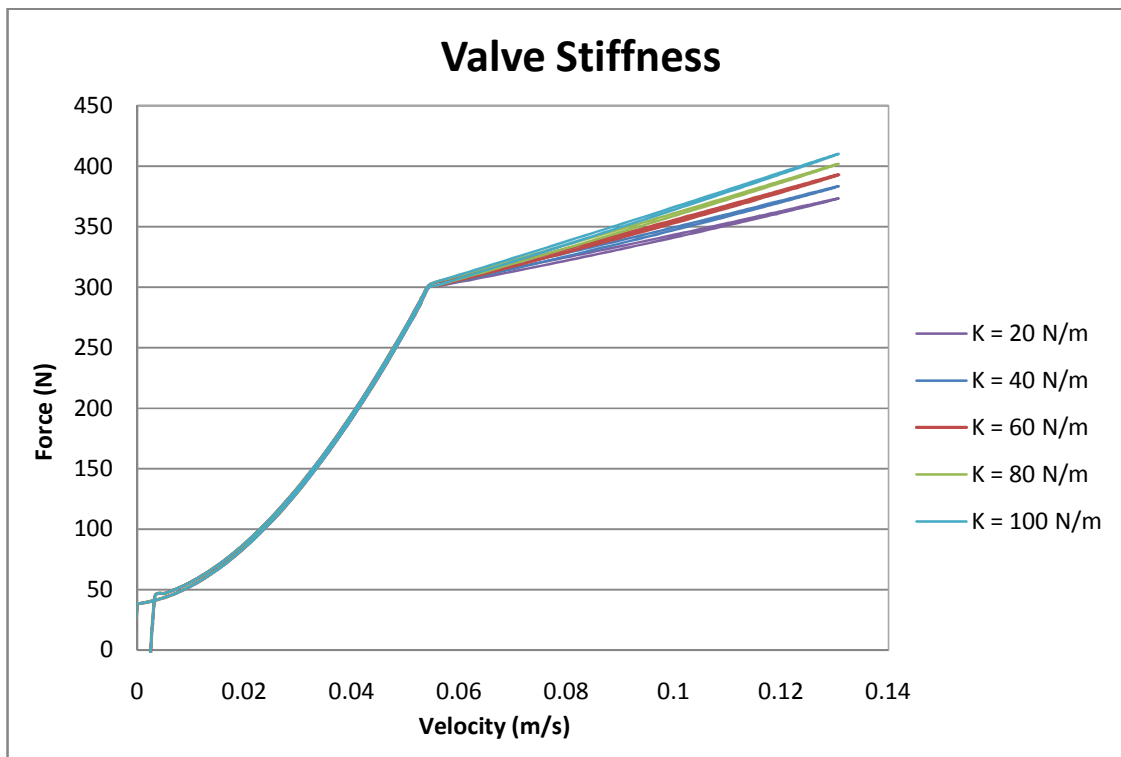


Figure 6.33: Characteristic Diagram of Valve Stiffness Parameter Study

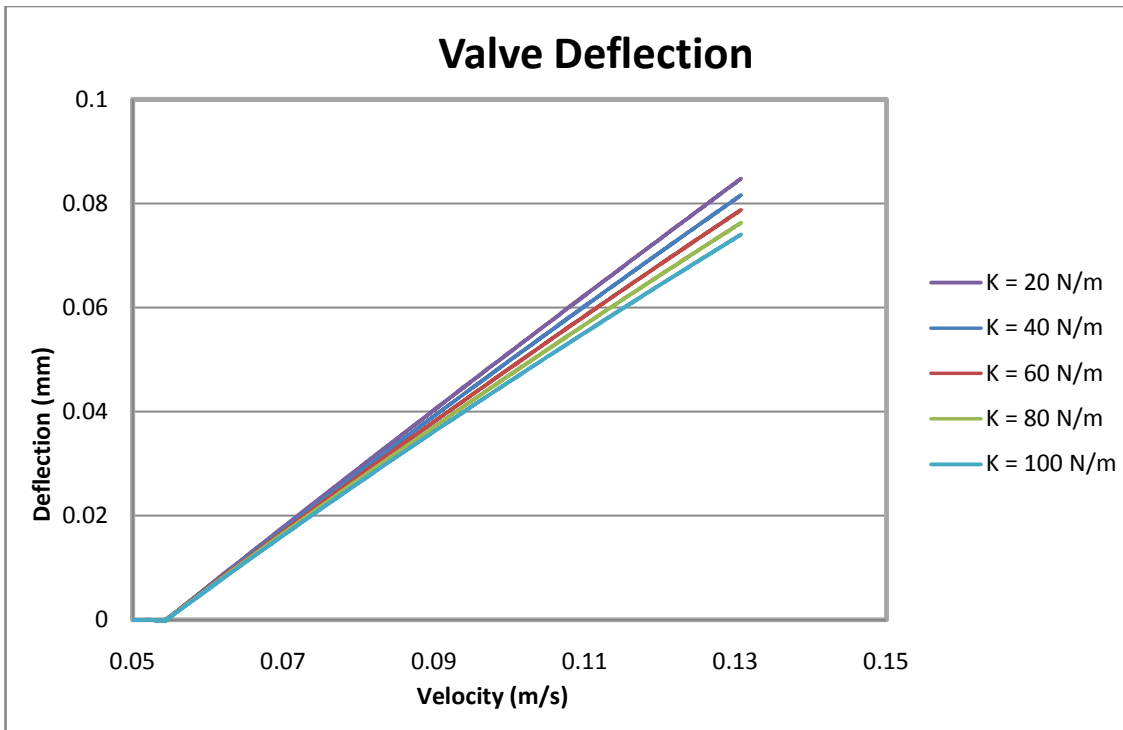


Figure 6.34: Valve Deflection from Valve Stiffness Parameter Study

#### 6.4.4 Piston Leakage Gap

If a damper is in good condition the leakage gap between the piston seal and damper chamber should not have a large affect on the damper performance. However since this parameter can change as the wear on the damper is increased it will be examined. The leakage gap around the piston should be very small. For the Cane Creek Damper it is approximately .04 mm. This was used as the starting value and then other gap sizes were tested. Figure 6.35 shows the results of these tests on the damper performance.

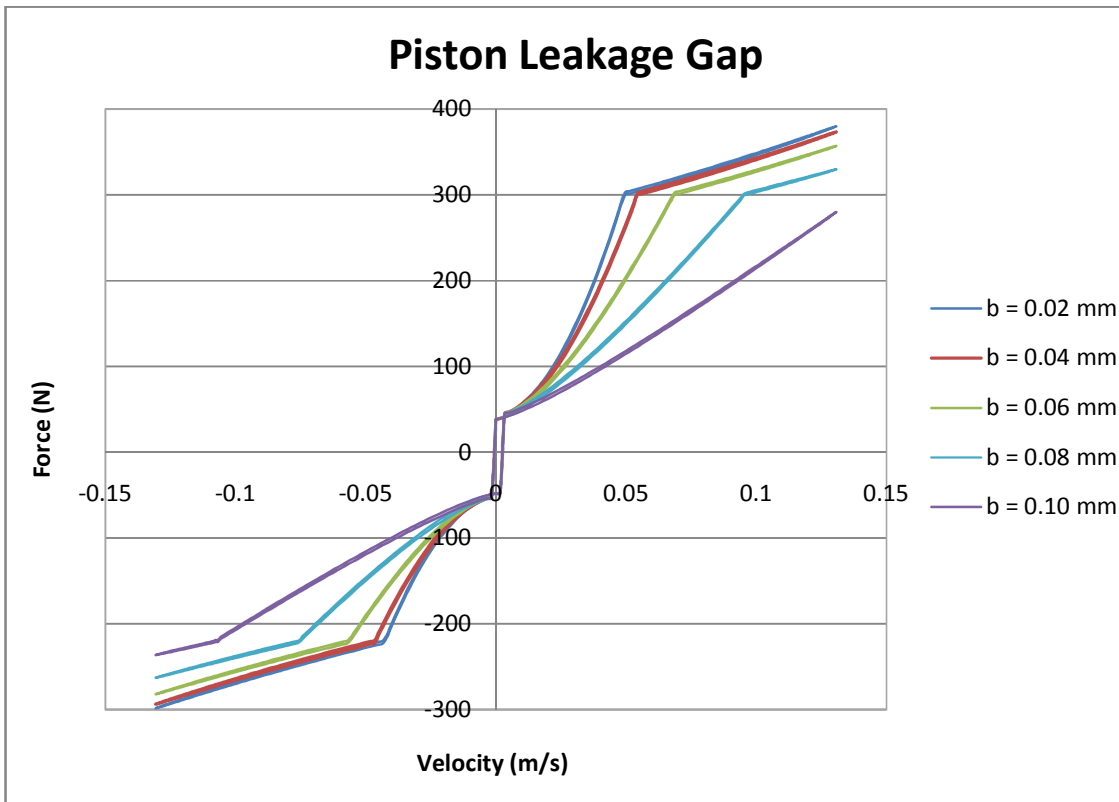


Figure 6.35: Characteristic Diagram of Piston Leakage Gap Parameter Study

It can be seen that for a properly operating damper decreasing the piston leakage gap will not have a large affect on the damper performance. The affect of it would most likely be insignificant compared to the change in friction of the damper. However as the leakage gap increases the damper force drops off dramatically. The force difference at the maximum velocity between the test of the .04 mm and .06 mm gap is 16.3 N and the maximum difference between the .04 mm and .08 mm gap was 43.5 N. Obviously these affects are very significant. This is one of the reasons why regular maintenance and seal replacement is often recommended for high performance dampers. The location of the knee is also severely affected. With a .10 mm gap the valve preload is never even overcome in compression.

Figure 6.36 shows the flow rate of the damper fluid through the piston leakage gap. The orange line is the total flow rate of all of fluid in the damper. It increases linearly as a function of the damper velocity. It can be seen that with a .10 mm gap over half of the fluid is flowing around the piston instead of through the valve and orifices. In addition to greatly reducing the damper force this would also significantly limit the effectiveness of the adjusters since they would be restricting significantly less fluid. With a .04 mm gap this flow is much less than one tenth of the overall flow and from the characteristic diagram it can be seen that it has a small effect on the damper performance.

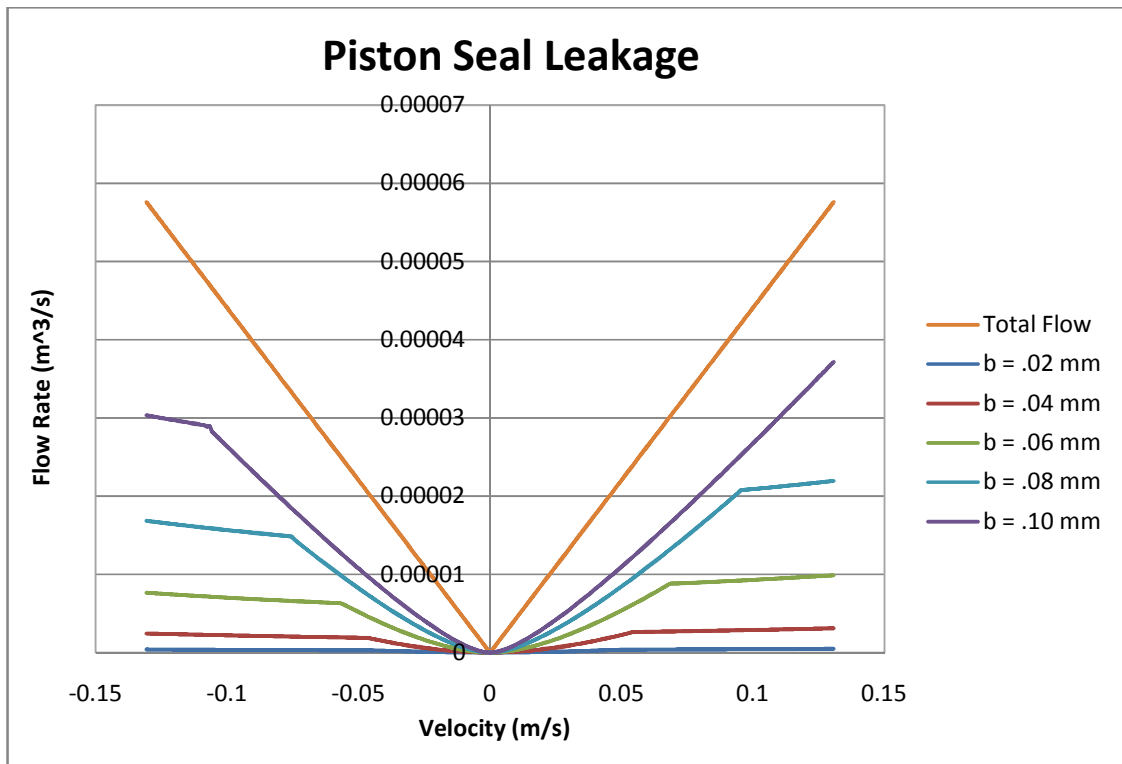


Figure 6.36: Flow Rate of Piston Leakage Gap

#### 6.4.5 Fluid Passage Width

In section 6.2 it was discovered that the viscous effects of the fluid flow through the circumferential passage of a modern twin tube damper was very significant to the performance of the damper. The effect of the width of this flow path will be investigated here. The width of the flow path in the Cane Creek damper is 2.20 mm. Multiple widths were tested to evaluate the effect of this parameter. The results are shown below in Figure 6.37.

The damper force increases significantly as the width is decreased. The force increase was significant over both the low and high speed regions of the curve. At maximum velocity the example with a width of 1.40 mm produced an additional 322.3 N compared to the example with a width of 2.20 mm. This is an increase of over 85%. The location of the knee is not affected by this parameter because it acts independently of the valve and does not affect the flow rate to the valve.

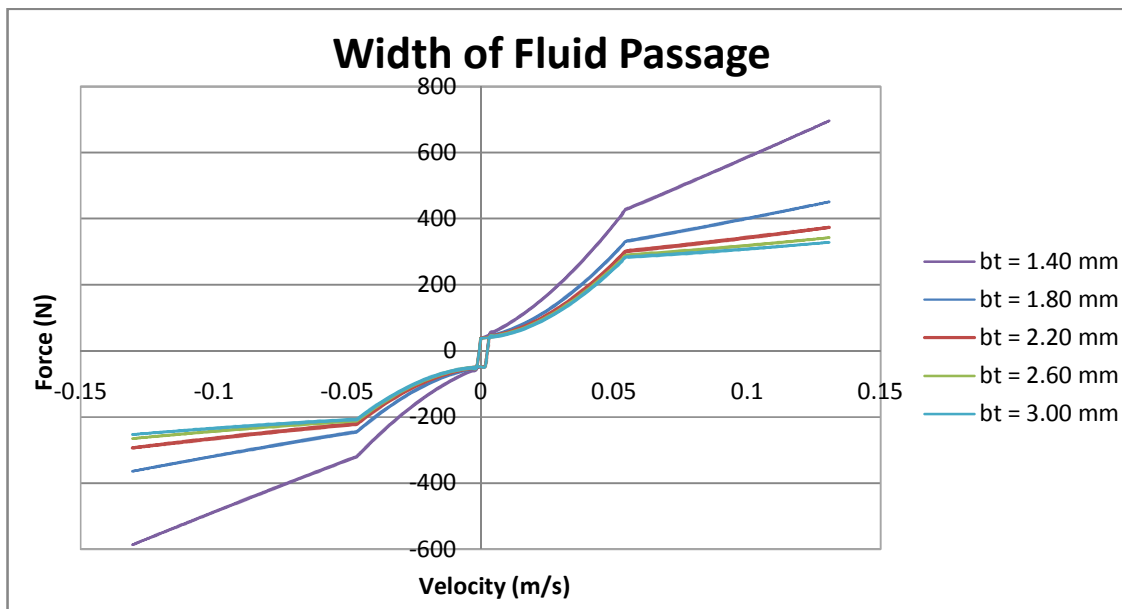


Figure 6.37: Characteristic Diagram of Fluid Passage Width Parameter Study

Figure 6.38 shows the increase in pressure caused by this effect. The rebound chamber pressure is represented by the black line. The pressure difference between the rebound chamber and the other lines is the additional compression chamber pressure caused by this effect. Therefore it is directly proportional to the additional force the damper produces.

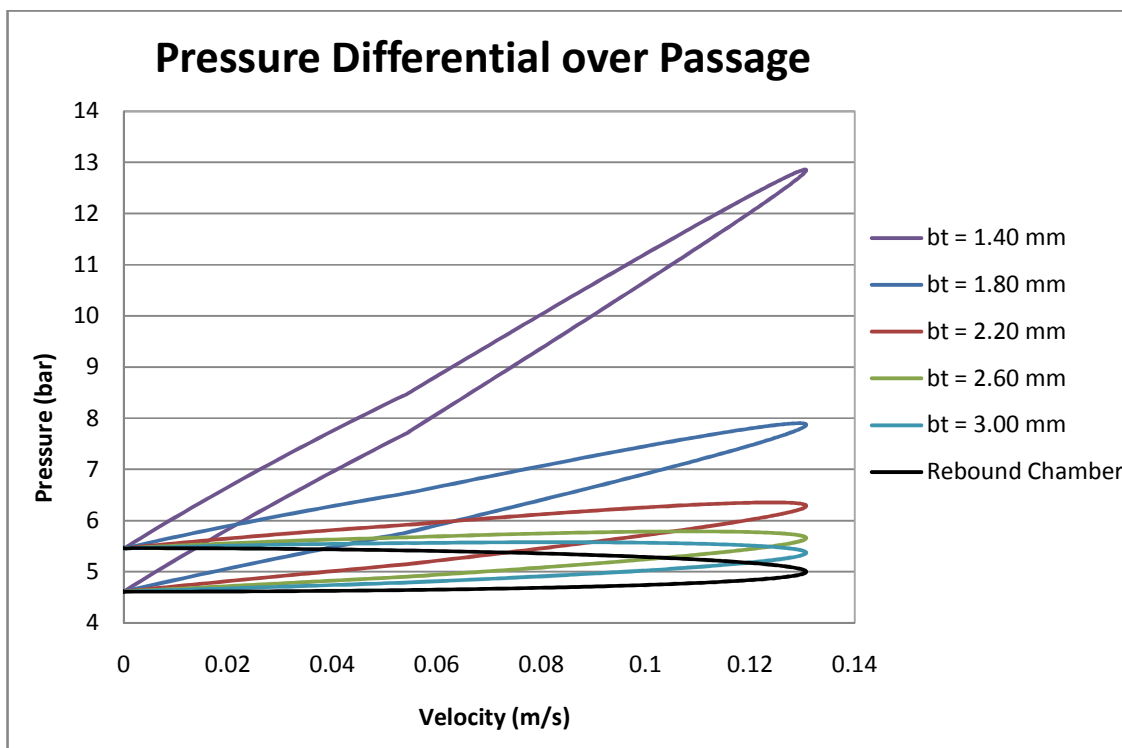


Figure 6.38: Pressure Differential over Fluid Passage

Understanding how and why different parameters of the damper affect its performance is very important. A good grasp of this knowledge can enable more accurate and quicker tuning of the damping to fit desired situations and a more scientific approach to damper design

## 6.5 Spring Mass Damper Model

The spring mass damper model that was developed in section 2.1 will now be used to evaluate a quarter car suspension with a nonlinear, asymmetric damper force. The damper force used will be inputted from the model. This will allow us to look at the effects of the damper characteristics on the displacement and acceleration of the sprung mass, and the tire load variation. The importance of these parameters was covered in section 2.1.

The system properties are the same as those evaluated in section 2.1 except the damper force is determined from the damper model instead of the linear coefficient. The model uses a tire stiffness of 120,000 N/m, a spring stiffness of 20,000 N/m, and sprung and unsprung masses of 60 and 12 kg. The tire damping is neglected. The response to a 300 N force applied to the sprung mass will be evaluated.

Three different settings of the Cane Creek damper will be evaluated. The characteristic diagrams from these settings are shown below in Figure 6.39. The “Under Damped” plot represents the softest possible settings for the low speed adjusters on the Cane Creek Double Barrel. The “Critically Damped” plot is near the middle of the adjustment range for the damper. It is not the exact critical damping for the system but the response reveals that it is very close to this value. The “Over Damped” plot represents a significantly stiffer setting of the damper.

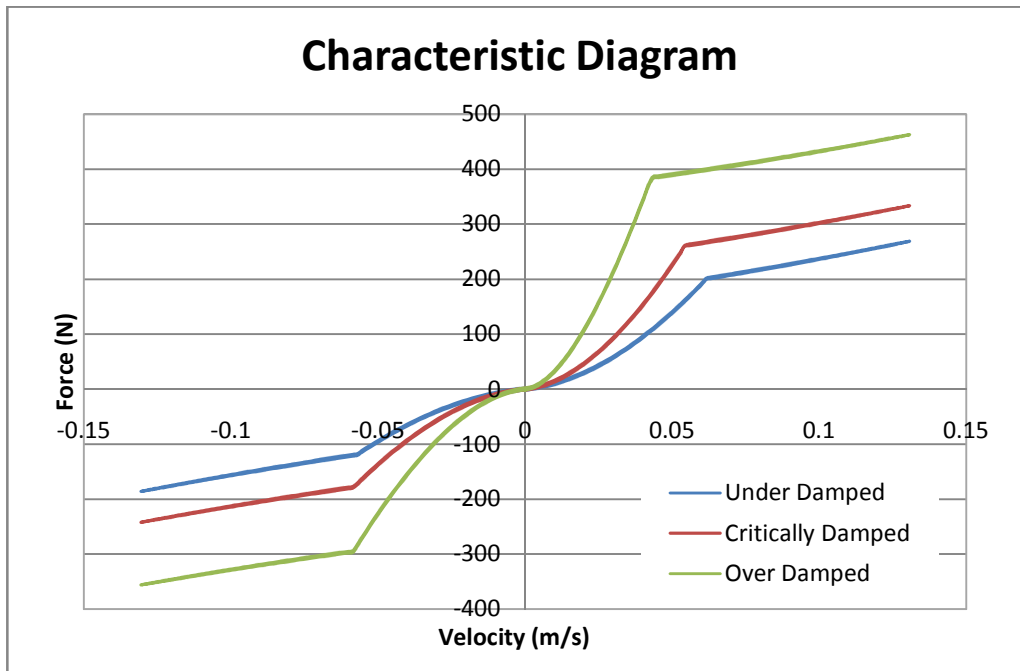


Figure 6.39: Characteristic Diagram for the Spring Mass Damper Model

Figure 6.40 below shows the response of the sprung mass to the force. As expected the over damped case takes much longer to reach steady state, the under damped case returns much more quickly with some oscillation, and the critically damped case reaches steady state with very little overshoot. Again this is only an approximate of critical damping because there are small amounts of overshoot and oscillation. The slight changes in slope that can be seen for the over damped case are where the sprung mass velocity became lower than the velocity of the knee. The same effect occurs for the under damped case but since the slope transition in the characteristic diagram is much more gradual than the other settings it is more difficult to see. The over damped case does not appear to ever go above the velocity of the knee.

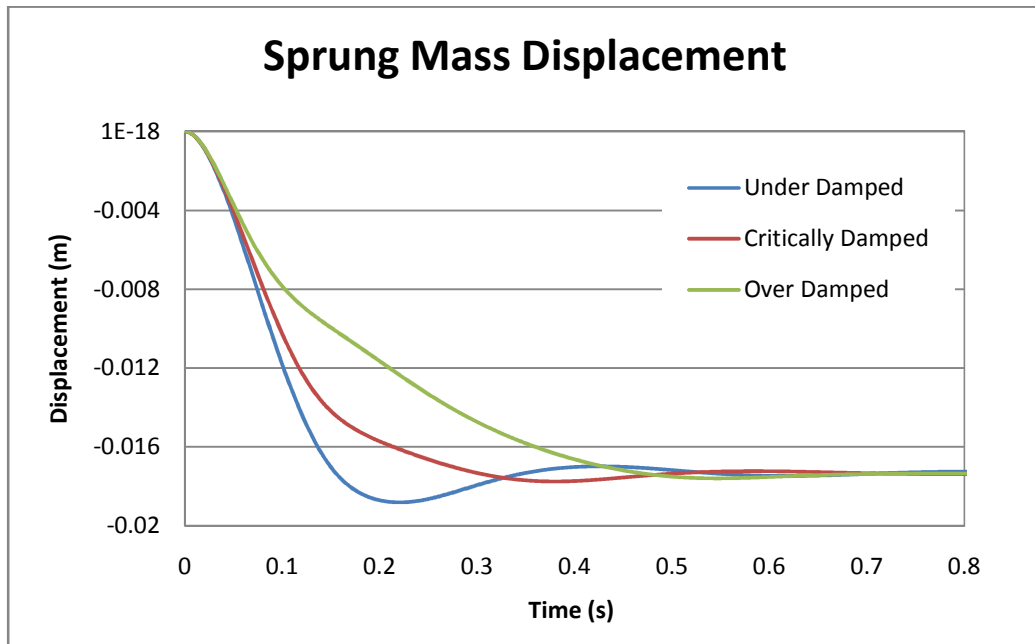


Figure 6.40: Sprung Mass Displacement with Damper Model Input

Figure 6.41 shows the acceleration of the sprung mass. The over damped case has the lowest sprung mass acceleration. For the majority of the response time it is operating in the low speed region of the characteristic diagram. Thus the damping coefficient is very high. There are dramatic changes in the sprung mass acceleration for the under damped and critically damped cases. This is due to the slope transition of the knee. Between about .025 and .125 seconds these systems are operating in the high speed region of the characteristic diagram. This prevents large forces from being transferred between the sprung and unsprung masses.

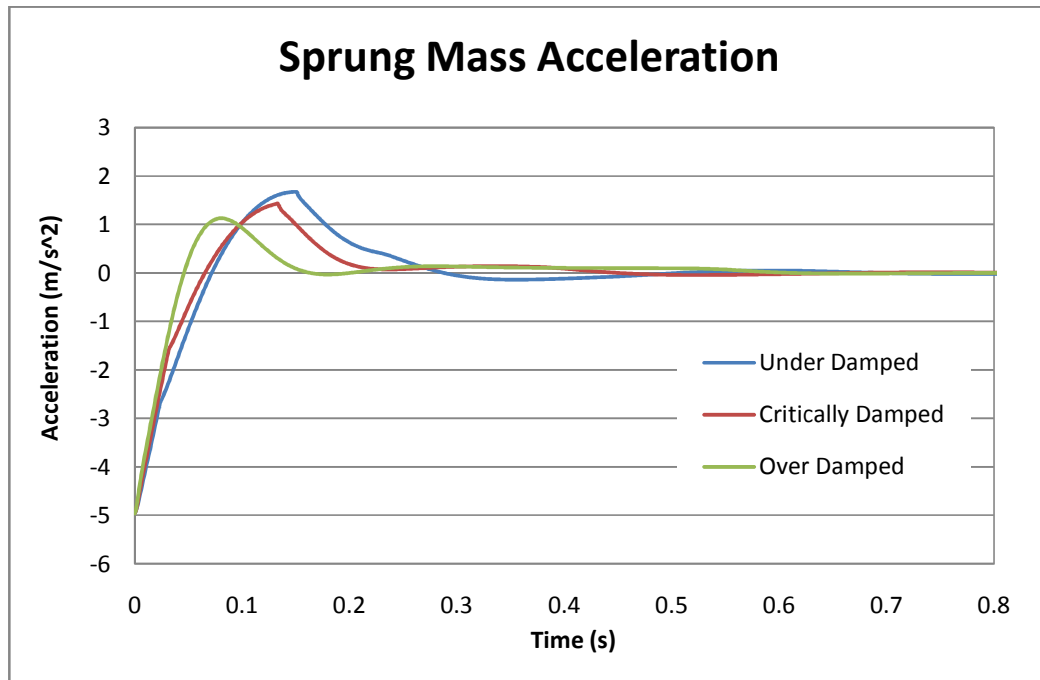


Figure 6.41: Sprung Mass Acceleration with Damper Model Input

Figure 6.42 shows the force outputted by the damper. From this it is very clear when the under damped and critically damped cases exceeded then dropped below the velocity at the knee. The transition and reduction in slope for both of these cases can clearly be seen. As expected it does not appear that the over damped case ever exceeds the velocity at the knee.

Figure 6.43 is the tire load variation. The transition at the knee causes a very high rate of load variation change. This is not good for vehicle handling because it disturbs the tire contact patch.

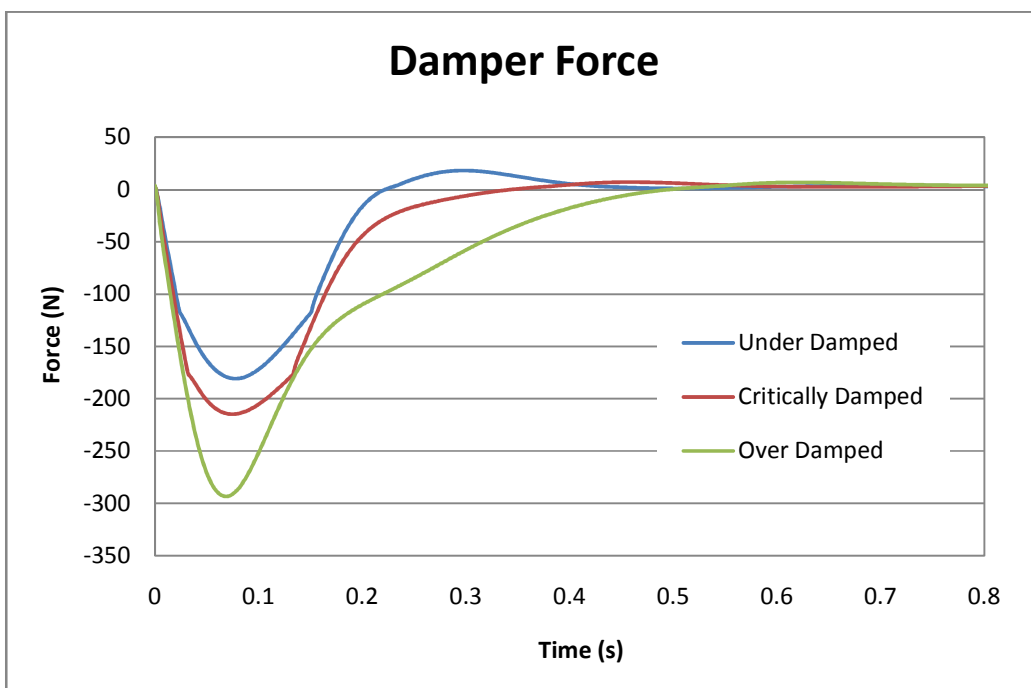


Figure 6.42: Damper Force from Damper Model Input

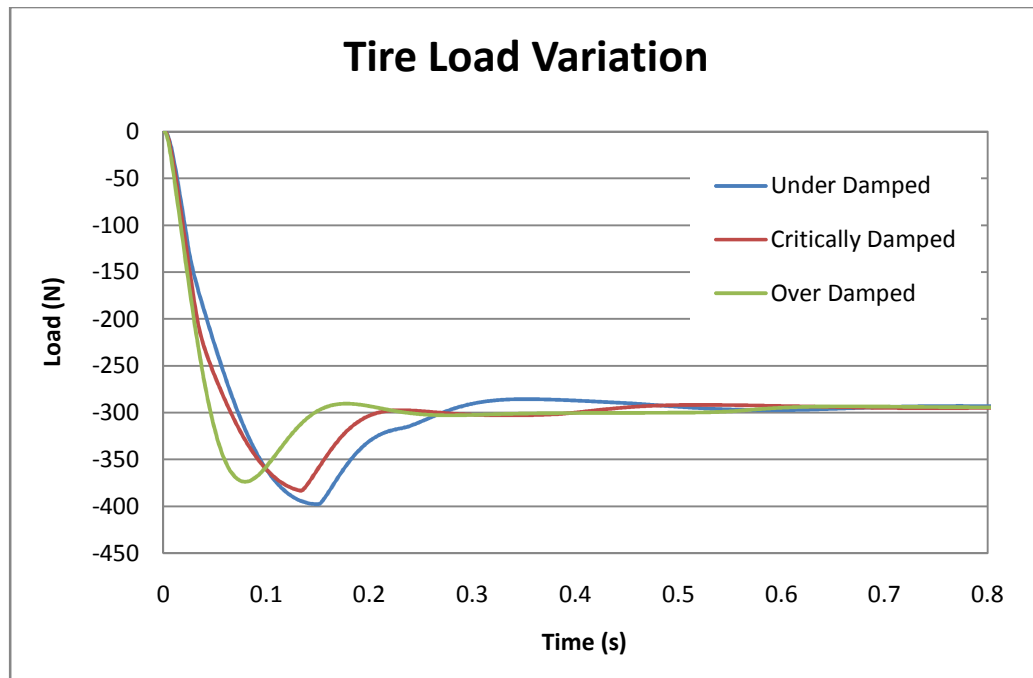


Figure 6.43: Tire Load Variation from Damper Model Input

For this specific input and depending on the desired response the over damped case might be the best compromise. The large force input and sharp slope transition at the knee cause the sprung mass acceleration and tire load variation to not be favorable. Another solution would be to increase the high speed adjusters so that the knee velocity is never exceeded. Further investigation with different force and displacement inputs and damper characteristics would be necessary to predict the ideal configuration.

Comparing these figures to those in section 2.1 illustrates the significance of the damper nonlinearity and asymmetry. The effect this can have on the response of the vehicle is very significant as well as the effect of friction and hysteresis. Therefore vehicle testing instead of calculations or computer models is often used to determine the optimal damper rates.

## **7. CONCLUSION AND RECOMMENDATIONS**

A physical model of a modern twin tube damper was successfully created and validated with experimental testing. The model was shown to accurately predict the nonlinear, asymmetric trends of the damper force over a large range of adjustment settings. The model also determines many other physical parameters of the damper such as flow rates, fluid pressures, and valve deflections.

The effect of fluid inertia and viscous effects were examined. The effect of the fluid inertia was negligible in comparison to the overall force output of the model for standard sinusoidal testing. However the viscous effects were revealed to be very significant. They were responsible for approximately 17 % of the force generated by the damper at high velocities.

It was shown that the primary mechanism for producing force is the increase in pressure in the chamber that is being compressed. This is in contrast to a monotube damper that produces force from changes in pressure both positive and negative of the rebound chamber while the compression chamber pressure stays relatively constant. This eliminates the possibility of cavitation from the rebound chamber pressure dropping below the vapor pressure of the fluid. This allows modern twin tube dampers to run much lower gas pressures and subsequently have much lower static gas force. The pressure increase in the compression chamber during compression also leads to an increase in damper force compared to a similar monotube damper.

Parameter studies were used to improve the understanding of the effect of the damper properties and adjustments. As expected the bleed orifice area was the primary factor in determining the low speed force as long as the piston leakage was not significant. The high speed force was influenced by the valve orifice and spring stiffness. The viscous effects of the fluid contributed significantly to both the high and low speed regions of the curve.

A spring mass damper model was also created to evaluate the effects of the damper characteristics on the vehicle response. This model represents one corner of a vehicle. It uses the output of the damper model to calculate the damper force. It also includes the tire stiffness and damping.

Further work could be performed on many different aspects of this model to improve its accuracy. The most significant improvement would most likely be including the effect of the fluid compressibility and damper compliance. This would allow the accurate prediction of hysteresis.

More detailed modeling of the fluid flow using computational fluid dynamics would increase the accuracy of the orifice and valve models. This could also include the effect of temperature on the fluid and resulting damper characteristics. Using variable discharge coefficients that are functions of the Reynolds number and the fluid acceleration could also improve the accuracy of the model.

A more complex model of the damper friction separating static and dynamic friction and a separate gas piston friction force could be incorporated into the model. Evaluation of the effect of parameters like gas pressure, piston leakage gap, damper fluid,

and seal design on the damper friction could be used to eliminate unnecessary friction in the damper.

Further testing and validation of other dampers would also be beneficial. This would further validate the accuracy of the model and would allow comparison between design differences between dampers. Comparison of other parameters besides the damper force could also be useful. For example chamber pressures could be measured while the damper is tested and compared to those calculated by the model data.

## REFERENCES

1. Talbot, M.S., Starkey J., “An Experimentally Validated Physical Model of a High Performance Mono-Tube Damper”, Society of Automotive Engineers, Warrendale, PA, Paper 2002-01-3337, 2002.
2. Rhoades, K.S., “Development and Experimental Verification of a Parametric Model of an Automotive Damper,” M.S. Thesis, Texas A&M University, College Station, TX, 2006.
3. Dixon, J.C., *Tires, Suspension, and Handling*, 2<sup>nd</sup> Edition, Society of Automotive Engineers, Warrendale, PA, 1996.
4. Thomson, W.T., Dahleen, M.D., *Theory of Vibrations with Applications*, 5<sup>th</sup> Edition, Prentice Hall, New Jersey, 1993.
5. Palm, W. J. III, Modeling, Analysis, and Control of Dynamic Systems, 2<sup>nd</sup> Edition, John Wiley and Sons, New York, 2000.
6. Gillespie, T. D., *Fundamentals of Vehicle Dynamics*, Society of Automotive Engineers, Warrendale, PA, 1992.
7. Rouelle, C. “Racecar Engineering and Data Acquisition Seminar,” OptimumG, September, 2006.
8. Milliken, W.F., Milliken, D.L., *Race Car Vehicle Dynamics*, Society of Automotive Engineers, Warrendale, PA, 1995.
9. Dixon, J.C., *The Shock Absorber Handbook*, 2<sup>nd</sup> Edition, John Wiley and Sons, England, 2007.
10. Ohlins Racing AB, “Stock Car Shock Absorbers: Owner’s Manual,” March 2002.
11. Ohlins Racing AB, “Road and Track Owner’s Manual,” April 2005.
12. Cane Creek, “Cane Creek Double Barrel Instructions,” August 2005.
13. Ohlins Racing AB, “Inside TTX: The Ohlins TTX40 Manual,” May 2005.
14. Roehrig Engineering, “General Product Information and Policies”, November 2007.

15. Lang, H.H., Segel, L., "The Mechanics of Automotive Hydraulic Dampers at High Stroking Frequencies," *The Dynamics of Vehicles on Roads and on Tracks*, pp. 194-214, 1982.
16. Lang, H.H., "A Study of the Characteristics of Automotive Hydraulic Dampers at High Stroking Frequencies," Ph.D. Dissertation, The University of Michigan, Ann Arbor, MI, 1977.
17. Reybrouck, K.G. "A Non Linear Parametric Model of an Automotive Shock Absorber," Society of Automotive Engineers, Warrendale, PA, Paper 940869, 1994.
18. Duym, S.W., Steins, R. Baron, G.V., Reybrouck, K.G., "Physical Modeling of the Hysteretic Behavior of Automotive Shock Absorbers," Society of Automotive Engineers, Warrendale, PA, Paper 970101, 1997.
19. Audendino, A.L., Belingardi, G., "Modeling of the Dynamic Behavior of a Motorcycle Damper," *Proceedings of the institution of Mechanical Engineers. Part D. Journal of Automobile Engineering*. v. 209 n. 4, pp. 249-262, 1995.
20. Mollica, R., Youcef-Toumi, K., "A Nonlinear Dynamic Model of a Monotube Shock Absorber," *Proceedings of the American Control Conference*, Albuquerque, NM, pp. 704-708, 1997.
21. Mollica, R., "Nonlinear Dynamic Model and Simulation of a High Pressure Monotube Shock Absorber Using the Bond Graph Method," M.S. Thesis, Massachusetts Institute of Technology, Cambridge, MA, 1997
22. Fitzhorn, P.A., "Fundamentals of Vehicle Dynamics: Struts and Dampers," Lecture Notes, Colorado State University, Fort Collins, CO, 2006.
23. Fox, R.W., McDonald, A.T., Pritchard, P.J., *Introduction to Fluid Mechanics*, 6<sup>th</sup> Edition, John Wiley & Sons, Inc., 2004.
24. Karnopp, D. C., "Bond Graph Models for Fluid Dynamic Systems," *Journal of Dynamic Systems, Measurements, and Control*, v. 94, n. 3, pp. 222-229, 1972.
25. Hoffman, J.D., *Numerical Methods for Engineers and Scientists*, 2<sup>nd</sup> Edition, Marcel Dekker, Inc., New York, 2001.
26. Coaplen, J., Cane Creek Representative, Personal Conversation, January 30, 2009.

27. Ott, R. L., Longnecker, M., *An Introduction to Statistical Methods and Data Analysis*, 5<sup>th</sup> Edition, Wadsworth Group, Pacific Grove, CA, 2001.
28. ZF Sachs, “Formula Matrix Damper Delivery Program”, November 2008.